A numerical perspective on wildfire plume-rise dynamics

by

Nadejda Moisseeva

A THESIS SUBMITTED IN PARTIAL FULFILLMENT

OF THE REQUIREMENTS FOR THE DEGREE OF

Doctor of Philosophy

in

THE FACULTY OF GRADUATE AND POSTDOCTORAL STUDIES

(Atmospheric Science)

The University of British Columbia

(Vancouver)

December 2020

The following individuals certify that they have read, and recommend to the Faculty of Graduate and Postdoctoral Studies for acceptance, the thesis entitled:

A numerical perspective on wildfire plume-rise dynamics

submitted by **Nadejda Moisseeva** in partial fulfillment of the requirements for the degree of **Doctor of Philosophy** in **Atmospheric Science**.

Examining Committee:

Roland Stull, Atmospheric Science, UBC
Supervisor

Douw Steyn, Atmospheric Science, UBC
Supervisory Committee Member

Phillip Austin, Atmospheric Science, UBC
Supervisory Committee Member

Adam Kochanski, Meteorology and Climate Science, SJSU
External Examiner

Lori Daniels, Forestry, UBC
University Examiner

Allan Bertram, Chemistry, UBC
University Examiner

Abstract

The buoyant rise of wildfire smoke and the resultant vertical distribution of emission products in the atmosphere have a strong influence on downwind pollutant concentrations at the surface, and provide key input into regional and global chemical transport models. Due to inherent complexity of wildfire plume dynamics, smoke injection height predictions are subject to large uncertainties. One of the obstacles to the development of new plume rise parameterizations has been the scarcity of detailed simultaneous observations of fire-generated turbulence, entrainment, smoke concentrations and fire behavior. This thesis makes contributions on two fronts: (i) it demonstrates the feasibility of using coupled fire-atmosphere large-eddy simulations to model wildfire smoke dynamics to produce "synthetic" plume data, and (ii) develops a new energy balance plume rise parameterization to predict the vertical distribution of smoke in the atmosphere.

The first part of the thesis focuses on evaluating the large-eddy simulation model used in this work with a detailed observational dataset from a real prescribed burn. The next portion explores the effect of various fire parameters and ambient atmospheric conditions on smoke plume behavior using a range of sensitivity studies. Analysis of flow dynamics shows that the updraft is shaped by complex interactions of fire-induced winds and vorticity generated in response to a near-surface convergence, and does not conform to commonly used mixing and entrainment assumptions.

With the knowledge gained through the above numerical experiments, the second half of the thesis introduces a simple parameterization for predicting the mean centerline height for penetrative plumes from fires of arbitrary shape and intensity. Lastly, the proposed parameterization is extended to capture the full vertical distribution of smoke in the atmosphere. The broad goal of this work is to better our understanding of plume rise dynamics and improve smoke dispersion predictions within air quality applications.

Lay Summary

This work aims to improve our understanding of how smoke from wildfires spreads in the atmosphere. The more we know about where and how the pollutants travel, the better we are able to predict hazardous air quality and inform downwind communities. Specifically, this thesis presents simple tools for estimating how high above the Earth's surface the smoke from a wildfire will rise. These methods can be used within existing air quality models and help improve their accuracy.

Preface

This dissertation is original work of the author, Nadejda Moisseeva, under the supervision of Roland Stull. Below are details of how papers (published and accepted for publication) included in thesis were modified into chapters.

- **Moisseeva, N.; Stull, R.: Capturing Plume Rise and Dispersion with a Coupled Large-Eddy Simulation: Case Study of a Prescribed Burn. Atmosphere 2019, 10, 579.**

  Excerpts from the article are included in Chapter 2. Chapter 3 is based in full on the paper, with the addition of brief introduction and 'Big picture' sections.

- **Moisseeva, N. and Stull, R.: Wildfire smoke-plume rise: a simple energy balance parameterization, Atmos. Chem. Phys. Discuss., https://doi.org/10.5194/acp-2020-827, accepted for publication, Dec 2020.**

  Excerpts from the article are included in Chapter 2. Chapter 4 and Chapter 6 are based in full on the paper, with the addition of brief introduction, expanded model configuration description and 'Big picture' sections.

For both publications, I was responsible for conceptualization, experimental design, methodology, analysis and visualization. Roland Stull was involved in concept formation, manuscript composition and provided supervisory support throughout the publishing process and the dissertation.

Datasets

Synthetic wildfire plume dataset produced for this dissertation is available via Federated Research Data Repository (FRDR):

- **Moisseeva N, (2020). WRF-SFIRE LES Synthetic Wildfire Plume Dataset. Federated Research Data Repository. https://doi.org/10.20383/102.0314.**

Externally-sourced graphics

The following figures and their corresponding original sources are included in Chapter 2 of the dissertation:

- **Figure 1.1**: Dalyup bushfire [48]
- **Figure 2.2**: Smoke modelling framework schematic. Figure produced by Chris Rodell for internal report to Natural Resources Canada.
- **Figure 2.3**: Process diagram for RxCADRE project [54]
- **Figure 2.4**: Conceptual diagram of spatial scales captured by field campaigns [61]

Open-source software

Smoke and trajectory visualizations included in Chapter 3 and Chapter 5 were produced using VAPOR open-source software [13].

Table of Contents

List of Tables

List of Figures

Glossary

ABL atmospheric boundary layer

AGL above ground level

AWI along-wind integrated

CALIOP Cloud-Aerosol Lidar with Orthogonal Polarization

CAWFE Coupled Atmosphere Wildland Fire-Environment

CO carbon monoxide

CWI crosswind-integrated

FASMEE Fire and Smoke Model Evaluation Experiment

FBP fire behavior package

FIREX-AQ Fire Influence on Regional to Global Environments and Air Quality

FRP fire radiative power

HIP Highly Instrumented Plot

IQR interquartile range

KE kinetic energy per unit mass

LES large-eddy simulation

LHS left-hand side

LWIR Long Wave Infrared

MAE mean absolute error

MINX MISR INteractive eXplorer

MISR Multi-angle Imaging Spectro-Radiometer

NASA National Aeronautics and Space Administration

NOAA National Oceanic and Atmospheric Administration

PE potential energy per unit mass

PM particulate matter

RANS Reynolds-averaged Navier–Stokes

RHS right-hand side

ROS rate of spread

RxCADRE Prescribed Fire Combustion and Atmospheric Dynamics Research Experiment

TKE turbulence kinetic energy

WFDS Wildland-Urban-Interface Fire Dynamics Simulator

WRF Weather Research and Forecasting Model

WRF-SFIRE Weather Research and Forecasting Model (WRF) combined with a semi-empirical Spread Fire model

Acknowledgments

Supervisory committee: This dissertation would not be possible without my supervisor **Roland Stull**. Roland's unwavering optimism, a firm belief that 'no challenge is too big (or too small)' and genuine enthusiasm have been a continuous source of motivation. Following his lead, I learned a tremendous amount about how to methodically untangle complex scientific ideas and even more about how to communicate them. Roland's care for the team (from uninterrupted supply of quick carbohydrates to late-night Slack consultations) and incredible passion for teaching reflect his mission of always putting students first. Most importantly, I want to thank Roland for giving me the opportunity to follow my own path, be it drifting off the team's weather prediction tracks or stepping away from research altogether to grow a family. I am deeply grateful for his support through each and every turn along the way.

Having **Douw Steyn**'s guidance for over a decade has been an incredible privilege. While Douw's formal status within my academic life has continually evolved, he has invariably remained my mentor. Never too far away to offer advice and support, he continually cultivated my scientific curiosity and has profoundly influenced my thinking as a researcher. Most of the academic opportunities and experiences I have been fortunate to enjoy, I owe to Douw's kindhearted belief in my abilities many years prior to my making a first scientific contribution.

I want to thank **Phil Austin** for being willing to be 'entrained' into my advisory committee at a later stage of the dissertation. While his formal membership is fairly recent, Phil's guidance and far-sighted scientific computing advice date back to my early years at UBC. His decade-long vision, mixed with extraordinary erudition and academic humor, turns any of his instructional talks into an indulging intellectual workout. Phil's ability to answer questions that have yet to ripen in a young researcher's head is truly fascinating.

I'd also like to thank **Neil Balmforth** for navigating me through half-century old literature on fluid dynamics fundamentals that curiously remained so topical, I revisited it at every stage of this dissertation.

Colleagues: Being a member of such a large and diverse research group has truly been a privilege. I want to thank **Rosie Howard** for her guidance on the doctoral path, her compassionate team work as well as for my newly acquired belief in human superpower. Thank you to **Chris Rodell** for his contagious enthusiasm to take on any novel challenge, openness and virtuoso ability to connect people. The support of our 'Fire Team' has been integral.

I want to sincerely thank **Julia Jiworrek** for her generous help with cluster access and **Tim Chui** for helping me (among a million other things) experiment with cloud computing. I also want to acknowledge **Greg West**, **David Siuta** and **Maggie Campbell** for their guidance on my early projects.

This work would not be possible without my **family**. I struggle to find words to express how deeply grateful I am to my parents. From my core values to any modest achievement, I owe it to their unconditional love and support. Thank you to my husband Lukasz for making sure I laugh daily and to my son Alik for redefining 'curiosity'. It truly takes a village to raise a researcher.

Chapter 1

Introduction

Wildfire smoke is a complex and dynamic pollutant. As wildfires become more frequent and intense under the changing global climate, smoke pollution is quickly emerging as one of the key issues facing air quality in the coming decades. Our ability to predict where and how smoke travels is crucial to mitigating its negative impacts for human health and the environment.

What is wildfire smoke plume rise? Intense heat above the fire creates updrafts, which simultaneously mix with and modify the ambient environment. These turbulent columns of hot air mixed with fire emissions are referred to as a plumes. The term plume rise is typically used to describe the initial buoyant phase of a smoke plume, which determines how high in the atmosphere the pollutants will travel.

Why is understanding smoke plume rise important? The ability to predict where in the atmosphere the majority of the smoke is released is key to accurately capturing subsequent pollutant dispersion. Due to vertical wind shear, small errors in plume rise predictions can have profound consequences for downwind dispersion and forecast smoke concentrations at the earth's surface. Figure 1.1 is a striking example of how sharply the wind direction can change between various levels of the atmosphere. This is why plume rise is often the pivotal point in smoke modelling process.

What are the challenges? Fundamental to understanding any physical process are good observations. Yet detailed and temporally linked 3D measurements of smoke dispersion and fire behavior are notoriously scarce. Moreover, wildfire plume dynamics involve complex nonlinear interactions and feedbacks between the fire and ambient atmosphere, which operate over a wide range of spatiotemporal scales. All these factors present a challenge for both modellers and experimentalists. This work aims to explore some of these challenges with the goal of improving our understanding of smoke plume rise dynamics.

Figure 1.1: Dalyup bushfire January 10, 2016 (Esperance, Australia) [48]

1.1 Overview of thesis

Wildfire dynamics are inherently an interdisciplinary scientific field. Hence, I begin by setting up the background for the thesis specifically in the context of air quality. Chapter 2 briefly summarizes the current state of knowledge and introduces smoke modelling frameworks (Section 2.1), plume rise parameterizations used within these systems (Section 2.2) and data sources available for their evaluation (Section 2.3). I discuss why coupled fire-atmosphere numerical models are gaining attention (Section 2.4) and outline the path forward for this thesis (Section 2.5).

The next part of the thesis focuses on a numerical modelling tool key to this work: the Weather Research and Forecasting Model (WRF) combined with a semi-empirical Spread Fire model (WRF-SFIRE). Chapter 3 summarizes my effort in evaluating the model, while Chapter 4 provides details of how I use WRF-SFIRE to generate surrogate smoke plume data. This "synthetic" dataset is explored in Chapter 5, to gain insights into how the fire interacts with the atmosphere (Section 5.1), breaks into multiple rotating cores (Section 5.2 - Section 5.4) and entrains ambient environmental air (Section 5.5).

In the remaining part of the thesis I step away from numerics and attempt to translate the knowledge gained from the simulations into a simple analytical method for predicting plume rise. Chapter 6 describes an energy-balance approach for estimating mean injection height of a smoke plume for a fire of arbitrary shape and intensity. I constrain and evaluate the proposed method with both numerical and observational data (Section 6.1 - Section 6.2), and demonstrate that there exists a linear dimensionless relationship between updraft velocity and plume vertical penetration distance (Section 6.3). Chapter 7 builds on this energy-balance approach, extending the method to parameterize the full vertical distribution of smoke in the atmosphere.

I conclude with a brief summary of key contributions of this thesis.

1.2 Purpose

My doctoral studies spanned some of the most devastating wildfire events both close to home (e.g. Fort McMurray Fire of 2016) and globally (e.g. Australian "Black Summer" and California wildfires of 2020). It is no coincidence, that the wildfire smoke modelling community has grown immensely in just the last few years. Yet the complex nature of wildfires makes for a uniquely interdisciplinary challenge to the scientific community. Current state of knowledge is a product of collaborative effort between atmospheric physicists, chemists, fire scientists, forestry and remote sensing experts, among many others.

This thesis is written with air quality researchers in mind. Each chapter concludes with a brief summary outlining its main purpose and/or contributions from a perspective of an atmospheric modeller. Yet many challenges and limitations of this work lay at the interface of multiple disciplines. For this reason, I added a "Big Picture" section at the end of each chapter. I hope this will help provide context, grasp the range of scales and perspectives involved and establish a common ground with researchers in other disciplines working to better our understanding of wildfire dynamics.

Chapter 2

Background: wildfire smoke in the atmosphere

Wildland fires are a fundamental global feature of the Earth system [5]. They cover a broad range of spatiotemporal scales and are shaped by the complex interactions of fuel, terrain, and meteorological conditions. Intense heat released during a wildland fire initiates convection, creating a rising smoke plume. This vertical transport of byproducts of combustion, including aerosols and trace gases, combined with complex dynamical feedbacks between the fire and ambient meteorological conditions, set wildfire smoke aside from other atmospheric pollutants [56].

Fire emissions can be injected far above the atmospheric boundary layer (ABL), making them susceptible to long-range transport. Such penetrative smoke plumes (i.e. plumes rising above the ABL), have far-reaching effects for chemical composition of the atmosphere, weather and climate. Plumes confined to the ABL, on the other hand, have direct impact on air quality on a local scale [38]. Between these extremes are plumes that penetrate, but remain near the ABL, in the region often associated with strong vertical windshear [70]. In some cases, a significant portion of the smoke associated with such plumes remains trapped in the ABL. Our ability to predict subsequent dispersion of pollutants and their impact, is hence, extremely sensitive to the dynamics of the initial buoyant phase of the smoke plume. Yet our understanding of plume rise has been limited due to both the complex nature of the phenomenon as well as challenges in obtaining detailed observations of smoke plumes.

In this chapter, I summarize our current state of knowledge of smoke plume rise dynamics. The first section sets the stage for examining plume rise in the context of air quality, highlighting the importance of smoke modelling and it's implications for human health and the environment (Section 2.1). Next, Section 2.2 provides a brief overview of existing plume-rise parameterizations and discusses their implementation within smoke modelling frameworks, noting the strengths and limitations of each approach. Section 2.3 summarizes common data sources used for creating, evaluating and constraining the above parameterizations, highlighting the gaps in the available observational data. The following Section 2.4 then takes a numerical perspective on studying plume rise dynamics, reviewing existing tools as well as modelling experiments. The last portion of the chapter (Section 2.5) synthesizes the knowledge gaps and charts the forward path for this thesis.

2.1 Context: air quality and smoke modelling frameworks

Wildfire emissions contain a wide range of pollutants, widely recognized as a hazard for human health, including carbon monoxide (CO), nitrogen dioxide, ozone, particulate matter (PM), polycyclic aromatic hydrocarbons, and volatile organic compounds and many others [29, 63]. Epidemiologists have repeatedly linked smoke exposure to respiratory morbidity, as well as overall increased mortality from all causes [23, 30, 47].

The ability of smoke dispersion models to make timely and accurate predictions of the development, spread and intensity of smoke events is central to successful mitigation of negative impacts for communities downwind. Typically, decision makers in a wide range of sectors, including health (public advisories and evacuations), transportation (safety), tourism (nuisance), weather forecasters (public advisories), wildfire response (downwind effects), and the public (health, nuisance), rely on smoke modelling frameworks to forecast surface pollutant concentrations from wildfires.

In North America several numerical air quality forecasting systems exist, which aim to capture emissions from wildfires. These include the BlueSky Framework operated by the US Forestry Service [39] and its Canadian version (BlueSky Canada, Figure 2.1) operated by the University of British Columbia [66], High-Resolution Rapid Refresh-Smoke system from the US National Oceanic and Atmospheric Administration [2], WRF coupled with Community Multiscale Air Quality model (WRF-CMAQ) used by the US National Weather Service [40], AIRPACT system operated by Washington State University [76] and the FireWork framework developed by Environment and Climate Change Canada [9]. While these systems differ in their approach, they typically share key components summarized in Figure 2.2.

Satellite and ground observations of "hot spots" are used to identify wildfire locations and sizes. This information is combined with fuel data to model emissions produced by combustion. Using meteorology from numerical weather forecasts, the vertical distribution of these emissions in the atmosphere is parameterized. From

Figure 2.1: Surface $PM_{2.5}$ forecast produced by BlueSky Canada smoke modelling framework.

there smoke dispersion is simulated (through either directly coupling chemistry with the numerical weather model or carrying out trajectory analysis). Typically, the output of such smoke modelling frameworks includes surface smoke concentrations (Figure 2.1) or column-integrated values, which can be compared with surface pollution observations or satellite data, respectively.

Traditionally, many operational smoke modelling frameworks relied on plume rise equations originally developed by Briggs [6] for industrial smokestacks [39, 57] to predict the vertical distribution of emissions in the atmosphere. Yet several studies suggest that this approach may not be appropriate for wildfires [20, 22, 57, 62]. Never-the-less, the Briggs plume rise scheme remains widely used today, hosted within well-established air quality and dispersion models such as HYSPLIT, CMAQ, and in the operational versions of BlueSky and FireWork, while often being recognized as a weak link within these systems [9, 74]. As a result, plume rise parameterization development remains an active area of research.

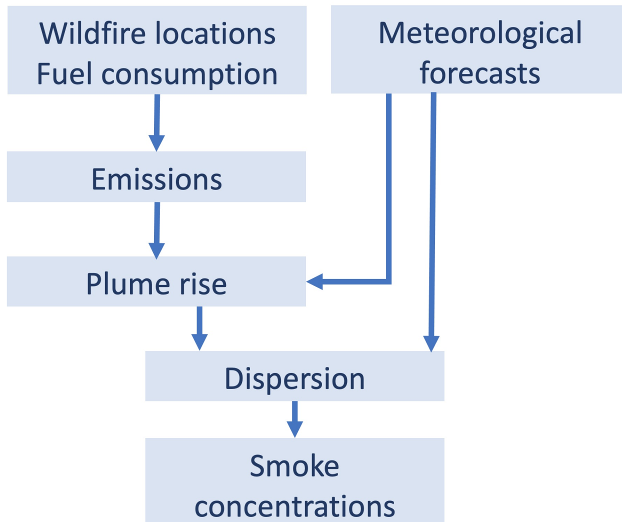

Figure 2.2: Simple schematic showing a typical structure of a smoke modelling framework. Figure produced by Chris Rodell for internal report.

2.2 Overview of existing parameterizations

Existing smoke plume prediction models span a vast range of complexity from simple empirical relations to the more recent coupled fire-atmosphere numerical approaches. Often the choice of model is dictated by the context of its application, subject to the trade-off between fidelity and timely execution. Typically, full-physics models, while being able to resolve the complexity of wildfire plumes, are too slow or computationally intensive to be used operationally [1]. Hence, simplified parameterizations are needed to make plume rise data available in a timely manner for large modelling domains with multiple active emission sources.

For clarity, from hereon I'll refer to numerical models used for forecasting meteorology (e.g. WRF) and creating highly-detailed simulations of the atmosphere (e.g. large-eddy simulations (LES)) as **models**. Simplified plume rise formulations typically hosted within air quality modelling systems will be referred to as **parameterizations**. The distinction is vital, as the goal of this thesis is to develop a plume rise parameterization with the help of a numerical model.

In a recent review of existing plume rise parameterizations, Paugam et al. [56] highlight three notable schemes that stand out in literature, as that of Freitas et al. [20], Sofiev et al. [69] and Rio et al. [64]. Both Freitas and Rio's methods use first principles to characterize plume temperature, vertical velocity and entrainment. While the former provides prognostic 1-D equations that can be solved as a stand-alone "offline" model, the latter is implemented as a sub-grid effect within a host chemistry transport model. Notably, both consider an idealized heat source to represent the fire. While subject to additional complexity and computational cost, the prognostic nature of these schemes offers an advantage over purely empirical or statistical methods under rapidly changing meteorological conditions. Another strength of these parameterizations, which is particularly important for global chemical transport modelling applications, is the inclusion of latent heat effects. Extreme pyroconvective plumes (classified as "flammagenitus" [52]) can gain additional buoyancy from energy released due to condensation [58]. While such events are not common [74], they can have a significant impact for atmospheric circulation on a global scale.

Sofiev's semi-empirical approach relies on energy balance and dimensional analysis [69], while using satellite data to both initialize and constrain the parameterization. The convenience of the method lies in the fact that it only relies on three input parameters (ABL height, Brunt-Vaïsälä frequency of the free troposphere and fire radiative power (FRP)) to obtain a smoke injection height estimate. The main limitation of the scheme, as expressed by Paugam et al. [56], is the exclusion of condensation and cloud formation from the scheme.

Another thermodynamics-based scheme was recently introduced within the experimental version of FireWork model [9]. The approach is based on a method developed by Anderson et al. [4], which aims to quantify the energy release of the fire and uses environmental and dry adiabatic lapse rates to estimate the vertical distribution of smoke.

Unlike Briggs's equations, all of the above models address wildfire plumes specifically, yet much research is needed to reduce the large prediction uncertainties [42]. Moreover, it is unclear, whether unreliable predictions should be attributed to the fire input parameters or the plume rise scheme itself. One of the central challenges in plume rise parameterization development has been the scarcity of comprehensive model evaluation data [15, 54]. Key sources of observational data and their corresponding limitations are summarized in the following section.

2.3 Sources of evaluation data

One of the challenges in obtaining a comprehensive dataset for evaluation of smoke plume-rise schemes is the fact that wildfires operate on a broad range of spatial and temporal scales. Fuel combustion, which is affected by the size, density and chemical properties of individual fuel elements as well as ambient environmental conditions, operates on micro- and local- scales. Smoke dispersion, on the other hand, can range from local to global scales, affected by both thermodynamics of the plume and meteorology.

To date, information on wildfire smoke emissions and dispersion has largely been derived from two distinct sources: remotely sensed data and prescribed burn campaigns. The "gold standard" for satellite plume observations has been the Multi-angle Imaging Spectro-Radiometer (MISR) instrument on board the Terra satellite [31]. The vertical distribution of aerosols can be reconstructed from MISR images with a stereoscopic altitude retrieval algorithm with roughly 500 m accuracy, typically aided by the MISR INteractive eXplorer (MINX) software tool [51]. MISR data has allowed for the development of plume "climatologies" over various global regions. Based on such comprehensive efforts [31, 73, 75], we know that only a small portion of wildfire smoke plumes are injected above the ABL (4-12%), and vast majority of plumes that do reach the free troposphere (83%) remain in the stable layers just above the ABL. A major drawback of using MISR data is that there is no way to differentiate clouds from smoke or dust. Also, the satellite overpass times are limited to morning hours, when wildfires are weakest and when the plumes have not fully matured [56, 75].

Smoke plume heights can also be obtained from the Cloud-Aerosol Lidar with Orthogonal Polarization (CALIOP), operated on board the CALIPSO satellite. With much better spatial (120 m in the vertical) and temporal resolution, daytime overpasses and ability to differentiate aerosols it offers several advantages over MISR. However, due to extremely narrow swath width (and, hence, infrequent overpasses) most of the plumes are not captured by CALIOP [31]. Apart from specific limitations of individual sensors and satellites, a common problem with remotely sensed data is obstruction by clouds and overall lack of direct spatiotemporal links to fire behavior [27]. As a result, until recently, evaluation of smoke plume models required a combination of studies, as no dataset was complete enough to rigorously constrain the problem [15].

To address this critical need for a comprehensive model evaluation dataset several field campaigns have taken place in recent years, ranging in scope and scale. FireFlux experiments I and II [10, 12] focused on micrometeorology and fire-atmosphere interactions. The main goal was to provide detailed measurements for evaluating fire behavior tools and next-generation physics-based fire models.

A collaborative effort between National Oceanic and Atmospheric Administration (NOAA) and National Aeronautics and Space Administration (NASA) called Fire Influence on Regional to Global Environments and Air Quality (FIREX-AQ) was designed with

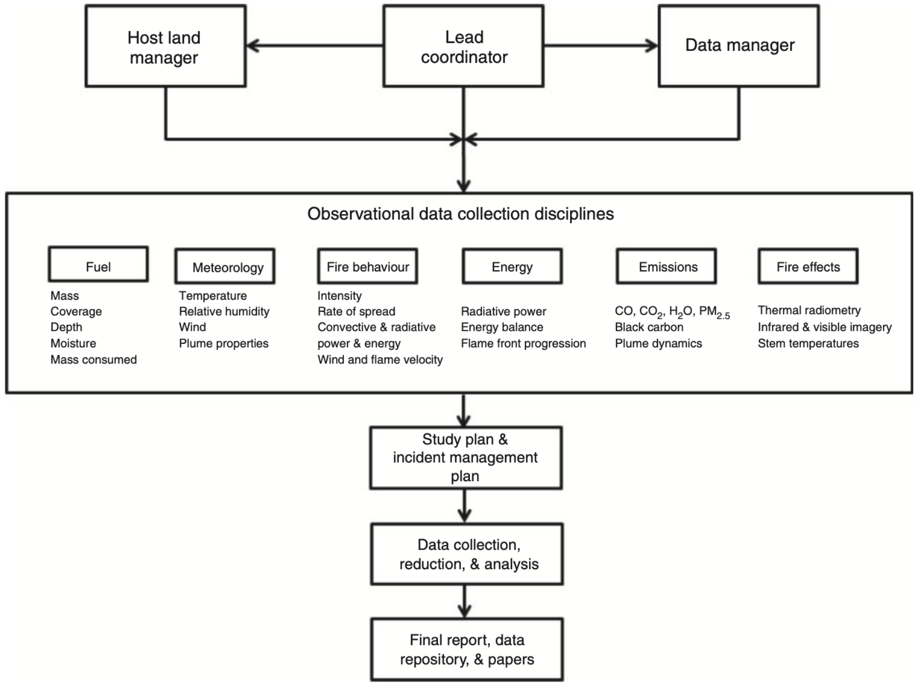

Figure 2.3: Process diagram for RxCADRE project, including a partial list of measured variables (figure extracted from [54]).

a focus on emissions and chemistry [65]. The campaign included a strong airborne component, allowing to track plumes downwind to assess chemical transformations and air quality impacts, but failed to provide any fire characterization data critical from the standpoint of plume-rise modelling.

One of the most diverse comprehensive campaigns to date has been the Prescribed Fire Combustion and Atmospheric Dynamics Research Experiment (RxCADRE) [54]. The project brought together researchers from a wide range of disciplines to collect data on fuel, meteorology, fire behavior, energy, smoke emissions and fire effects. Experimental burns captured by this campaign required extensive planning, management and coordination, but produced a well-integrated dataset spanning a wide range of measurement techniques, as illustrated in Figure 2.3. Another important aspect of RxCADRE dataset is that it captures a range of spatiotemporal scales most relevant to evaluation of coupled fire-atmosphere numerical models (Figure 2.4).

Due to success of RxCADRE an even more extensive and complex Fire and Smoke Model Evaluation Experiment (FASMEE) is currently underway [61]. While still in early stages, the campaign is focused on large wildfires and aims to provide detailed mutli-

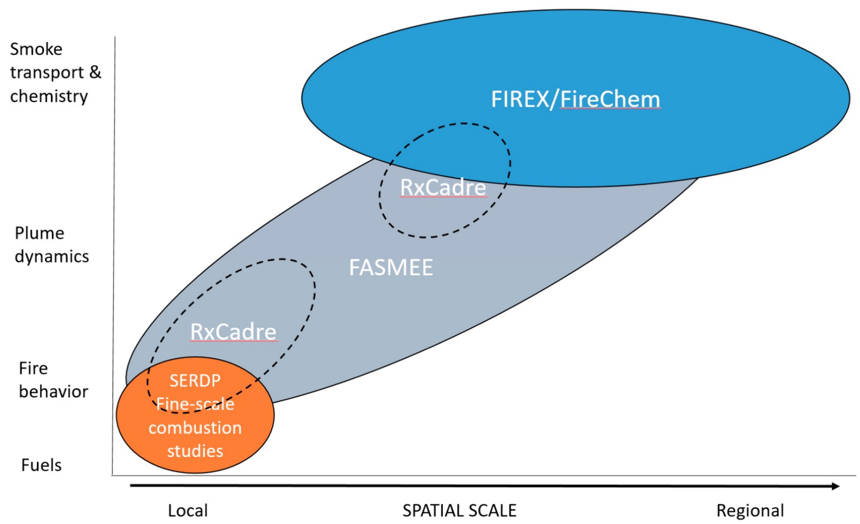

Figure 2.4: Conceptual diagram of spatial scales captured by various field campaigns (figure extracted from [61]).

scale observations ranging from local to regional scale (Figure 2.4).

While comprehensive field experiments summarized above provide the necessary level of detail for model evaluation studies, they typically capture a modest range of fire and atmospheric conditions. Given the required coordinated effort (as shown in Figure 2.3) and high costs of such campaigns, the use of "synthetic" numerical experiment "data" produced by coupled fire-atmosphere models has been gaining attention, as described in the following section.

2.4 Related work on numerical studies of plume dynamics

Rapid increase in computational power in the recent years has aided the development of complex physics-based numerical models, that allow fire-atmosphere coupling. Several such models exist today, covering a range of scales and various levels of idealization of the modelled fire and atmosphere.

Wildland-Urban-Interface Fire Dynamics Simulator (WFDS) [49] and FIRETEC [41] explicitly resolve combustion and, hence, require very fine model grid (on the order of meters). The advantage is that fire behavior is captured without the use of simplifying parameterizations. High computational demand of such systems, however, typically limits the size of modelled domains to less than 1 km^2 [61].

In contrast, WRF-SFIRE [45, 46], MesoNH-ForeFire [18], and Coupled Atmosphere

Wildland Fire-Environment (CAWFE) [14] have a strong focus on the atmosphere. Fire behavior is parameterized allowing faster run time and larger scale simulations than those performed with WFDS and FIRETEC [61]. Plume dynamics, however, are resolved to the level of detail which can hardly be matched by even the most extensive observational campaign. This is typically made possible by the use of large-eddy simulations (LES): a computational fluid dynamics method that explicitly resolves turbulent atmospheric motion, while only parameterizing small-scale eddies. It is, therefore, critical to confirm whether the output of such models is physically realistic.

Overall, WRF-SFIRE has been one of the most actively developed models. Several studies have examined its ability to capture the ground-spread behavior of a fire line, near-surface temperatures and winds [34, 35]. Large-scale simulations of two real fires were carried out [36], comparing modelled plume tops with satellite data. Notably, WRF-SFIRE was recently used to capture radiative feedbacks between the smoke and the atmosphere [37] in a first study of its kind. Current developmental work includes the addition of canopy parameterization, which accounts for the effects of modified wind profile over forested land types [44]. Promising results of the above modelling studies, as well as the presence of an active development community, were key in selecting WRF-SFIRE as the central tool for this thesis.

While a growing number of evaluation studies of coupled fire-atmosphere models are encouraging, there remains a general lack of research focusing on the vertical distribution of smoke emissions in the atmosphere [42]. This knowledge gap can, in part, be explained by the difficulty of constraining potential sources of error in both inputs and the model itself.

2.5 Knowledge gaps and research questions

While, at first, modelling plume rise may appear to be purely an atmospheric dynamics exercise, the subject is truly interdisciplinary in nature. Many aspects of plume rise modelling lie at the interface of atmospheric physics, fire behavior science, numerical methods, air quality, meteorology and remote sensing. This section aims to recap what we know from each field and to identify the existing gaps in our knowledge, while putting together a road map for the thesis.

What are the challenges in modelling wildfire smoke? Smoke is a harmful pollutant. Understanding its movement in the atmosphere (and being able to predict it) is crucial to mitigating negative air quality impacts. A weak link in our effort to model smoke pollution is plume rise dynamics. Remotely sensed data suggests that vast majority of the plumes remain in or near the ABL [73]. However, the ability to determine which plumes will remain in the ABL vs. penetrate it and reach the free troposphere is critical for accurate downwind smoke predictions [69]. In addition, the penetration distance within the free troposphere can matter significantly due to vertical wind shear [75].

Complex combustion-resolving models are too slow and computationally intensive to be useful for operational air quality applications. That is why smoke modelling frameworks typically rely on simplified parameterizations to predict smoke injection height. Such parameterizations remain subject to large errors, due to the complex nature of the processes involved, uncertainties associated with fire behavior and the limited observational data available.

How can we address these challenges? Comprehensive model evaluation data on wildfire smoke plume rise is extremely scarce. Recent developments in coupled fire-atmosphere models offer an opportunity to examine plume rise from a numerical perspective. This approach, however, still needs to be evaluated. This dissertation aims to make a contribution at the interface of numerical and analytical modelling, guided by the following broad research questions:

- **Can a coupled fire-atmosphere numerical model accurately simulate smoke plume rise from a real fire?**

  The focus of Chapter 3 is to provide a "proof of concept" for using WRF-SFIRE to simulate plume dynamics, using a real-life case study from the RxCADRE campaign. Based on the results of this model evaluation, Chapter 4 introduces a synthetic plume dataset, capturing a wide range of fire and atmospheric conditions.

- **What can we learn about the behavior of the atmosphere around the fire from numerical experiments?**

  Chapter 5 examines the effects of various fire parameters and environmental conditions on modelled plume rise using the simulations described in Chapter 4.

- **Can synthetic data be used to parameterize smoke plume rise for air quality applications?**

  Based on insights gained from the numerical experiments, Chapter 6 introduces a simple energy-balance plume rise parameterization to estimate the mean smoke injection height for penetrative plumes. Chapter 7 then extends this approach to predict the full vertical distribution of smoke in the atmosphere. Lastly, Chapter 8 summarizes the main contributions of this thesis.

While the broad research topics above highlight the overarching goals of this work, each chapter will introduce more specific questions to help focus and guide this investingation.

Chapter 3

Proof of concept: Capturing plume rise and dispersion with a large-eddy simulation

Plume rise is a result of a complex set of physical phenomena, spanning multiple spatiotemporal scales. Until recently comprehensive integrated datasets, combining measurements of fire behavior, meteorology and smoke dispersion were not available [61]. Hence, evaluation studies of coupled fire-atmospheric models focusing on plume rise are scarce [42].

RxCADRE, a recent mutli-scale prescribed burn campaign designed to address this need [54], provides a rare opportunity to examine the ability of a coupled fire-atmosphere model (WRF-SFIRE) to capture smoke plume dynamics. In this chapter, I hope to provide a "proof of concept" for using WRF-SFIRE simulations as a surrogate for real-life observational data.

Note that the main focus of this chapter is the evaluation of the model's ability to capture the atmospheric response to a simulated fire of known bulk properties, rather than the fire behavior itself. Effectively, the work aims to validate the relationship between the simulated surface forcing due to a fire and the resultant turbulent convection.

3.1 Methods

3.1.1 Observational data

The RxCADRE campaign consisted of 10 operational and 6 small replicate prescribed fires in Florida. Collected data are accessible via a US Forest Service online repository, as referenced below. Smoke dispersion and emissions measurements are available for three large fires: L1G and L2G grass fires and L2F sub-forest canopy surface fire.

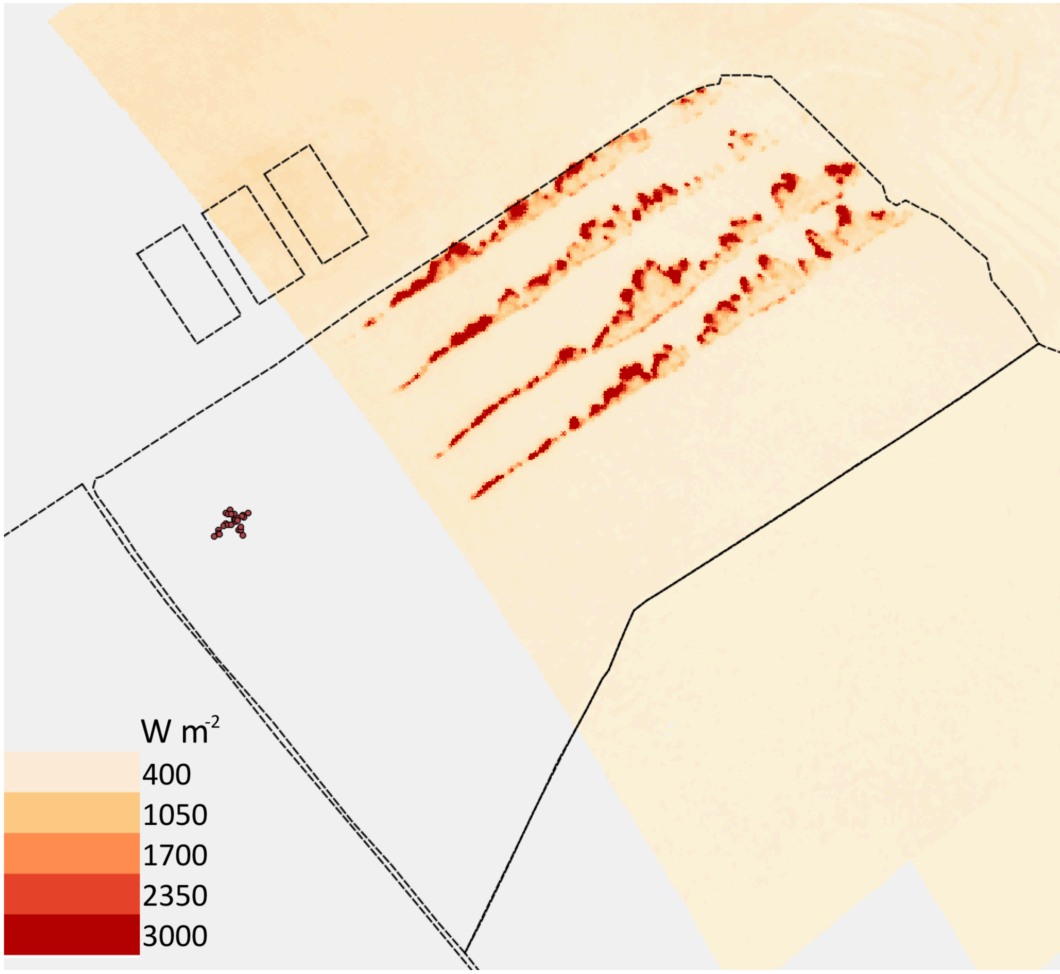

Figure 3.1: Long Wave Infrared (LWIR) image of L2G plot during ignition (12:32:02 CST) with dashed black lines denoting burn perimeters. Red scatter points correspond to Highly Instrumented Plot (HIP) #1 fire behavior package (FBP), each containing a system of airflow, temperature and energy sensors. Data source: RxCADRE field experiment [24–26].

For the purpose of model evaluation, I selected L2G (10 November 2012) grassland fire as a case study, based on its reported uniformity and consistency of flame propagation [7]. Figure 3.1 shows a sample snapshot of the burn plot during the ignition. The overall meteorological conditions and instrumental design of the L2G experimental burn are described in detail in Clements et al. [11]. The individual datasets obtained from the US Forest Service online archive used for this study are summarized below.

Georeferencing data, including plot location and burn perimeters, are available from Hudak and Bright [25]. Analysis of fire rate of spread (ROS) and intensity as well as a detailed description of three Highly Instrumented Plots (HIPs) used to produce the estimates can be found in Butler et al. [7]. Locations of HIPs are available from Hudak et al. [24]. HIP1, used for this evaluation, is shown in Figure 3.1. Near-surface wind and temperature sonic anemometer time series for in-situ and background locations are available from Seto and Clements [67, 68]. Ignitions timing and locations were obtained from field-grade GPS units, mounted on-board firing vehicles [26]. Fuel data used for this evaluation study included photographs of pre-burn samples, as well as measurements of size, loading and moisture content of species groups. Data collection methodology is detailed in [53]. Dispersion and emissions measurements included volume-mixing ratio of CO_2, CO, CH_4, and water vapor at a rate of 0.5 Hz, obtained from aircraft-mounted sensors [72]. The georeferenced data consisted of horizontal transects at multiple elevations, as well as "corkscrew" and "parking garage" flight profiles.

3.1.2 Numerical configuration

I configured WRF-SFIRE [45, 46] in idealized LES mode. One of the primary advantages of using this model is that it allows for two-way coupling between fire and the atmosphere. While WRF-SFIRE does not model combustion directly, the spread and intensity of the fire are parameterized using a semi-empirical approach. The latent heat flux is computed based on the fuel consumption and stoichiometric combustion of cellulose. Heat and moisture fluxes from the simulated burn provide forcing to the atmosphere, which in turn influences fire behavior.

A 10.4 km $\times$ 14 km domain with 40 m horizontal grid spacing, 3000 m model top and 51 hyperbolically stretched vertical levels was initialized using the 10:00 CST (16:00 UTC) sounding [11]. While this may appear to be a shallow domain compared to mesoscale ("Real") WRF simulations, such model top is substantially higher than that found in several existing published WRF-SFIRE evaluation studies [15, 32, 35]. Five lowest model grid centers were located at approximately 8 m, 24 m, 42 m, 60 m and 80 m above ground level (AGL). I allowed the simulation to spin up the ambient background flow for 2 h 23 min prior to ignition at $\sim$12:23 CST (time varied slightly for different firelines). To aid the formation of buoyancy-driven ambient background turbulence typical for a daytime ABL, I imposed a lower-boundary surface thermal flux (tke_heat_flux). The value was estimated from the sonic anemometer time series of vertical wind velocity and temperature over the time period leading up to ignition. As shown in Figure 3.2, based on the measurements, the ambient background surface heat flux remained fairly constant over the entire spin-up period. Hence, the lower-

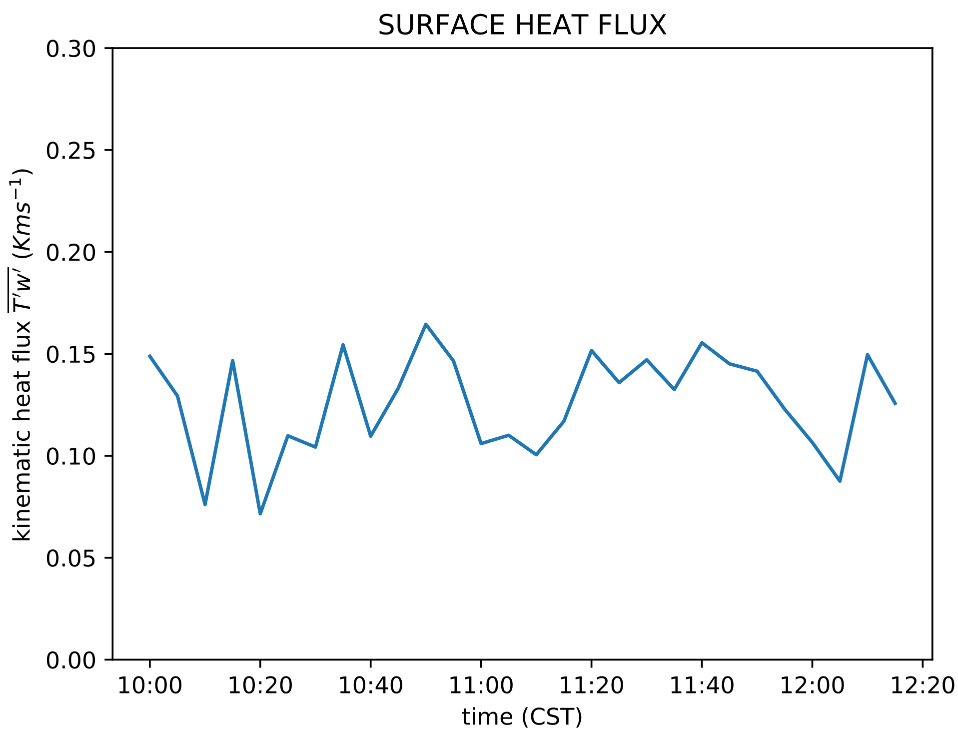

Figure 3.2: Five-minute averaged kinematic surface heat flux $\overline{T'w'}$ derived from 1 Hz wind and temperature sonic anemometer time series of the background ambient environment. Data source: RxCADRE field experiment [68].

.

boundary surface forcing was idealized for the LES simulation as being uniform in space and constant in time. I used full surface initialization (sfc_full_init =.true.), with the lower boundary moisture flux and surface roughness characteristics set to standard USGS values for "Grassland" land use category.

To help trigger the ambient background convection in a horizontally uniform initial domain, I added a small temperature perturbation "bubble". With periodic boundary conditions, near-stationary turbulence spectrum was achieved within $\sim$40 min of run start. The well-mixed modeled ABL continued to turn over and warm for a total of 2 h 23 min (10:00:00 CST–12:23:00 CST). I used the restart file generated at 12:23:00 CST as initial conditions for the main burn simulation (12:23:00 CST–13:12:00 CST), ensuring the fire was ignited into a well developed convective ABL. Other key configuration details can be found in Table 3.1, as well as in the complete namelist initialization files in published supplementary material [50].

Table 3.1: Key parameters of numerical domain setup.

Simulation Parameter	Value/Description
Model version	24 May 2019 (git #ced5955)
Horizontal grid spacing	40 m
Domain size	260 grids (east-west) $\times$ 350 grids (north-south)
Time step	0.1 s
Model top	3000 m AGL
Spinup timing	10:00:00–12:23:00 CST (CST = UTC $-$ 6 h)
Fire (restart) simulation timing	12:23:00–13:12:00 CST
Sub-grid scale closure	1.5 turbulence kinetic energy (TKE)
Lateral boundary conditions	periodic
Surface physics	Monin–Obukhov similarity (sf_sfclay_physics = 1)
Land surface model	thermal diffusion (sf_surface_physics = 1)
Ambient surface heat flux	160 W m^{-2} (tke_heat_flux = 0.13)

Following the LES spin up, I ignited the northwestern half of the simulated L2G plot with four roughly parallel fire lines mimicking strip head fire method used during the real-life burn (Figure 3.1). During the campaign, the prescribed burn was ignited with drip torches attached to moving all-terrain vehicles (ATVs). Using GPS data from these vehicles (available from [26]), I extracted the locations of start and end points of the four firelines, as well as their individual start and end ignition times. While the real-life ignition process was not perfectly uniform in time, I approximated the modeled fire lines as being ignited at a constant speed, such that the time and location of the start and end points matched those of the real burn (see published supplementary material [50]). Timing varied slightly for each of the four modeled firelines. I approximated the ignitions as straight lines between observed start and end points, as the ATVs' deflections from a straight path during the real burn remained within a single atmospheric grid in my modeled domain.

Ignited cells in WRF-SFIRE proceeded to spread, while each fire line continued to advance until reaching the opposite end of the L2G plot. I excluded subsequent upwind ignitions of the remaining plot area to reduce the computational load of the simulation. Taking into account the downwind location and timing of smoke plume observations, this simplification should have no effect on the proposed evaluation. The simulation was allowed to proceed for 49 min, until the emissions reached the downwind end of the domain.

Summary of fire and fuel parameters can be found in Table 3.2. Based on photographs and average measurements of fuel size, composition and type, I determined

Table 3.2: Details of fire and ignition parameters in LES setup.

Simulation parameter	**Value**
Fire mesh refinement	10
Ignition duration	12:23–12:36 CST (varied for each fireline)
Rate of spread during ignition	0.2 m s^{-1}
Fuel category	1 (short grass)
Surface dead fuel moisture	8.46%
Heat of combustion of dry fuel	1.64×10^7 J kg^{-1}

Anderson's fuel Category 1 (short grass) [3] to be the best fit for L2G ground cover. Actual burn perimeters were used to mask the remaining domain as containing no fuel to prevent spread of the simulated burn outside of the burn plot. I replaced the standard fuel loading and depth associated with Type 1 fuels with average measured values of 0.267 kg m^{-2} and 0.18 m, respectively. Surface dead fuel moisture content was set to 8.46% based on observations. I adjusted the heat of combustion of dry fuel to 16.4×10^6 J kg^{-1} as per estimates for grasslands [55].

As the central goal of this work is to evaluate the model's ability to capture wildfire smoke plume dynamics, I did not incorporate chemistry coupling into the simulation. Modeled "smoke plume" was represented by two passive tracers released proportionally to the mass and type of fuel burned. The rate of release for each tracer representing CO and CO_2 was controlled by assigned emission factors, based on values for grasslands provided by Prichard et al. [60].

3.2 Results

The overall evolution of the simulated L2G burn and the associated smoke plume is best visualized with a 3D animation (see Animation S1 in published supplementary material [50]). Figure 3.3 shows a still image of the simulated smoke plume at the end of the animation. The supplement [50] also includes an animated view of the cross-wind modeled CO_2 mixing ratio (Animation S2). The latter demonstrates the ability of the LES to capture typical plume behavior. As seen in the animation, the initial rise of moist buoyant air results in a temporary overshoot of the equilibrium plume height, followed by the gradual settling of the plume to its final injection height near the top of the ABL (1060 m at the end of LES spinup) for this case. While the ability of WRF-SFIRE to qualitatively capture typical plume dynamics is reassuring, the following sections take a more quantitative approach to model evaluation.

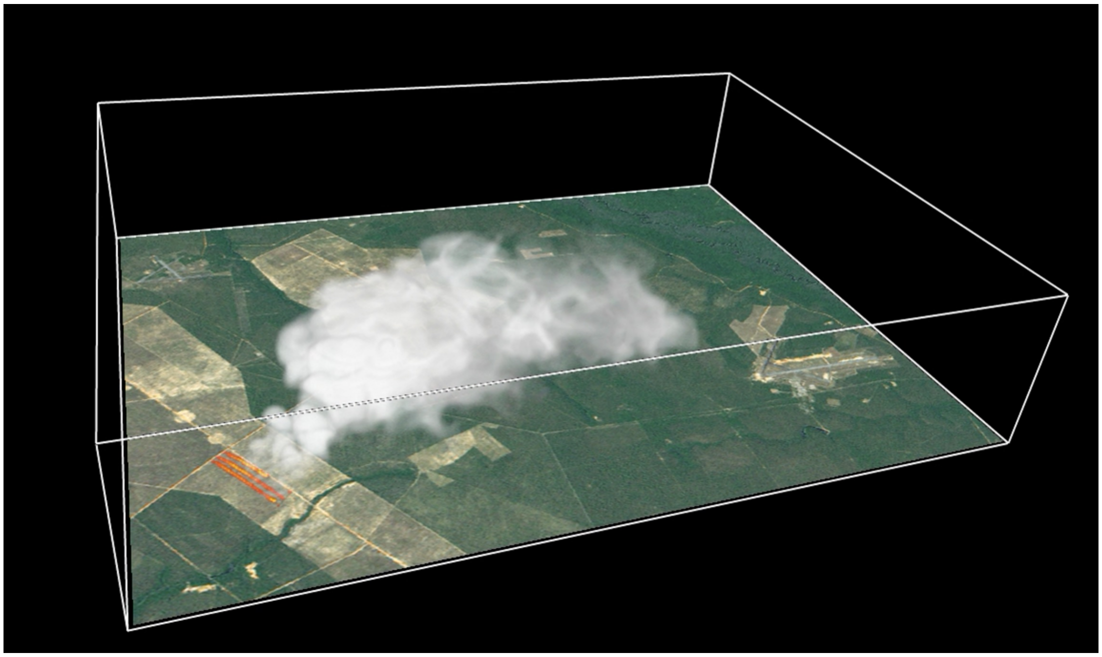

Figure 3.3: WRF-SFIRE simulation of L2G burn. Modelled fire and smoke are superimposed on surface satellite imagery for reference. Figure produced using VAPOR software [13].

3.2.1 Fire behavior

Prior to evaluating the ability of WRF-SFIRE to capture plume rise and dispersion, it is important to ensure that the model is able to simulate fire behavior with reasonable accuracy. Initial surface and fuel conditions have the potential to strongly impact fire growth and intensity, and, hence, affect the location and buoyancy of the smoke plume. This approach does not constitute a comprehensive fire behavior evaluation study, but rather aims to ensure that WRF-SFIRE captures the bulk properties of combustion and supplies a reasonable surface forcing to the simulated atmosphere.

My evaluation is based on the analysis of fire energy transport of RxCADRE observational data for L2G burn carried out by Butler et al. [7]. The study provides measurement-based values as well as error margins for ROS, and peak and average heat fluxes of the fire, which I use to assess the performance of the semi-empirical fire algorithm driving the LES simulation.

Figure 3.4a,b compares LES-derived average and peak total heat fluxes for HIP1 and entire burn area over the flaming period with observations. For HIP1 point-to-point comparison, I use output from the nearest modelled grid points. L2G average observed values include measurements from all three HIP lots. The corresponding simulated estimates are calculated using the entire burn area (roughly half of the L2G plot).

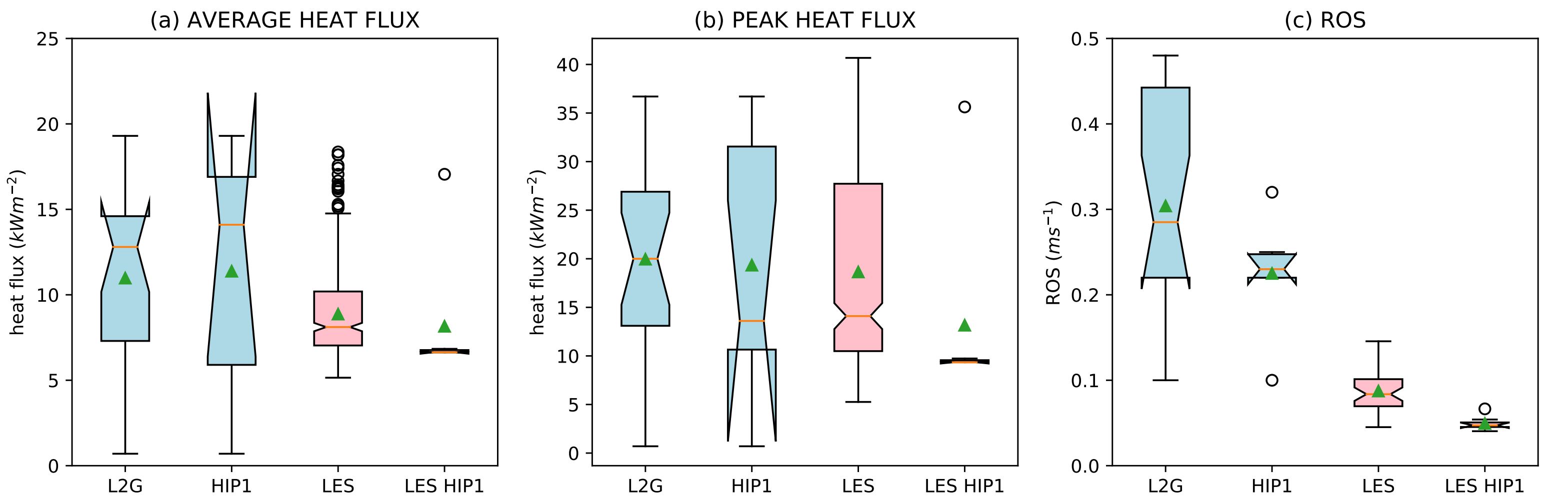

Figure 3.4: Comparison of observed (blue) and modeled (red) fire behavior. The box and whiskers span interquartile range (IQR) and 1.5 $\times$ IQR, respectively, with the notch denoting the 95% confidence interval of the median (median $\pm 1.57 \times$ IQR/n$^{\frac{1}{2}}$). Red line and green triangle correspond to median and mean, respectively. (**a**) Average heat flux during flaming period. (**b**) Peak fire heat flux during flaming period. (**c**) Rate of spread.

The start and end times of the flaming period are defined as simulation frames at which total heat flux at the location exceeded 5 kW m^{-2} [7]. For both burn-wide and point comparisons, the flaming period is determined separately for each individual grid point. Only ignited grids are included in the analysis. This approach allows me to mimic the analysis performed by Butler et al. [7] in the absence of true combustion modeling in WRF-SFIRE.

For the entire burn area the observed mean and peak heat fluxes associated with the fire (not the background environment) are 11 kW m^{-2} and 20 kW m^{-2}, compared to LES-derived values of 8.9 kW m^{-2} and 19 kW m^{-2}, respectively. For HIP1 lot the corresponding values were 11.4 kW m^{-2} and 19.4 kW m^{-2} (observed) versus 8.2 kW m^{-2} and 13 kW m^{-2} (modeled). Note that, due to close proximity of the HIP1 sensors to each other, four out of seven of them fall into the same atmospheric grid within the modeled domain. Modeled HIP1 averages should therefore be treated with caution, as they consist of only four unique values. Moreover, the large spread of observed HIP1 heat fluxes renders the differences between model and measurements not statistically significant. Overall, the results shown in Figure 3.4 suggest that on average the surface thermal forcing to the modeled atmosphere due to the fire is reasonably captured by the model, subject to a slight negative bias (significant and non-significant for average and peak heat fluxes, respectively).

Observed rates of spread during the L2G burn were estimated using two methods in the study by Butler et al. [7]: flame arrival time from ignition and video images. The former approach takes into account the ignition time of the nearest fire line (perpendicular to fire advance vector) and the distance to the individual HIP1 sensors. The resultant values appear to have lower associated uncertainty than the latter image-derived method. To ensure consistency, I mimicked the above methodology in my simulated domain. Using the high-resolution fire domain, I calculated the upwind distance between each HIP1 point and the ignition line and the time it took the flame to reach each sensor location. To estimate ROS for the entire burn area, I created a mid-fire cross-section of 50 point-pairs between second and third ignition lines. Similar to the approach above, I derived the distance and flame travel time for each pair to calculate ROS. As shown in Figure 3.4c, mean LES-based HIP1 and L2G ROS values of 0.049 m s^{-1} and 0.087 m s^{-1} are significantly lower then the corresponding observed rates of spread (0.23 m s^{-1} and 0.30 m s^{-1}, respectively). Possible implications and sensitivity of my results to this deficiency are addressed in Section 3.3.

3.2.2 Plume dynamics

Airborne emissions data collected during RxCADRE campaign is central to my evaluation of WRF-SFIRE's ability to capture plume rise and dispersion. The emissions dataset [72] contains smoke plume entry and exit points along the flight path, which were calculated using background CO baseline concentrations. The measurements were taken along horizontal transects passing through the plume at various vertical levels ("parking garage" profile), beginning close to the ground and moving towards the top of the plume, for a total of 9 crossings.

I compared the identified in-plume segments with modeled CO mixing ratios along the same flight path extracted from the geo- and time-referenced LES domain. Figure 3.5 shows the time series of the flight path simulated emissions, overlaid with observations-derived plume segments. The results suggest good overall agreement in both location and timing between the modeled and observed emissions dispersion throughout majority of the ABL depth. The coinciding model CO peaks and observed smoke segments indicate that the horizontal width of the smoke plume is well represented in the model. Potential shortcomings include excess smoke near the ground, as suggested by the early peaks (12:36 and 12:40 CST) not identified as a plume crossing, as well as a slight skew of the overall smoke distribution towards higher levels. A small phase shift appears in the modeled peaks toward the later parts of the simulation (12:50 CST and beyond).

To evaluate the vertical distribution of WRF-SFIRE emissions, I compared the model-generated CO_2 concentrations with airborne measurements obtained during the "parking garage" and "corkscrew" (spiral ascent or descent) maneuvers. As shown in Figure 3.6a, there is a good overall agreement in injection heights for fire-generated emissions during the earlier "parking garage" profile. Plume top is accurately captured. Modeled concentrations tend to have a negative bias of $\sim$5 ppmv throughout the bulk of the plume thickness (500–1300 m), and be slightly over-predicted for the very top and bottom of the smoke column (at 400 m and 1500 m).

The "corkscrew" profile corresponds to a time near the very end of our simulation. As shown in Figure 3.6b, the band of modeled emissions appears to be very narrow and severely under-predicts the smoke concentrations. I discuss possible reasons for this behavior in Section 3.3.

The above assessment of model performance can be easily quantified with a variety of accuracy metrics. However, given the prescribed emission factors in WRF-SFIRE, the absolute magnitudes of such quantitative measures would hardly be useful. Hence,

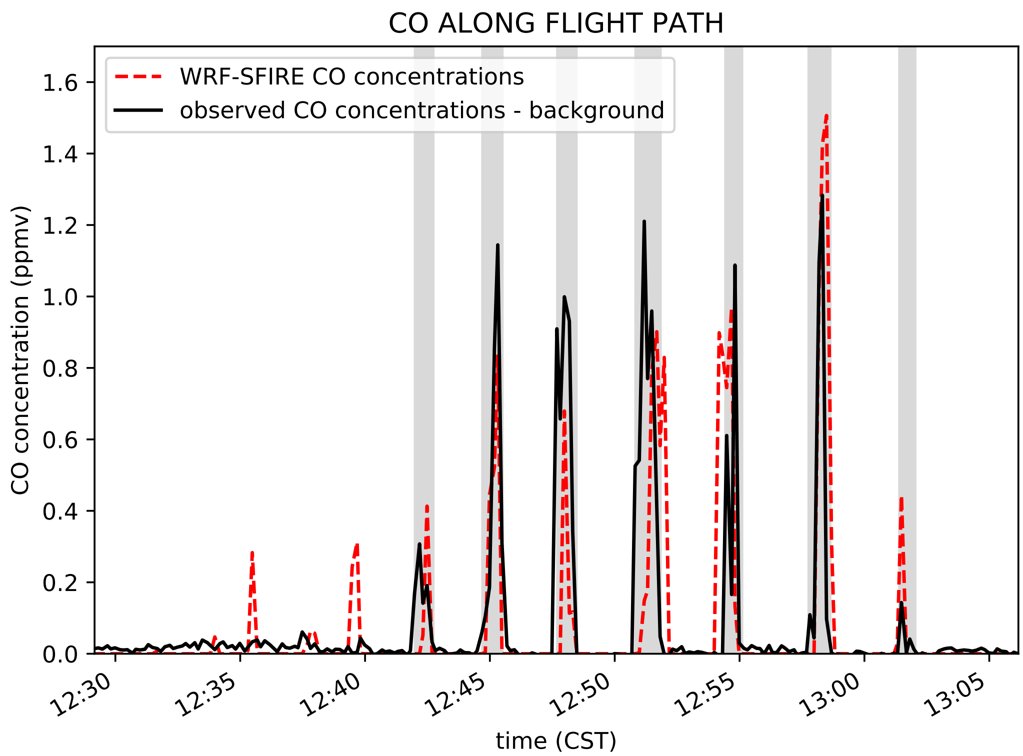

Figure 3.5: Simulated CO mixing ratio along RxCADRE flight path. Red dashed and solid black lines correspond to LES-derived and observed values, respectively. Gray shading indicates observed smoke time periods (not magnitudes) as identified from CO measurements along the flight path.

this evaluation focuses on the ability of the model to capture the relative distribution of modelled smoke in the atmosphere, rather than attempting to quantify concentration prediction errors.

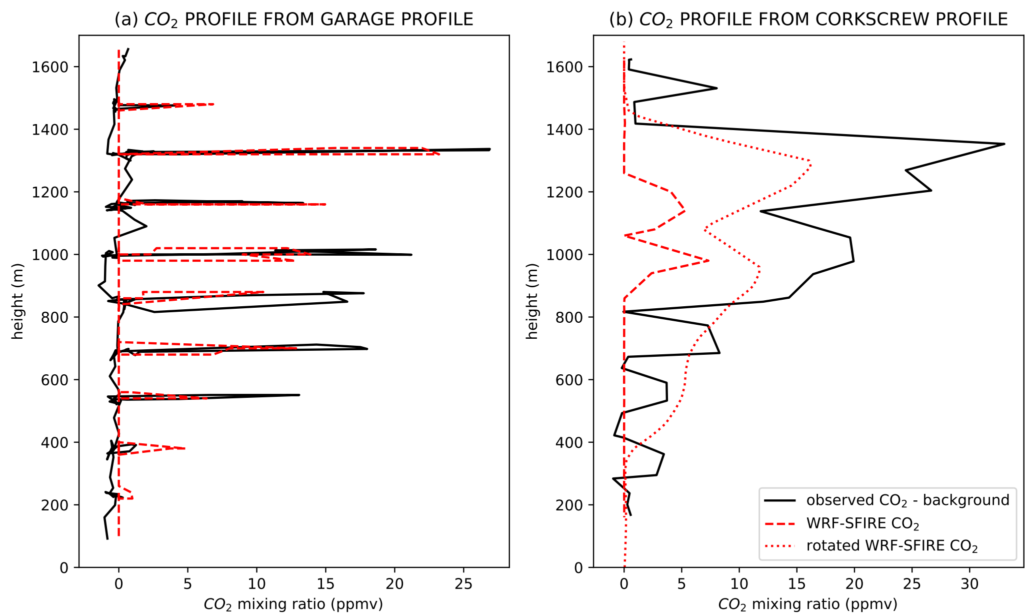

Figure 3.6: Observed (black) and modeled (red) vertical CO_2 emissions distribution during: (**a**) "parking garage" maneuver; and (**b**) corkscrew maneuver.

3.3 Discussion

The aim of this WRF-SFIRE evaluation is to assess its ability to capture fire-generated emissions in the context of air quality. Hence, I examine the above results based on their potential applications for wildfire smoke plume rise and dispersion modeling. The following sections discuss model performance and accuracy from the perspective of atmospheric dynamics, as well as address potential implications of uncertainty in fire behavior and the associated input parameters.

3.3.1 Vertical plume rise in the boundary layer

As demonstrated in my results summary in Section 3.2.2, initially WRF-SFIRE produced a fairly accurate near-source emissions distribution and plume top with a slight underprediction of concentrations (Figure 3.6a).

Over time model performance appears to deteriorate. Given that the fire thermal forcing compares relatively well with observations (Section 3.2.1), a likely cause for the increasing difference between model and observations is background ABL dynamics. The simulated atmosphere was initialized with 10:00 CST sounding, and continually forced with an observations-based constant surface heat flux. However, the cyclic lateral boundary conditions maintained the same vertical wind profile as initially supplied by the sounding at 10:00 CST, irrespective of potentially changing mesoscale conditions in the real atmosphere. Over the course of more than three hours between spin up start and the final minutes of the fire simulation, from which the "corkscrew" emissions distribution was obtained (Figure 3.6b), the real atmospheric wind profile likely evolved.

With time and further downwind the effects of any small changes in mesoscale conditions become more pronounced, which is why initially encouraging model performance deteriorated towards the end of the simulation. The markedly narrow band of emissions in Figure 3.6b suggests that the "corkscrew" location in the LES domain corresponded to the very edge of the plume rather than the center, indicating a shift in mesoscale wind conditions.

Indeed, analysis of observed background 30 m wind direction leading up to and during the burn shows a significant shift to the west, resulting in the LES "corkscrew" profile being extracted from the edge of the plume, rather then the intended center (Figure 3.7). Accounting for this observed wind rotation, it is possible to extract a wind-corrected smoke profile, such as shown with a red dotted line in Figure 3.6b. Assuming an average 30 degree rotation over the course of available wind observations (based on the slope of linear regression shown Figure 3.7a), the corrected location of the "corkscrew" maneuver indeed corresponds to the center of the plume (Figure 3.7b). The wind-corrected profile shown in Figure 3.6b is a notable improvement from the original non-rotated estimate. Note that this adjustment is extremely crude, as it is based on an estimated wind rotation at one point on a single vertical level and does not take into account potential changes in vertical wind shear.

Unfortunately, unlike the Real-mode WRF simulations, there is no way to account for changing lateral boundary conditions in WRF-SFIRE large-eddy mode. Hence, we can expect the ability of the model to accurately capture dispersion to depend strongly on the variability of real background conditions as well as the simulation length and spatial extent of the modeled domain. Namely, an LES will provide better simulations for situations where that actual atmosphere is horizontally uniform and temporally steady. While this presents a limitation for smoke plume rise and dispersion modellers, it is important to consider it in the context of existing alternative sources of field data. Given a typical uncertainty of $\sim$500 m associated with the most accurate widely available plume height dataset from MISR [75], WRF-SFIRE provides a valuable alternative source for generating comparatively accurate "synthetic plume height data".

Moreover, unlike instantaneous observational point measurements or overpass-

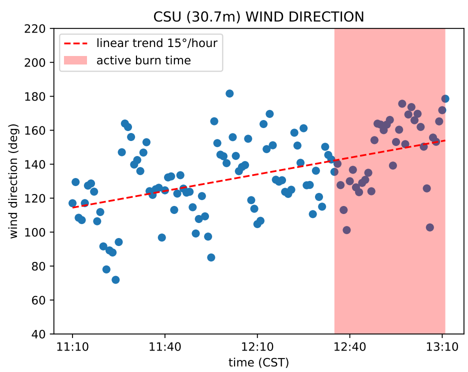

(**a**)

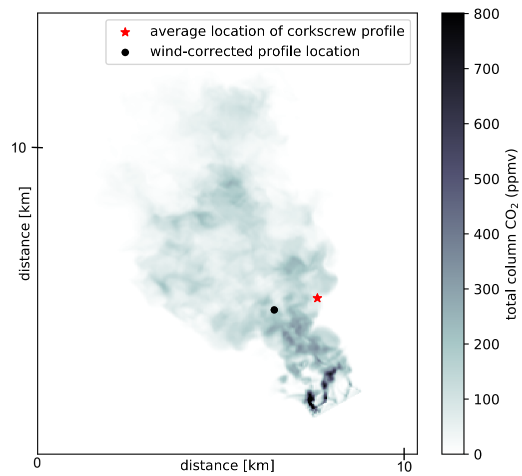

(**b**)

Figure 3.7: The effects of changing mesoscale wind conditions on plume observations (**a**) Observed 30 m wind direction prior to and during the burn (scatter points). Significant linear trend is shown with a red dashed line; active burn time shaded in red. (**b**) Top view of modeled smoke plume during the "corkscrew" maneuver by the instrumented aircraft. Black dot and red star indicate the average location of the "corkscrew" profile from flight with and without wind-correction, respectively.

limited derived satellite data, the LES allows me to examine the domain-wide temporal evolution of the plume and identify key features, which are likely to be of interest to dispersion modellers. As shown in Figure 3.8 and Animation S2 (see published supplementary material [50]), the vertical distribution of emissions in the domain changes throughout the simulation. Following an initial overshoot and a period of active smoke production near the ground, most of the emissions rise and end up near the top of the ABL (1060 m at the end of LES spinup), accumulating just above the inversion level in a wide span of heights. While this vertical distribution may contain modelling and initial condition biases, it is likely to offer dispersion modellers an advantage over the common current approach of using a single empirically derived injection height [42].

3.3.2 Importance of fire input parameters

As noted in the chapter introduction, this evaluation work is focused on assessing the relationship between coupled surface forcing and the atmosphere in WRF-SFIRE rather than on fire behavior. However, the following discussion on fire input parameters might be of interest to future modellers using WRF-SFIRE.

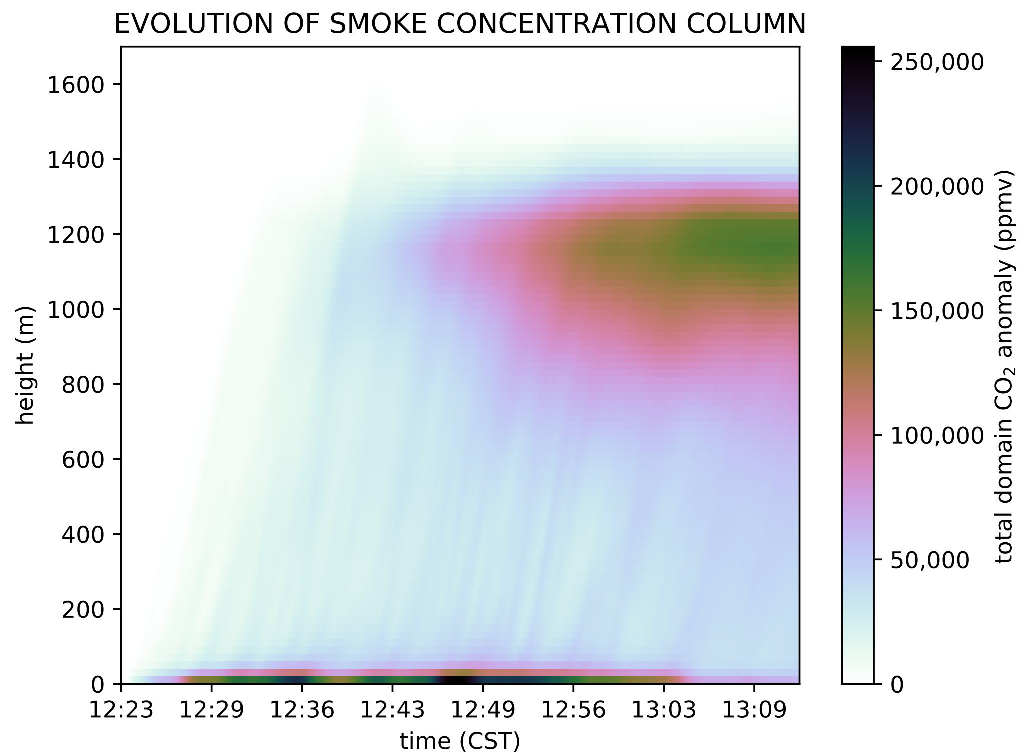

Figure 3.8: Temporal evolution of total column CO_2 anomaly in LES domain.

Similar to Kochanski et al. [34], I found that the fire behavior model is particularly sensitive to the choice of fuel moisture. This parameter in WRF-SFIRE does not depend on the selected fuel category and was based entirely on field data in my simulation. I also modified the standard fuel depth and loading parameters associated with Category 1 fuels to match observations, which resulted in very accurate surface heat flux forcing but substantially lower ROS values than observed or those obtained with standard settings.

Notably, similar thermal forcing to the atmosphere can be produced using a range of combinations of fuel categories and parameters in the model. I have not carried out a formal sensitivity analysis as it was beyond the scope of this study, however, future modelers may find the following information helpful. As preliminary tests for my study, I have used Category 1 and Category 3 fuels (short and tall grass) with various combinations of both standard and measurement-based fuel depth and loading parameters to achieve similar surface forcing. The relationships between these parameters are highly non-linear, which makes determining the "correct" choice (in the absence of detailed observational data) difficult. What I found to be encouraging is that while the absolute value of modeled concentrations and ROS changed dramatically depending on the chosen fuel category for a given fire intensity, the relative spatial distribution of emissions did not. The simulated atmosphere is forced solely by the parameterized heat and moisture fluxes, so WRF-SFIRE does not discriminate which combination of fuel characteristics produced a given heat flux that drives the buoyant plume rise.

Given any thermal forcing, the atmospheric response appears to be fairly robust, irrespective of the particular combination of fuel parameters or ROS with which it was achieved. While this study does not aim to establish whether the model sensitivity to fuel conditions is physical, it does suggest that the LES produces realistic plume rise for the given fire intensity.

3.3.3 ROS and biases in modelled emissions

The model's poor performance for ROS in my case study likely resulted in reduced simulated emissions concentrations due to lower parameterized fuel consumption rate. This is consistent with the notable negative bias in my modeled CO_2 profiles.

As mentioned above, the low ROS values on my simulation are largely a result of my use of non-standard fuel depth and loading parameters. To eliminate alternative causes for slow fireline advance, I compared horizontal winds at the first and second model levels (at $\sim$8 m and $\sim$25 m AGL) with data obtained from 2D sonic anemometers mounted at multiple heights of the CSU-MAPS meteorological tower. As shown in Figure 3.9, the near-surface winds are generally accurately captured by the model. At the lowest vertical level, there tends to be a slight positive bias, which one would expect to contribute to higher rather than lower ROS values.

Apart from their dependency on ROS and fuel consumption, the absolute values of WRF-SFIRE emissions are also controlled by user-prescribed emission factors. In my case study, these factors were not derived from measurements, but were rather based on standard values typical for the Grassland fuel category (see Section 3.1.2). Hence, the negative bias in our modeled smoke distribution could potentially be reduced, should observations-based emissions factors become available.

3.3.4 Experimental design considerations

One of the shortcomings of the RxCADRE dataset and this experiment is the substantial (nearly 2.5 h) difference in timing between the sounding balloon launch and the fire ignition. Availability of an additional vertical profile for model evaluation just prior to

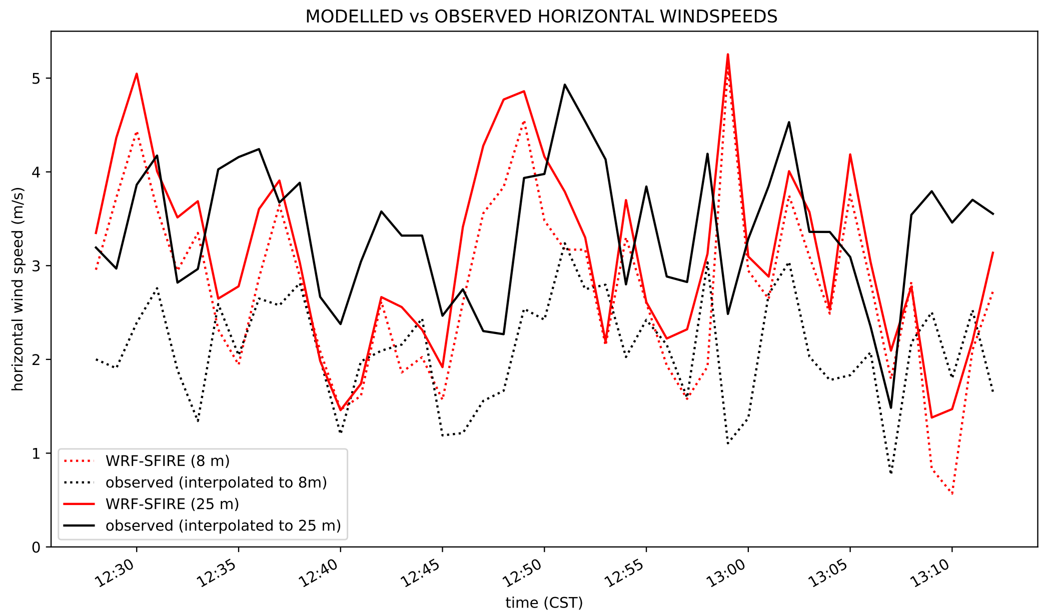

Figure 3.9: Modeled (red) and observed (black) near-surface horizontal wind.

ignition would have been extremely helpful in mitigating some of the sources of error mentioned in the above sections. A similar recommendation was offered by Kochanski et al. [35], who suggested that an on-site sounding just prior to the burn rather than a few hours earlier would be most useful.

While the challenges of coordinating balloon launches in the presence of aircraft over the fire are obvious, a potential alternative would be to include on-board temperature and wind sensor data from flight with the smoke dispersion measurements.

3.4 Summary

This chapter aimed to assess the ability of a coupled fire-atmosphere WRF-SFIRE LES model to simulate a case study of fire smoke plume growth and dispersion. I examined the L2G burn from the RxCADRE 2012 campaign - a comprehensive experiment combining simultaneous monitoring of fuel, fire behavior, meteorology and emissions.

My model evaluation demonstrates good overall agreement between the LES and the observations, subject to accuracy and timeliness of model initialization data. Using the emissions and dispersion data collected from an airborne platform during the RxCADRE experiment, I show that LES reasonably captures the timing, rise and dispersion of the fire plume. I examine the possible relationships among model biases, fire behavior and changes in ambient atmospheric conditions.

This work demonstrates the feasibility of using WRF-SFIRE LES in studying fire plume dynamics. The scarcity of detailed plume observations presents one of the central challenges for smoke-model development. WRF-SFIRE's ability to capture the rise and spread of fire emissions for cases such as studied here has the potential to address this critical research need and provide alternative "synthetic" data for future development of parameterizations for wildfire smoke plume rise.

3.4.1 Limitations

Recent studies suggest that the heat extinction depth parameter in WRF-SFIRE (or e-folding distance) has a strong influence on the modeled fire and near surface plume behavior [33, 35]. Currently, there is no clear theory in the literature on how the vertical distribution of fire-released heat above the ground affects near-ground air temperatures as well as ROS. As the relationship appears to be highly non-linear, I have not examined its implications in our simulations.

Overall, my findings suggest that the ability of WRF-SFIRE to capture plume dynamics of a specific real fire largely depends on the availability of timely atmospheric initial conditions and accurate simulation of fire intensity. Owing to the detail and comprehensive nature of the data provided by the RxCADRE experiment, these critical inputs could generally be derived from measurements for the current case study. This sensitivity, however, could present a challenge for future real-time fire simulations, where few or no such measurements would be available.

3.4.2 Big picture

The case study discussed in this chapter can likely be considered a good representation of a "typical" smoke plume, from the perspective of remotely sensed plume "climatology" (Section 2.3). It occurred during daytime atmospheric conditions and most of the smoke was injected into the atmospheric layers just above the ABL top. While these findings may be reassuring for regional air quality modellers, the bulk approach to fire behavior evaluation may spark many interesting questions for combustion researchers.

In particular, fire modellers may consider whether it is feasible to use the fire spread algorithm implemented within WRF-SFIRE with non-standard fuel category parameters and whether the produced behavior (and, in particular ROS) can be considered physical. Another theoretical consideration relating to micro-scale dynamics is what the effects of upscaling heat fluxes (and the inevitable smoothing associated with it) from fire to atmospheric grid are. More broadly: how meaningful is the comparison of in-situ fire heat flux sensor measurements with grid-averaged values representing heat flux in the model? These questions could serve as a helpful starting point for additional investigations by fire behavior scientists.

Chapter 4

Synthetic data: Simulating smoke plumes under a wide range of fire and atmospheric conditions

In this chapter I introduce a synthetic plume dataset produced using a coupled fire-atmosphere model WRF-SFIRE [45, 46]. The broad goal of this effort is to capture a wide range of fire and atmospheric conditions and examine their effect on modelled smoke plume rise. This surrogate "data" addresses many of the challenges of working with available observations (Section 2.3). The following chapter details the numerical setup, scope of the dataset, as well as my approach to defining "ground truth" for plume injection height model evaluation.

4.1 Generating plume data

4.1.1 Numerical configuration

WRF-SFIRE was configured in idealized large-eddy resolving mode. Much of my numerical setup was adopted from the case study detailed in the previous chapter (Chapter 3), to ensure the simulations represent physical conditions backed by model evaluation. Due to high computational demands of LES runs, I focused on the local- and meso-gamma scales (1 km - 20 km), considering only the initial buoyant plume rise of smoke in typical daytime clear non-precipitating atmospheres. Key parameters varied were ambient wind, fuel category, vertical potential temperature profile and fire-line length, denoted as conditions **W**,**F**,**R** and **L**, respectively (detailed further in Section 4.1.2).

I initialize each 10 km x 20 km domain with 40 m horizontal grid spacing with uniform ambient west wind **W** and vertical temperature profile **R**. Depending on the sounding **R**, the simulations were performed in either a shallow (3000 m) or a deep (5000 m) domain, with 51 or 71 hyperbolically stretched vertical levels, respectively. A constant uniform lower boundary surface thermal flux (tke_heat_flux) in the ambient environment and lateral periodic boundary conditions were imposed to produce a turbulent well-mixed layer in the ambient environment. I used full surface initialization (sfc_full_init =.true.), with the lower boundary characteristics set to USGS values for land use most closely matching the Anderson fuel category **F** [3]. The corresponding surface roughness lengths added various levels of wind shear to each domain to produce a more realistic non-uniform vertical wind profile during spinup of the environment before the fire was initialized in the LES.

Initial convection in the ambient environment was triggered using a perturbed surface temperature field. On average, a near-stationary turbulence spectrum was achieved within the first 30 min of run start. The "restart" file generated at the end of one hour of spinup was used to initialize the main burn simulation, ensuring the fire was ignited in a well-mixed turbulent ABL.

I initialized the fire over a one-minute interval using a straight line of length **L**. The ignition line was placed one kilometer downwind of the western edge of the domain (perpendicular to ambient wind) and centered in the north-south direction. With a refinement ratio of 10 in each horizontal direction, the fire was simulated on a 4 m sub-grid mesh.

The "smoke plume" was modelled with a passive tracer emitted proportionally to the mass and type of fuel burned. The rate of release was controlled by an assigned emission factor representing $PM_{2.5}$ for each fuel category, based on values provided by Prichard et al. [60] (see namelist.fire_emissions in downloadable supplement referenced in Appendix A.1).

A summary of key configuration details can be found in Table 4.1, as well as in sample namelist initialization files available for download (Appendix A.1).

4.1.2 Test conditions

Table 4.2 summarizes the key parameters that were varied to produce the synthetic dataset.

The range of ambient winds tested was bound largely by numerical constraints. Due to cyclic boundary conditions, wind speeds higher than 12 ms^{-1} would require a much larger domain to prevent smoke recirculation. For the lower bound on my wind condition **W**, I needed to ensure that sufficient wind speed was maintained to

Table 4.1: Key parameters of numerical domain setup.

Simulation Parameter	Value/Description
Model version	May 24, 2019 (git #ced5955)
Horizontal grid spacing	40 m
Domain size	500 grids cells (east-west) x 250 grids cells (north-south)
Time step	0.1 s
Model top	3000 m (shallow) / 5000 m (deep)
Spinup timing	11:30:00 - 12:30:00
Fire (restart) simulation timing	12:30:00 - 12:50:00 (shallow) / 12:30:00 - 13:00:00 (deep)
Sub-grid scale closure	1.5 TKE (TKE = Turbulence kinetic energy)
Lateral boundary conditions	periodic
Surface physics	Monin-Obukhov similarity (sf_sfclay_physics = 1)
Land surface model	thermal diffusion (sf_surface_physics = 1)
Ambient surface heat flux	240 W m^{-2}(tke_heat_flux=0.2)
Fire mesh refinement	10
Ignition duration	13:00:10 – 13:01:10
Heat of combustion of dry fuel	16.4 MJ kg^{-1}

Table 4.2: Test conditions included in synthetic plume dataset. The count indicates the number of unique values used within the specified range.

Condition (Tag)	Range	Count	Description
Ambient wind (**W**)	3 - 12 ms^{-1}	10	Uniform horizontal wind magnitude used to initialize model spinup
Stability profile (**R**)	R0-R8	9	Atmospheric sounding with variable ABL height, temperature and inversion strength
Fuel (**F**)	1 - 13	13	Anderson fuel category assigned at lower boundary
Fireline length (**L**)	1 - 4 km	3	Length of ignition line
			Total number of experiments = 140

propagate the fire. The spread algorithm used within the LES applies a correction factor under low wind speed conditions to prevent the fire from extinguishing itself. While necessary for numerical reasons this effect is not physical, so winds below 3 ms^{-1} were excluded from my dataset.

I used 9 different atmospheric profiles (**R** condition) to initialize the model. I varied the following features for each initialization:

- initial ABL height (500 m - 1600 m)

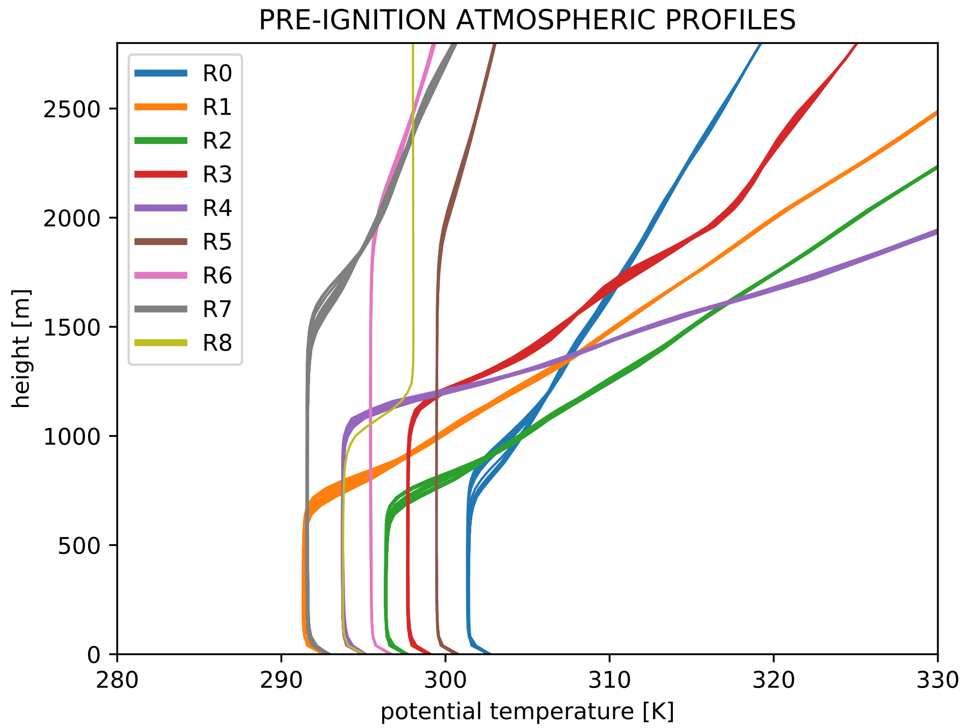

Figure 4.1: Pre-ignition potential temperature profiles (stability condition **R**). Colors correspond to initial soundings used for model spinup.

- potential temperature lapse rate above inversion (0 K km^{-1} - 20 K km^{-1})
- initial (pre-spinup) ABL temperature (290 K - 300 K)

Following spinup (Section 4.1) under variable winds and surface conditions, this produced 9 sets of soundings, shown in Figure 4.1 with ABL depths of approximately 600m - 2000 m. I tested all fuel categories available within the model (**F** condition), and varied the length of the fireline (**L** condition) between 1 and 4 km.

Table 4.3 and Table 4.4 summarize the tested combinations of fire and atmospheric conditions captured by the synthetic plume dataset. Colored cells (blue and red) correspond to completed simulations. Tall boundary layers of **R5** and **R6** domains required low winds (5 ms^{-1} and below) and high intensity fires (fuel categories 4, 6, 7, 12 and 13) to reach ABL top within the simulation runtime and/or avoid smoke recirculation. Hence, alternative combinations (white cells in **R5** and **R6** columns) would require considerably different domain setup from other runs. For this reason these combinations were not tested. Also, a single run was performed for **R8** condition (adiabatic free atmosphere) as an extreme case scenario.

Red cells highlight simulations that were completed, but subsequently excluded from analysis presented in Chapter 6. This was done based on visual inspection of LES fields. There were two possible reasons for exclusion: (i) the plume reached the top of the domain or (ii) the plume appeared to be non-penetrative (see sample in Appendix A.2). In the former case, it's questionable whether the fields are physical, as the plume could potentially be affected by the absorbing layer near domain top, designed to prevent numerical instability. The latter rendered the plume irrelevant for the purpose of modelling smoke injection height (Chapter 6). These non-penetrative runs, however, were included for testing the plume classification method presented in Section 7.1.

Table 4.3: Combinations of test conditions resulting in penetrative plumes, as captured by the LES datasets. Green cell highlights fireline length condition (**L**) runs. Intensity of blue color corresponds to the number of runs for fuel condition (**F**) represented by the cell. Row 'W5' is expanded in Table 4.4 below.

R/W	**R0**	**R1**	**R2**	**R3**	**R4**	**R5*†**	**R6*†**	**R7***	**R8***
W3	F7	F7	F7	F7	F7	F7	F7	F7	
W4	F7	F7	F7	F7	F7L1 F7L2 F7L4	F7	F7	F7	
W5	F1 - F12, excl:F4	F1 - F13, excl:F9	F1 - F13	F2 - F13, excl:F8,F9	F1 - F13	F4 F6 F7 F12 F13	F4 F6 F7 F12 F13	F2 - F13, excl:F8,F9	F7
W6	F7	F7	F7	F7	F7			F7	
W7	F7	F7	F7	F7	F7			F7	
W8	F7	F7	F7	F7	F7			F7	
W9	F7	F7	F7	F7	F7			F7	
W10	F7	F7	F7	F7	F7			F7	
W11	F7	F7	F7	F7	F7			F7	
W12	F7	F7	F7	F7	F7			F7	

*Deep domain (5 km). †Extended runtime (30 min).

Table 4.4: Tested combinations of fuel and ABL conditions (blue and red colored cells).

R/W	R0	R1	R2	R3	R4	R5*†	R6*†	R7*	R8*
F1				ABL plume				ABL plume	
F2									
F3									
F4	smoke at domain top								
F5									
F6									
F7									
F8				ABL plume				ABL plume	
F9		ABL plume		ABL plume				ABL plume	
F10									
F11									
F12									
F13	smoke at domain top								

Note, that varying a single condition while holding the rest constant does not result in a controlled experiment isolating its impact on plume rise. Because WRF-SFIRE incorporates fire-atmosphere coupling, the problem is not well-constrained. For example, by varying fuel type **F** alone, while holding the rest of test conditions constant, I obtain a set of fires with diverse shapes, sizes, intensities, fireline depths, rates of spread and heat release. This reflects the complexity of non-linear interactions that exist between the fire and the atmosphere (discussed further in Chapter 5). As a result, the parameter space captured within my LES dataset is much greater then the four conditions described in Table 4.2.

4.2 Defining smoke injection height

Given non-stationary fire and atmospheric conditions, determining a consistent definition of an equilibrium smoke injection height is not a trivial task. It requires separating buoyant rise from dispersion, while excluding the effects of initial momentum overshoot and accounting for the advection due to varying ambient and fire-generated winds.

A common way of examining vertical distributions of pollutants in the context of air quality is to consider crosswind-integrated (CWI) concentrations. This allows one to reduce the problem to two dimensions, with plume centerline being defined simply as the CWI concentration maximum at each location downwind of the source. Theoretically, under stationary conditions there exists an equilibrium height, around which the centerline eventually oscillates. In reality, as well as in my LES experiments, neither the ambient nor the fire conditions are stationary. The changing location, shape and intensity of the fire, ABL warming and growth, as well as the development of fire-coupled winds and vorticity continually modify the conditions.

As a result, my approach is based on defining a region, where the concentration distribution is quasi-stationary. I consider the last frame of each simulation for this analysis. Using CWI tracer values, I locate the plume centerline (Figure 4.2a). To obtain the quasi-stationary region for each individual plume, I first calculate the change in tracer concentration along the centerline. I then use a smoothing function to reduce the effect of random turbulent oscillations in both the centerline height and the tracer concentration gradient along the centerline. The downwind region where both of these parameters are not changing rapidly are then then considered quasi-stationary. Additional details of this filtering method are provided in Appendix A.3.

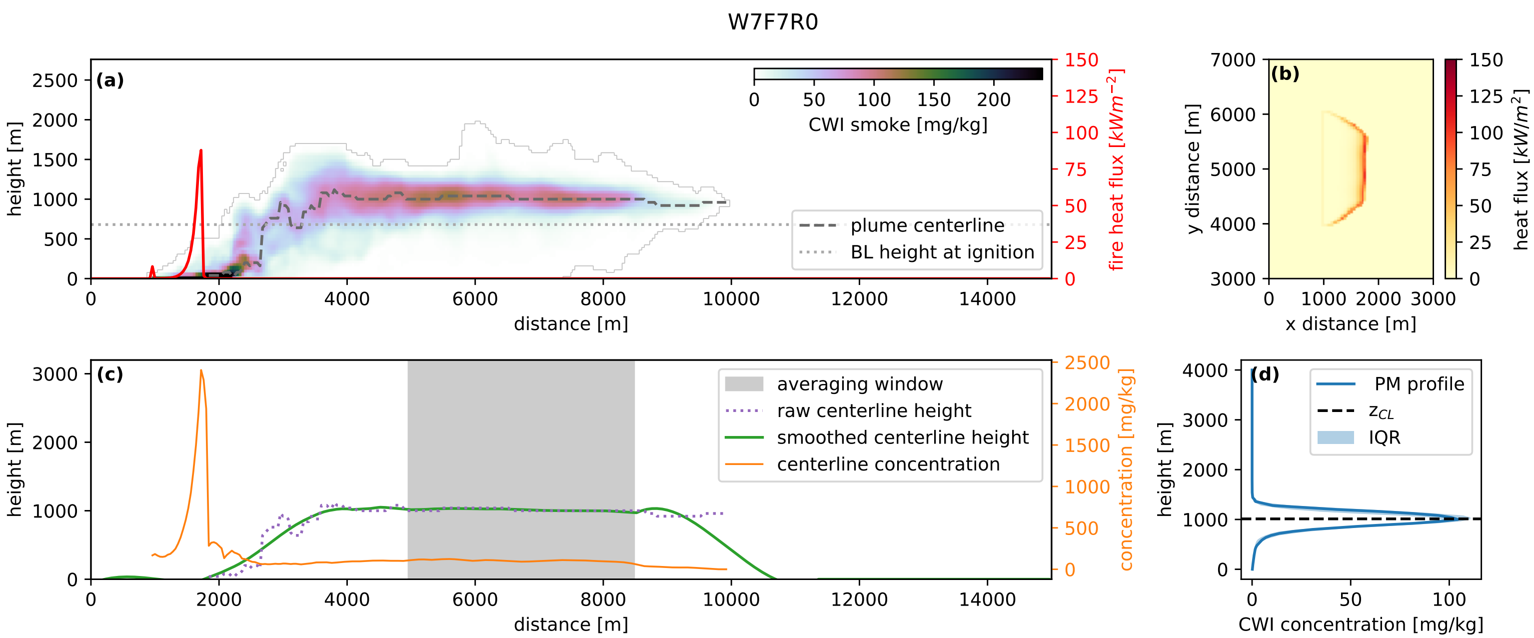

Figure 4.2: Illustration of the approach to identifying a quasi-stationary downwind region in CWI smoke distribution using a sample LES experiment. (**a**) CWI smoke concentrations. Also shown are plume centerline height (dashed), z_i (dotted) and CWI fireline intensity (solid red, secondary axis). (**b**) Plan view of fire heat flux showing the fireline. (**c**) Quasi-stationary region (grey shading). Also shown are raw (dotted purple) and smoothed (solid green) centerline heights and tracer concentrations (solid orange, secondary axis). (**d**) Representative downwind smoke distribution. The profile (solid blue line) is obtained by horizontally averaging the CWI smoke concentrations in the quasi-stationary region. Also shown are interquartile range (IQR) (light blue shading) and the derived smoke injection centerline height z_{CL} (dashed black).

I then average the vertical CWI distribution of tracers in the downwind direction over the identified quasi-stationary regions (shaded in grey on the Figure 4.2c) to produce a representative downwind distribution for each plume (Figure 4.2d). I define the "true" injection height z_{CL} as the mean height of smoothed centerline over the averaging region. The resultant dataset of z_{CL} values is used to constrain and evaluate the proposed smoke injection height parameterization introduced in the following chapters.

4.3 Summary

The synthetic plume dataset (Section 4.1) and the derived injection height dataset (Section 4.2) described above provide a rich source of training and evaluation data for future models and parameterizations (see Appendix A.4 for access information). The approach introduced in this chapter allows for creation of controllable and repeatable numerical experiments, which can capture a range of fire and atmospheric conditions not possible with real-life observational campaigns.

4.3.1 Limitations

The presented dataset is limited to initial plume rise from fires occurring under daytime fair-weather conditions on a local/regional scale over flat terrain. While representative of vast majority of smoke plumes [73], the examples captured by the dataset are limited to penetrative plumes, which remain in the stable layers of the free troposphere above the ABL. I have not considered the effects of latent heat: all plumes in the dataset are non-condensing.

4.3.2 Big picture

The range of fire and atmospheric conditions captured here is most applicable for regional air quality applications. Future researchers interested in examining plume rise in the context of global chemical transport models, where cloud formation and potential stratospheric injection of aerosols are of great importance, could extend the proposed approach for deeper simulated domains over complex terrain. It would be interesting to compare plume injection heights obtained from WRF-SFIRE simulations configured in LES vs Reynolds-averaged Navier–Stokes (RANS) mode and reanalysis-driven boundary conditions. Relatively fast run-time (compared to LES) and ability of WRF to incorporate realistic initial conditions and chemistry in RANS simulations, combined with increasing computational power, could pave the way for broad use of WRF-SFIRE in operational smoke modelling [43].

Chapter 5

Fire-atmosphere coupling: qualitative analysis of local-scale dynamics

The past decade has seen significant developments in complex, coupled, physics-driven atmospheric numerical models, including WRF-SFIRE, which resulted in enormous improvement in our ability to simulate wildfire and smoke behavior. These sophisticated models offer the promise of giving insight into the underlying dynamics of interactions between the fire and the atmosphere [61]. Our current understanding of the subject is limited, and large uncertainties remain due to lack of observational data (Section 2.3).

While the evaluation case study presented in Chapter 3 is a step towards greater confidence in model performance, much research is still needed to understand all the physical processes involved. Yet without proper knowledge of what the dynamical mechanisms and feedbacks are, it is impossible to assess how well the current models represent them. Comprehensive observational campaigns, such as FASMEE (Section 2.3) will hopefully help shed light on the subject in the near future.

In the mean time, existing plume rise parameterizations have to rely on simplifying assumptions about how the fire interacts with the ambient atmosphere. A vast majority of operational schemes [9, 39, 66], consider the smoke plume to be rising through a static atmosphere, entraining ambient environmental air along its path. While suitable for small-diameter low buoyancy sources like industrial smoke stacks, exclusion of any possible feedbacks between the fire and the atmosphere may contribute to large errors associated with applying such schemes to wildfires.

This chapter asks the following question: **What can a coupled fire-atmosphere model tell about dynamic interactions around wildfires?** While still subject to comprehensive evaluation, the answers to this question may help inform current and future plume rise parameterization development.

5.1 Fire-induced winds

As noted in the previous chapter, the synthetic dataset produced with WRF-SFIRE consists of a diverse set of smoke plumes with unique characteristics, combining the effects of imposed initial conditions, fire-atmosphere coupling and background ABL turbulence. The detailed nature of synthetic LES data, however, allows us to identify dynamical flow features that are common to vast majority of the modelled plumes.

One such effect is the formation of a convergence zone at the fire front. Shown in Figure 5.1 is a typical example of a flow pattern produced by WRF-SFIRE. The top panel represents cross-wind-integrated CWI smoke (Figure 5.1a), shown with ambient wind direction. The remaining subplots display horizontal and vertical flow generated by the fire (along with background turbulence), **relative** to mean ambient winds. I.e. the wind fields displayed in the figure can be superimposed on average ambient atmospheric conditions to give the total flow field.

As shown in the horizontal velocity subplot (Figure 5.1b), the fire generates a large region of slowing winds extending far downwind. A well-defined convergence zone forms at the fire front, where these slowing winds meet accelerated horizontal flow from behind the fireline (i.e. from upwind of the fireline). Once the rising air reaches equilibrium height, the smoke is pushed into a wide range of outflow levels, marked by increased advection relative to ambient wind. Lastly, as demonstrated in the vertical velocity subplot (Figure 5.1c), the downwind ABL region is generally dominated by sinking air, which aids smoke recirculation and fumigation of elevated pollutants back to the surface.

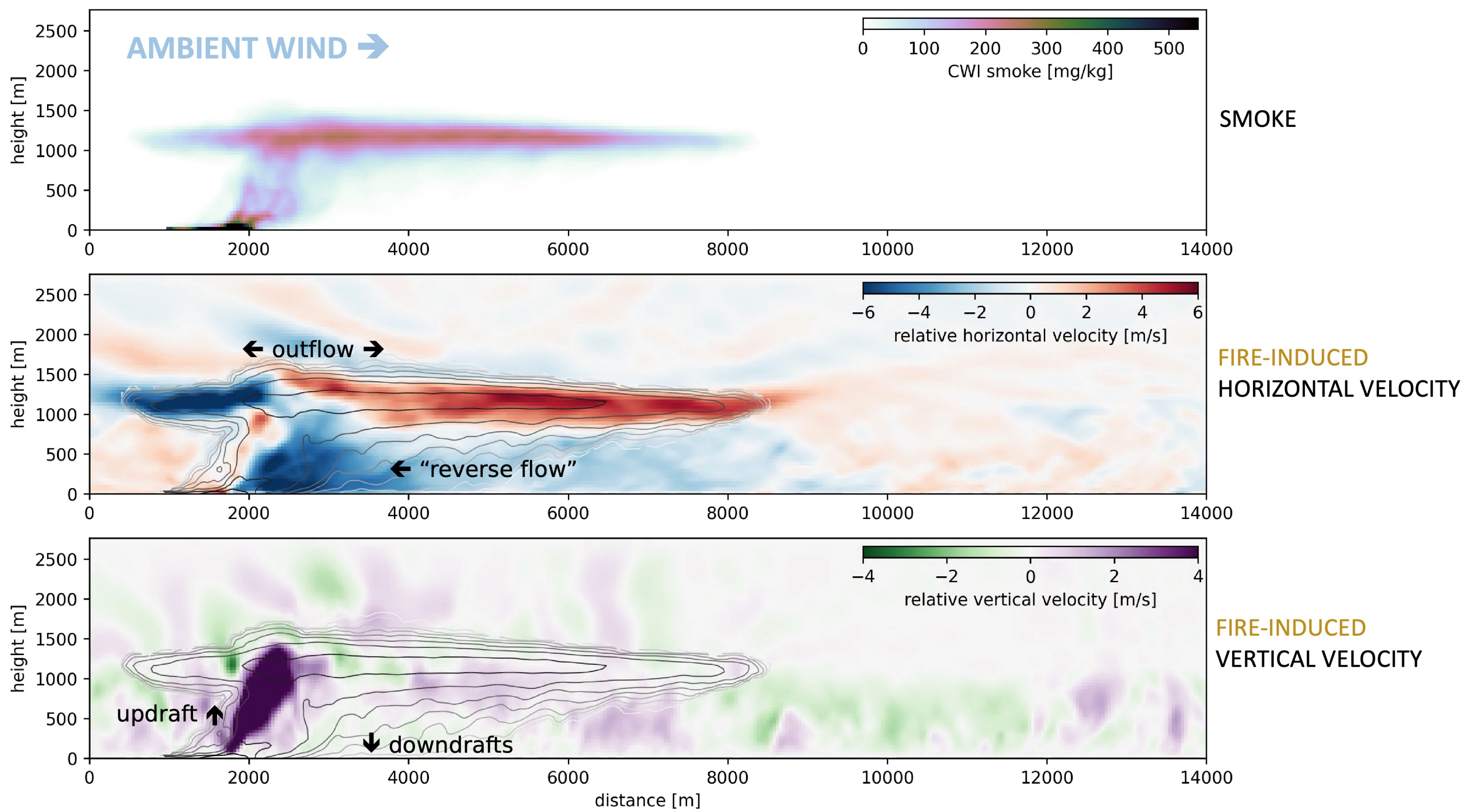

Figure 5.1: Cross-wind integrated (CWI) smoke concentrations (top). Fire-induced horizontal flow relative to ambient conditions (middle). Fire-induced vertical flow relative to ambient conditions (bottom).

5.2 Vorticity

To examine how wildfire plumes entrain air I used the LES fields to perform trajectory analysis for air parcels located just outside of the fire. I placed equally spaced source points to the side of the fireline (laterally) and tracked the streaklines as they mixed with the smoke plume. As shown Figure 5.2, clean air is pulled towards the head of the fire, creating a large lateral vortex.

Examination the temporal evolution of various LES fields, the fire-atmospheric coupling mechanism appears to be as follows:

- low pressure in the center of the updraft results in a horizontal pressure gradient force
- wind shear induces vortices that bring clean air into the plume and maintain mass continuity
- cross-wind flow creates a curved fireline (eg. Figure 5.3) resulting in less occlusion of the firefront and decreasing the strength of the reverse flow

There is no clear theory on which buoyancy and wind conditions induce vortex formation and, in extreme cases, plume bifurcation [19]. However, Cunningham et al. [16] have previously shown using numerical experiments, that the degree to which the smoke splits is related to surface wind shear. More importantly, they found that plume bifurcation does not affect plume rise. Though the study stops short of quantifying these effects, it represents the most detailed investigation of vorticity in wildfires to date.

Overall, vortices appear to be a transient feature in wildfires [59]. They are continually mediated by fluctuations in ambient winds (as shown in further detail in Section 5.4), and generally occur under light wind conditions [16].

Notably, the lateral wind flow generated in response to the updraft and the associated vorticity appear to be a very efficient mixing mechanism. The color of the streaklines shown in Figure 5.3, corresponding to smoke concentration, indicates that the most rapid entrainment of ambient air occurs close to the surface. This result is interesting, because most plume models rely on a common entrainment assumption, which suggests that mixing rate is proportional to the local vertical velocity of the updraft [71]. Yet near the ground this velocity is still relatively low, compared to near the top of ABL, where most of plume's buoyancy has been converted into kinetic energy.

These findings could in part explain why wildfire plume behavior differs from that suggested by common Gaussian plume models.

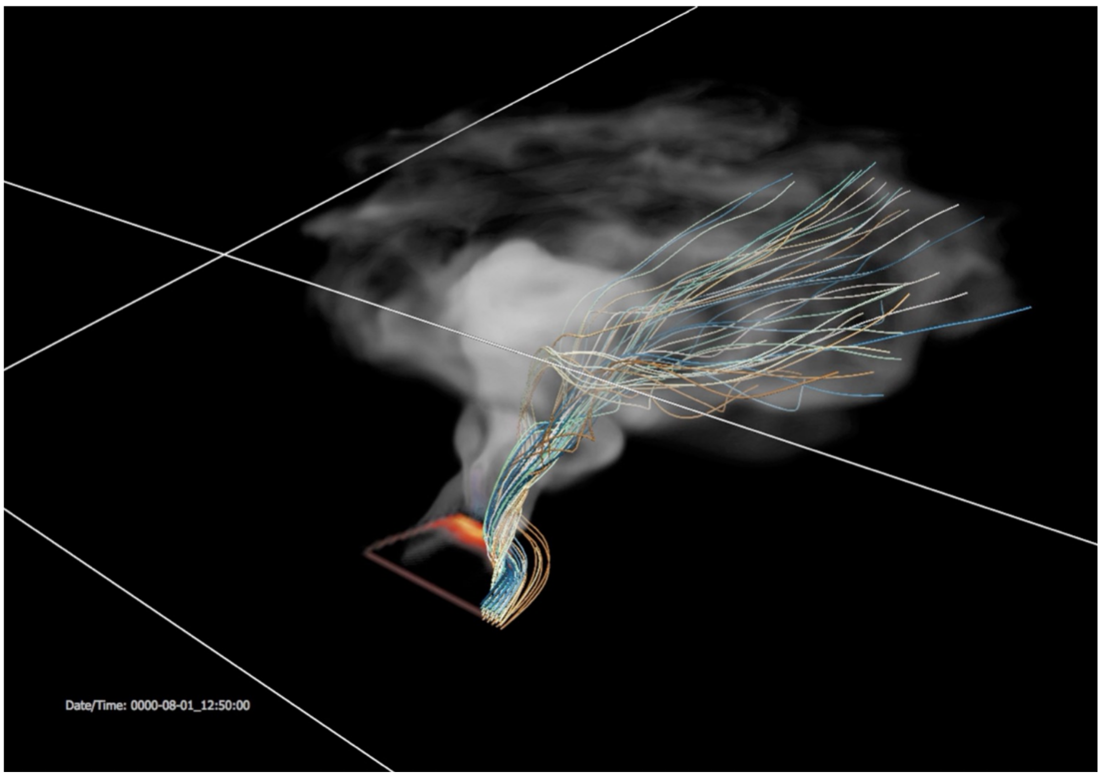

Figure 5.2: Formation of a lateral vortex around a fireline. 200 m x 200 m trajectory source mesh is located next to ignition line (outside of the fire) at the surface. Colors correspond to trajectory index to aid visualization. Figure produced using VAPOR software [13]

Figure 5.3: Illustration of fire-atmosphere feedbacks between updraft, lateral winds and fireline curvature with trajectories. Colors correspond to tracer concentration along each path. Equally spaced trajectory sources were placed on each edge of the fireline, extending between 50 m and 200m AGL. Figure produced using VAPOR software [13]

5.3 Effects of fireline length

Most existing plume rise parameterizations [4, 6, 20, 64] idealize the shape of the fire, usually assuming it's radially symmetric. In other words, the plume is often represented by a cone or a cylinder. However, a wildfire often consists of an intense firefront (at the leading edge of the fire) where peak heat fluxes occur, followed by a wide smouldering region, and sometimes a backing fire. The length of the fireline can extend many kilometers. For modelling purposes, it is therefore convenient to consider the fire and the smoke plume in two dimensions (x,z) as viewed from a cross-wind direction (y). This raises a question: how does the length of the fireline affect plume rise and the vertical distribution of smoke?

Figure 5.4 compares the time-averaged fire-generated 2-D (x,z) horizontal flow for 1 km, 2 km and 4 km firelines (in the cross-wind direction) under the same initial fire and atmospheric conditions. I found that the magnitude of the downwind region of slowing air is greater for longer firelines. Moreover, longer firelines produced a wider, stronger range of smoke outflow levels compared to shorter ones. Irrespective of the magnitude of the fire-induced horizontal wind, the convergence zone remained stationary at the firefront.

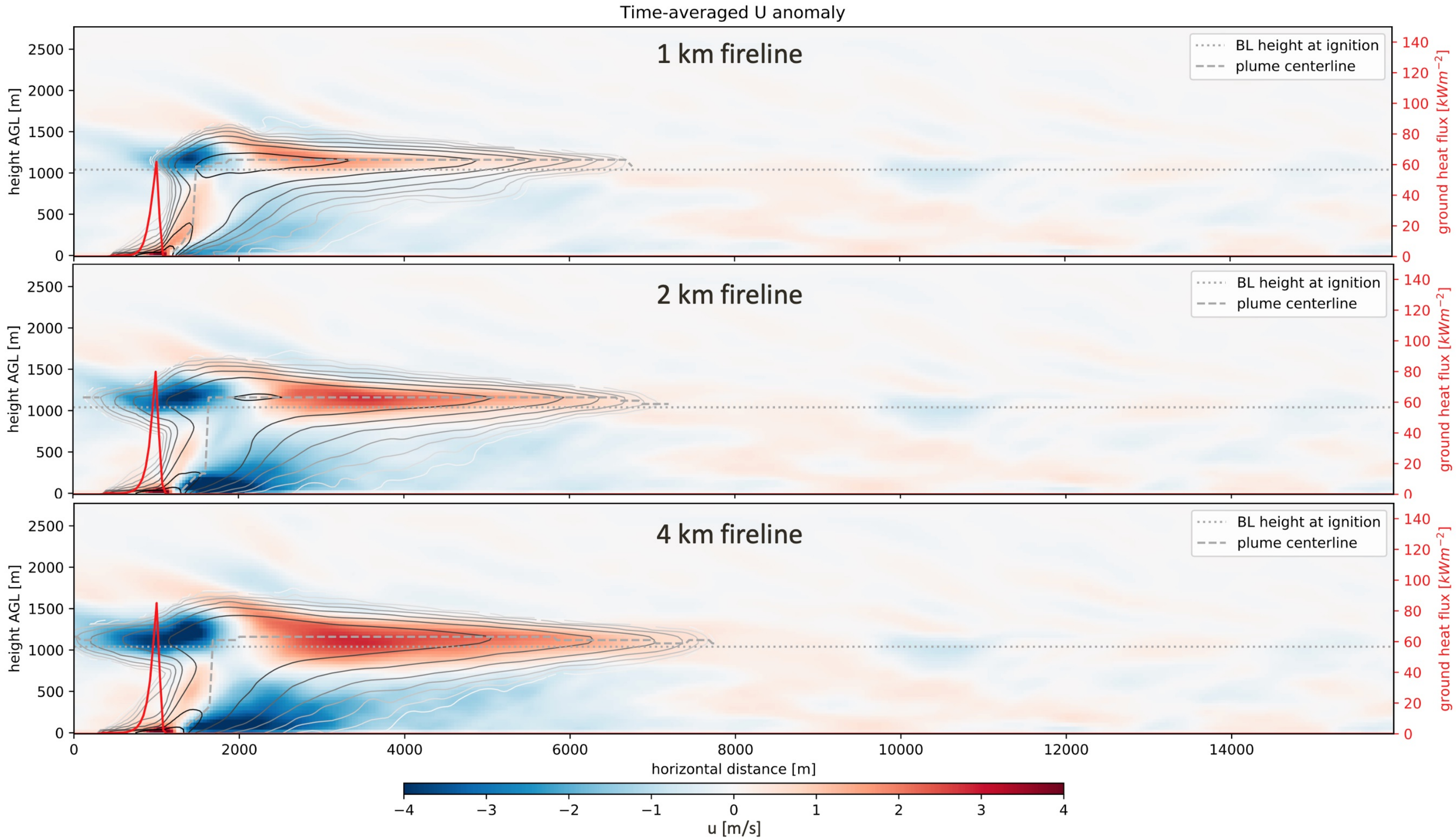

Figure 5.4: Time-averaged relative horizontal velocity plots for 1 km (top), 2 km (middle) and 4 km (bottom) firelines. Fireline-following moving averaging was performed over the last 15 min of the simulation using mean vertical cross section of the horizontal flow field (averaged over the central 800 m of the fireline in the y-direction) . Grey contours correspond to time-averaged smoke concentrations. Fireline heat flux is plotted on a secondary (red) axis. Dotted and dashed lines denote ABL height and the plume centerline, respectively.

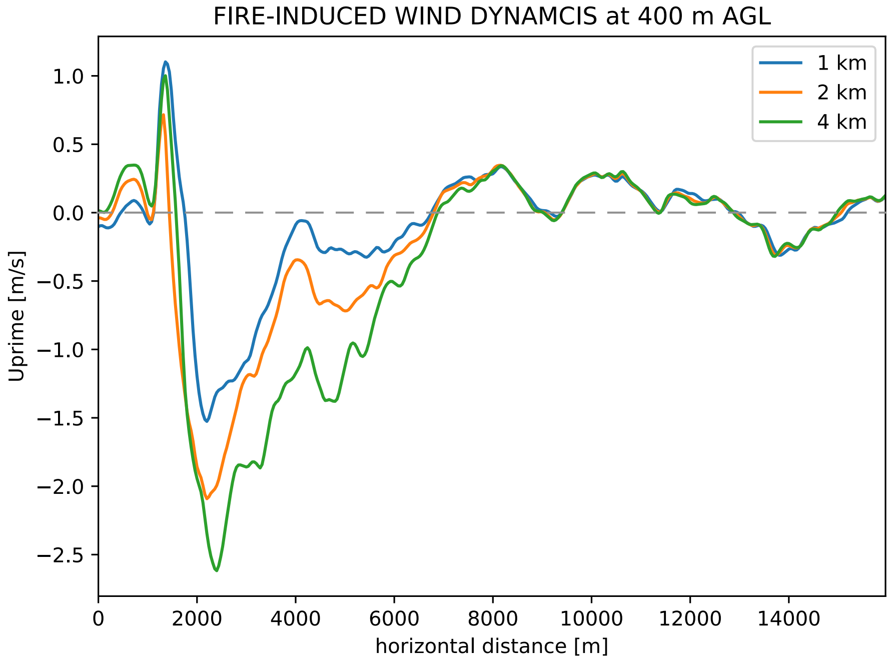

Figure 5.5: Magnitude of fire-induced horizontal winds U' (relative to ambient flow) at 400 m above ground level (~half of ABL height).

Figure 5.5 provides a more direct comparison of the effect of fireline length on fire-induced horizontal wind magnitude by examining a mid-ABL slice. Following a region of brief acceleration, longer firelines produce a sharper drop across the plume, followed by a gradual convergence to average ABL conditions. This carries implications for local near-fire dynamics, as it results in stronger recirculation of smoke back to the firefront and higher relative smoke concentrations near the surface. As shown in Figure 5.6, this effect eases with downwind distance, as relative vertical smoke distributions converge to a fairly similar shape further away from the fire. The differences are most pronounced close to the fire. Notably the distribution maximum (in other words the mean smoke injection height) is nearly identical for all three firelines.

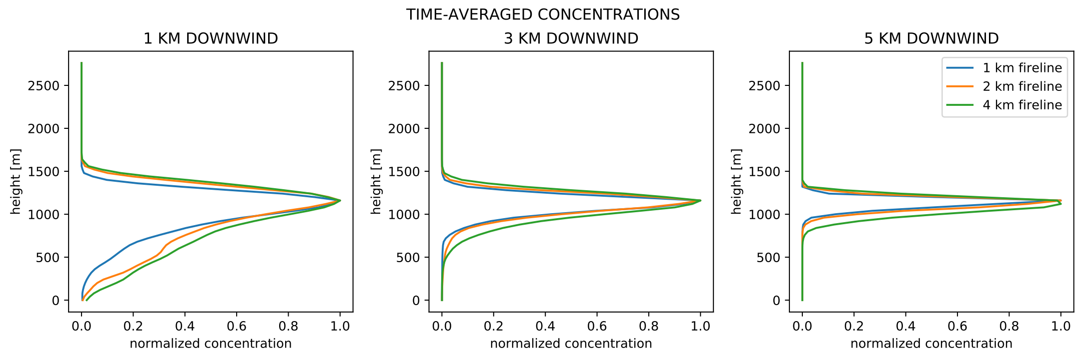

Figure 5.6: Normalized vertical CWI smoke distributions at 1 km (left), 3 km (middle) and 5 km (right) downwind of the fireline for various fireline lengths.

5.4 Modulation of the fire by passing ambient thermals

One interesting observation noted in the above Section 5.3, is the fact that the location of the horizontal wind convergence remains at the firefront, irrespective of the length of the fireline. From mass continuity perspective, a larger (or longer) updraft would require more air to be drawn towards the head of the fire. In part, this is supported by higher horizontal fire-induced wind magnitudes (Figure 5.1). However, if this was the only mechanism, one would expect formation of larger lateral vortices as well as greater fireline curvature for longer firelines. Yet neither of these features differ greatly between the various fireline length simulations.

In an attempt to explain how longer updrafts are supported, I repeated the trajectory analysis for the 4 km fireline now placing equally spaced sources upwind of the ignition. The results are shown in Figure 5.7: as clean air is accelerated towards the head of the fire, the flow breaks up into multiple cores. This multi-vortex structure is transient: individual cores are not stationary in space or time. This behavior is likely the result of interaction between the plume and the passing ambient ABL thermals.

Random velocity perturbation due to ABL turbulence allow for fireline "fingering", as certain portions of an initially uniform ignition line are advected faster/slower by local eddies relative to their surroundings. Because WRF-SFIRE spread algorithm responds to local winds, these turbulent fluctuations naturally distort the fireline, aiding the formation of multiple cores. While the parameterized fire behavior in WRF-SFIRE remains subject to evaluation, this tendency for more prominent fingering for longer firelines appears to be supported by models with explicitly resolved combustion [8]. In real life, this effect is likely further enhanced by fuel and surface heterogeneity.

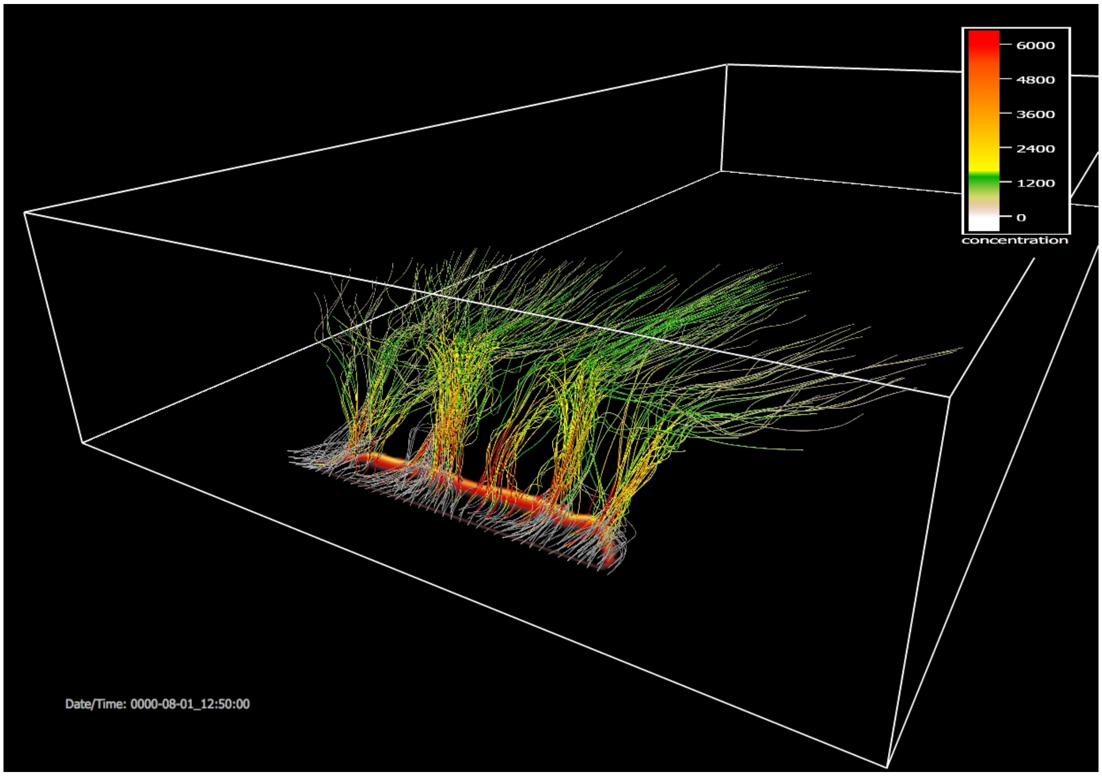

Figure 5.7: Trajectory analysis of clean air entrainment from behind a 4 km fireline. Individual paths are colored by smoke concentration. Figure produced using VAPOR software [13]

5.5 Plume mixing and the boundary layer

The trajectory analysis discussed in the previous sections suggests that most rapid mixing of the plume with clean environmental air occurs near the surface. In other words, based on the observed kinematics, one would expect most of the plume dilution (and, hence, cooling) to occur in the lower levels of the ABL as well.

Using the synthetic plume dataset (Chapter 4) I examined the vertical distribution of plume centerline potential temperature for each run. Shown in Figure 5.8 is a typical example of such a profile. It suggests that rapid cooling of the plume's core indeed occurs in the lower half of the ABL, after which its potential temperature remains largely unchanged (or on the order of random turbulent perturbations).

Apart from radiative cooling and effective mixing due to fire induced winds and vorticity, this may also be attributed to growth and widening of the smoke plume. As the edges of the plume move further away, the core becomes less and less affected by the ambient environmental conditions. A penetrative plume entering the free tro-

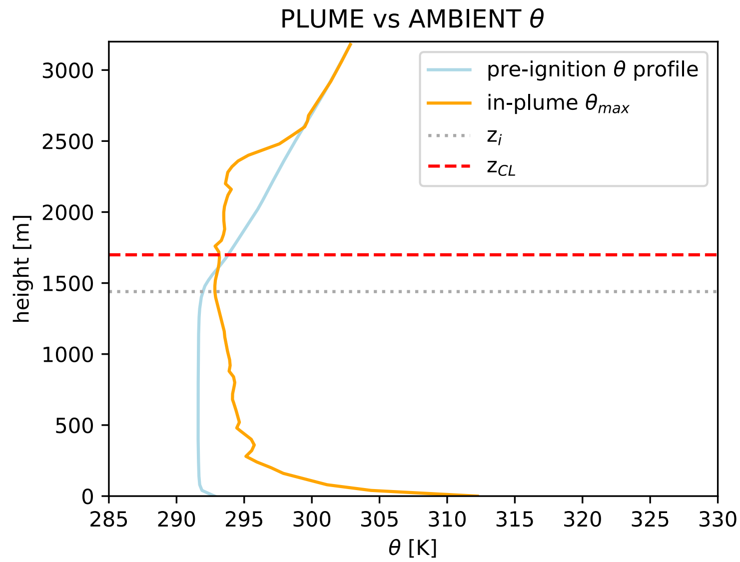

Figure 5.8: Vertical potential temperature profile of the mean ambient pre-ignition environment (light blue) and plume core (orange) temperature. Also shown: ABL height z_i before ignition (dotted grey) and smoke injection height z_{CL} (dashed red), based on the definition provided in Section 4.2

posphere above the ABL is still warmer then the surrounding atmosphere, hence it continues to move up into the stable layers. However, our LES simulations suggest that there is relatively little cooling and mixing occurring above the ABL. Following a momentum-driven overshoot the plume centerline eventually oscillates around its equilibrium height, where its core temperature roughly matches that of the ambient environment. This concept is best demonstrated with conserved variable plots, such as one shown in Figure 5.9.

Scatter point color in Figure 5.9 indicates the relative height (normalized by the height of the ABL) of the plume centerline, from which the dry static energy and tracer concentrations were obtained. Note that the theoretical mixing line connecting warm, smokey points (lower right) and the equilibrium cluster (upper left) is generally brown, suggesting that most dilution occurs below mixed layer top z_i.

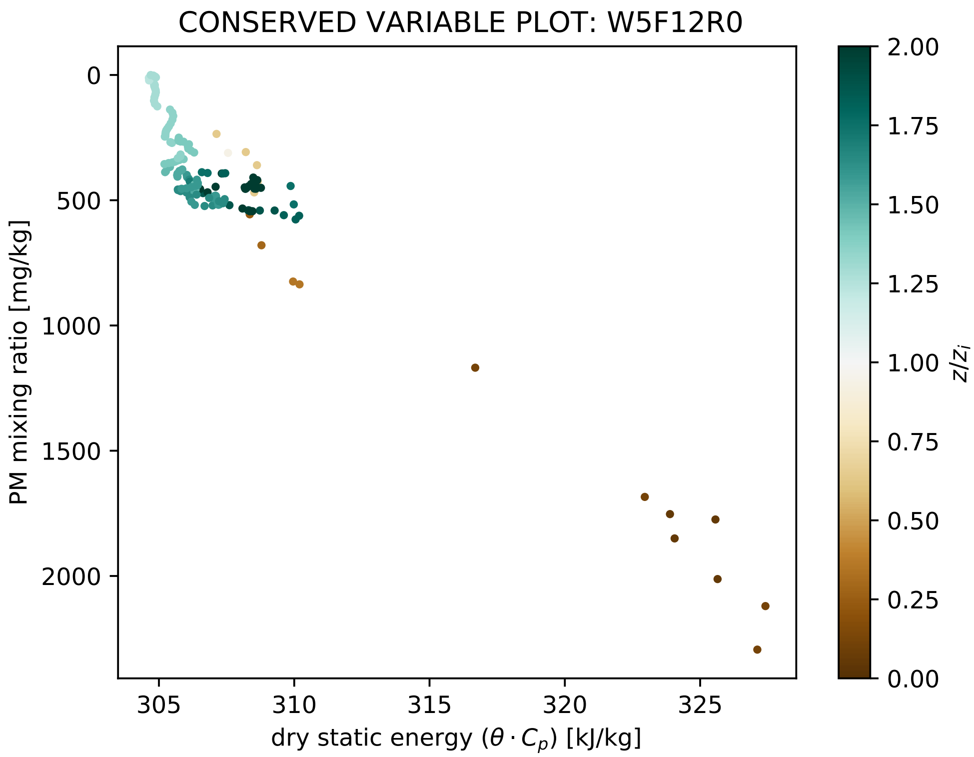

Figure 5.9: Dry static energy vs. concentration along the CWI plume centerline. Values are obtained at 20 min after simulation start. Scatter point color corresponds to relative (to ABL top z_i) height from which the values were obtained.

5.6 Summary

This chapter provided a qualitative discussion of several fire-atmosphere dynamical feedback mechanisms observed in LES plume data. Key features included the formation of horizontal flow convergence at the firefront and the associated lateral wind shear and vorticity. Fireline curvature and fingering appear to be influenced by ambient ABL conditions as well as fire geometry. Based on LES data, most of plume mixing and dilution occurs in the lower levels of the ABL, beyond which the plume core temperature remains largely unaffected by the ambient environment.

5.6.1 Big picture

Some of the fire-atmosphere interactions discussed in this chapter may help inform plume rise parameterization development (including the one introduced in this thesis).

However, most still lack evaluation with observational data. While this may require an exceptionally complex and expensive effort, numerical simulations, similar to those used in this chapter, could potentially facilitate planning field experiments. Optimizing instrument placement as well as anticipating weather impacts could help save cost and increase the chance of collected data being useful and relevant.

Chapter 6

Smoke injection height: A simple energy balance parameterization for penetrative plumes

This chapter introduces a new simple parameterization for predicting the mean injection level of wildfire smoke plumes. The method is derived from basic energy balance, using simplifying assumptions motivated by numerical insights from the previous Chapter 5.

6.1 Formulation

A common approach to predicting the final equilibrium centerline height of wildfire smoke is to first estimate the initial buoyant energy of the hot rising smoke [4, 6, 69]. After the smoke plume entrains surrounding ABL environmental air and cools, the remaining energy is spent doing work to push the cooled smoke plume up into the statically stable capping inversion.

The relationship between final and initial energies is often rewritten to show that the potential energy per unit mass (PE) of smoke penetration equals some fraction c_1 of initial heat released from the fire. In kinematic units, the initial heat input has units similar to kinetic energy per unit mass (KE). The empirical parameter c_1 is usually estimated based on concepts of entrainment into the rising smoke plume [17].

$$PE = c_1 KE \tag{6.1}$$

The PE of smoke-plume penetration into the capping inversion can be written as

$$PE = g'z' \tag{6.2}$$

where the penetration distance z' of the final equilibrium smoke centerline z_{CL} above reference height z_s (near the top of the well-mixed portion of ABL) is

$$z' = z_{CL} - z_s \tag{6.3}$$

The static-stability variable g' for the plume-penetration region is

$$g' = g\frac{\theta_{CL} - \theta_s}{\theta_s} = g\frac{\theta'}{\theta_s} \tag{6.4}$$

where θ_{CL} and θ_s are the potential temperatures of the ambient environment at z_{CL} and z_s, respectively, and $\theta_{CL} - \theta_s = \theta'$.

Typically, expression for plume buoyancy includes a potential temperature perturbation relative to ambient environment within the same vertical level in the atmosphere. However, as discussed in Section 5.5, based on LES data, little cooling occurs beyond upper ABL. This allows me to express θ' in Equation 6.4 in terms of plume core potential temperature θ_{CL} at injection level.

The KE can be estimated using a velocity scale w_f as

$$KE = 0.5w_f^2 \tag{6.5}$$

Typically, the bulk potential-temperature difference across the smoke-plume penetration region θ' is expected to be relevant for only the PE portion of Equation 6.1. However, I found from the LES runs for a wide range of fire and environment conditions that the KE also depends on the same potential temperature difference. This dependence can be expressed in the velocity scale:

$$w_f = \frac{I}{z_i\theta'} \tag{6.6}$$

This velocity scale is related to the fireline intensity parameter $I = \int^r H dr$, which is the kinematic heat flux into the atmosphere H integrated across the fireline depth r (in units of K m^2 s^{-1}), and to the mixed-layer depth z_i. The mathematical form of w_f is discussed further in Appendix B.2.

One could speculate that this interesting result is because smoke from a fire does not rise through a passive environment, as is often assumed for Briggs types of plume entrainment models. Instead, the fire and the environment interact in many complex ways. Some of these, detailed in Chapter 5 include: vertical-to-bent-over vortices on the ends of the fire line that rapidly mix environmental air into the buoyant smoke plume; modulation of fire intensity and fire updrafts by translation of ambient thermals across the fire line; plumes of enhanced convergence and updraft along the fire line; mass conservation as descending air beneath the extended smoke plume lowers the local mixed-layer depth; and possibly other factors.

Thus, Equation 6.1 becomes

$$g'z' = c_2 \left[\frac{I}{z_i \theta'} \right]^2 \tag{6.7}$$

where $c_2 = 0.5c_1$.

The above can be rearranged into the following form (see Appendix B.1):

$$z_{CL} - z_s = C \left[\frac{g\left(\theta_{CL} - \theta_s\right)}{\theta_s\left(z_{CL} - z_s\right)} \right]^{-\frac{1}{2}} \left\{ \frac{gI\left(z_{CL} - z_s\right)}{\theta_s z_i} \right\}^{\frac{1}{3}} \tag{6.8}$$

where C is a dimensionless empirical parameter. The factors in square and curly brackets with their corresponding powers have units of time and velocity, respectively. This relationship is plotted in Figure 6.1. It provides quite an acceptable fit to the data over a wide range of 140 combinations of fire and atmospheric conditions simulated. Scatter points largely fall close to 1:1 line, suggesting $C \approx 1$. Model bias will be addressed in further detail in Section 6.2.2.

Equation 6.8 suggests that the relevant length and temperature scales (z', θ') depend not on the capping inversion strength alone, or on the tropospheric lapse rate above the capping inversion alone, but on the bulk potential-temperature differences across the smoke-plume penetration region, z'. Equation 6.8 is implicit, in that the desired plume centerline equilibrium height z_{CL} appears in both the left and right sides of the equation. The plume centerline height also defines where θ_{CL} is retrieved from the atmospheric sounding; namely, z_{CL} is implicit in both Equation 6.7 and Equation 6.8. However, for any specific fire and environment conditions, values of z_{CL} are easily found by iteration (see Appendix B.4). Steps to estimating input parameters required for the proposed injection model from the LES data are summarized in Appendix B.3.

Alternatively, for a small sacrifice in accuracy, it is possible to obtain an explicit solution by considering an idealized version of the atmospheric profile, consisting of an adiabatic mixed layer, entrainment zone and a stable uniformly stratified free atmosphere above (Figure 6.2). In such case γ is defined as the overall potential temperature gradient of the free atmosphere and z_s as the height corresponding to the intercept of γ and the well mixed portion of the ABL profile. Then, using Equation 6.8,

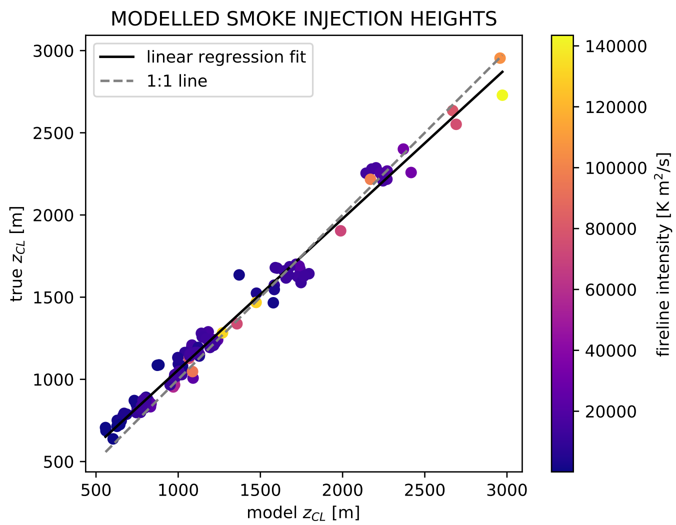

Figure 6.1: Comparison of true (as shown in Figure 4.2) and modelled (from Equation 6.8) smoke injection heights. Scatter points represent the 140 individual plume experiments within the LES dataset, with colors corresponding to fireline intensity I. Solid black and grey dashed lines denote linear regression fit and unity, respectively.

z_{CL} can be found explicitly as:

$$z_{CL} = \left[\frac{\theta_s}{g}\right]^{\frac{1}{4}} \left[\frac{I}{z_i}\right]^{\frac{1}{2}} \left[\frac{1}{\gamma}\right]^{\frac{3}{4}} + z_s \quad (6.9)$$

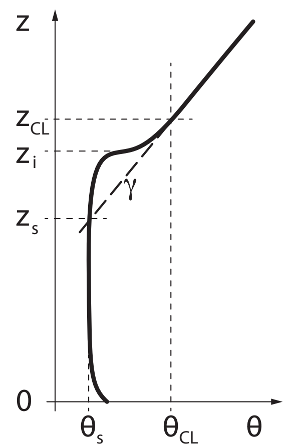

Figure 6.2: Idealized potential temperature profile θ vs. height with constant stable layer lapse rate. γ.

6.2 Model evaluation

To assess the accuracy of the proposed smoke injection height parameterization (Equation 6.8), I perform two sets of verification studies. The first approach is based on using the synthetic plume dataset from Chapter 4 to carry out model evaluation, bias correction and sensitivity analysis with idealized data. The second portion of this section applies my approach to the case study of a real prescribed burn (RxCADRE 2012) discussed in Chapter 3.

6.2.1 Numerical results

Shown in Figure 6.1 are "true" and parameterized smoke injection heights. The former is obtained directly from the LES, as per Section 4.2. The latter is determined iteratively using the proposed smoke injection height parameterization (see Appendix B.4 for implementation details).

Individual prediction errors do not appear to be a function fireline intensity, as indicated by scatter point color in Figure 6.1, or ambient winds (not shown). While overall the scheme's performance is encouraging, the small discrepancy between the unity and regression lines suggests a linear bias. This can be remedied by applying bias correction using regression parameters from the fit shown in Figure 6.1. This optimized model produces errors on the order of 20 - 30 m for equilibrium plume centerline height z_{CL}, as suggested by the interquartile range shown in Figure 6.3d. Model bias will be

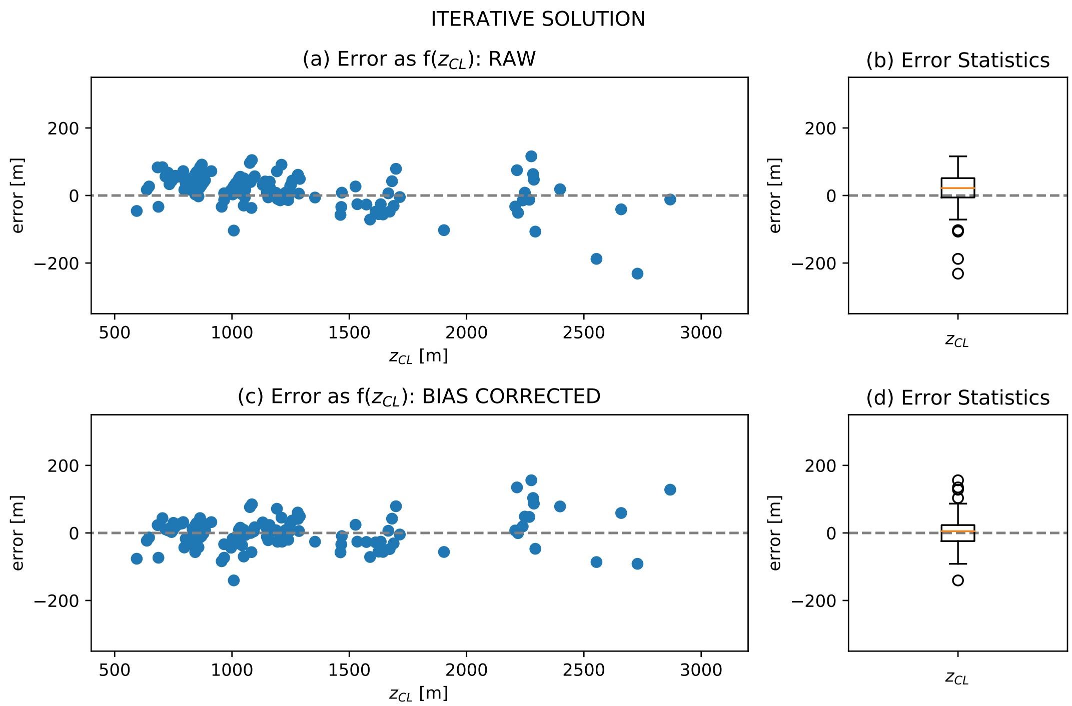

Figure 6.3: Performance of the smoke injection height parameterization based on the iterative solution (Equation 6.8). (a) Non-bias corrected prediction error (true - modelled z_{CL}) as a function of z_{CL}. (b) Error statistics for non-bias corrected values. The box and whiskers span IQR and 1.5 x IQR, respectively. Median value shown in orange. (c) Bias-corrected prediction error as a function of z_{CL}. (d) Error statistics for bias-corrected values.

addressed in further detail in Section 6.3.

Given smooth averaged profiles from the synthetic dataset and excluding condition **R8** (adiabatic free atmosphere), the explicit solution using Equation 6.9 offers comparable accuracy to the iterative version for both raw and bias corrected datasets (Figure 6.4) . I address the limitations of using the explicit approach in Section 6.4.1.

6.2.2 Model sensitivity

To asses how sensitive the smoke injection model performance is to the particular choice of bias correction parameters, I partition my original plume dataset into training and testing groups through random sampling. I obtain the linear bias correction parameters using training data only (80% of runs). I then apply our bias-corrected iterative solution to the test group (remaining 20% of the runs) and assess model

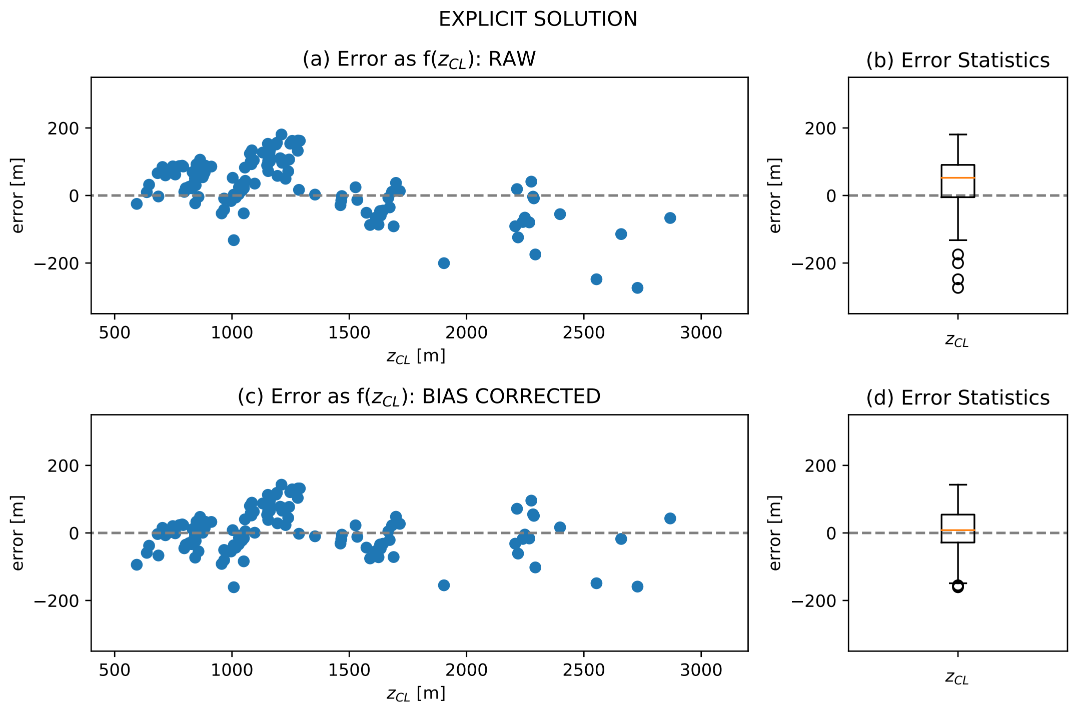

Figure 6.4: Performance of the smoke injection height parameterization based on the explicit solution (Equation 6.9)). (a) Non-bias corrected prediction error (true - modelled z_{CL}) as a function of z_{CL}. (b) Error statistics for non-bias corrected values. The box and whiskers span IQR and 1.5 x IQR, respectively. Median value shown in orange. (c) Bias-corrected prediction error as a function of z_{CL}. (d) Error statistics for bias-corrected values.

accuracy. Figure 6.5 summarizes the performance and sensitivity of the proposed parameterization, based on 10 trials of sampling with replacement. Consistently high Pearson correlation shown in the trial histogram in Figure 6.5c, are encouraging, and suggest that the particular choice of simulations used in bias correction does not have a strong impact on accuracy.

6.2.3 Evaluation with observations

Next, I apply the proposed parameterization to a real-life case-study. I use observational data from the RxCADRE L2G prescribed burn (Section 2.3) and it's numerical simulation detailed in Chapter 3.

Recall the strip headfire pattern used to ignite the grass lot (shown in Figure 3.1). I estimate the burn's input fireline intensity parameter I for this complex ignition in two

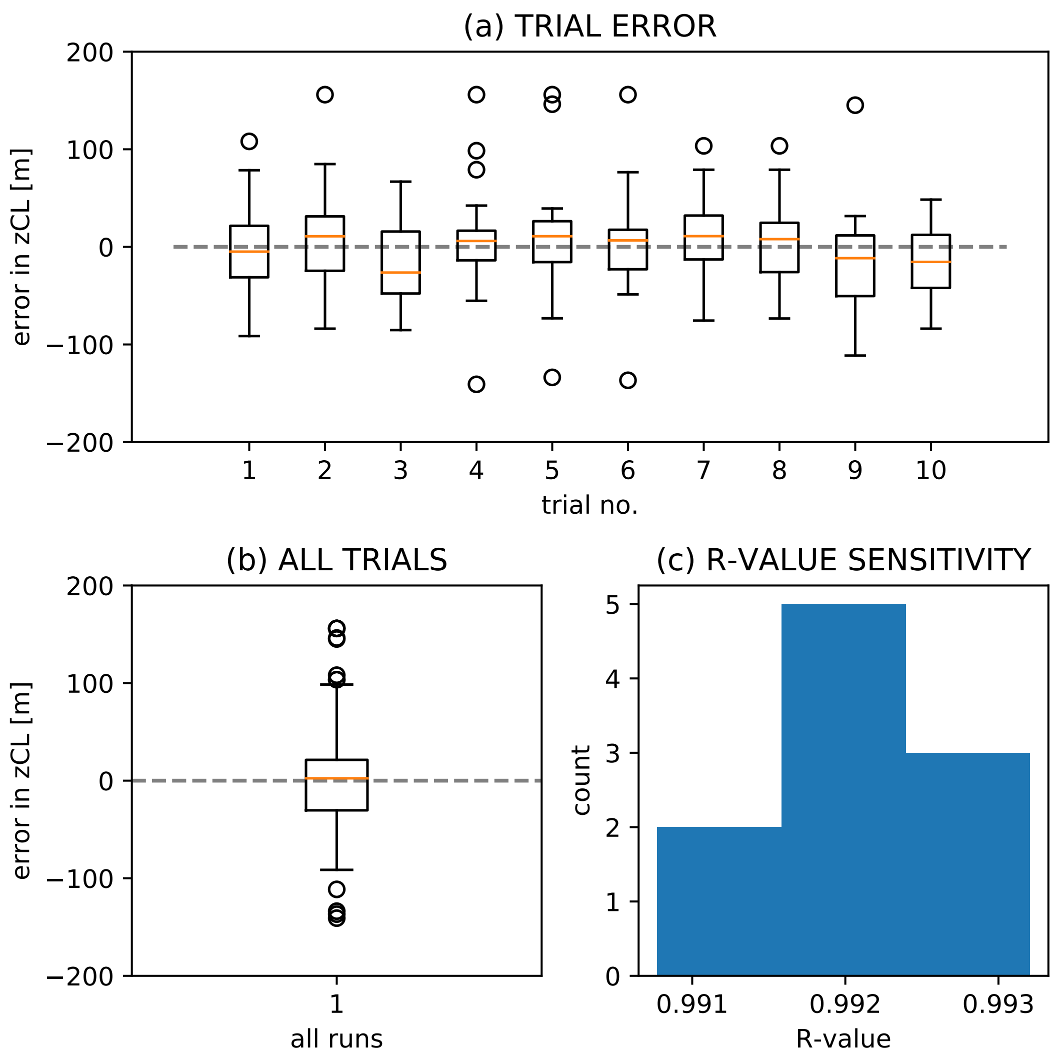

Figure 6.5: Analysis of model sensitivity to the choice of bias correction parameters. (a) Error distributions for individual trials using independent (test) data. (b) Error distribution for all trials using independent (test) data. (c) Sensitivity of R-value (correlation coefficient) for all trials.

different ways: from raw data collected during the burn as well as from the numerical simulation. The observations-based value I_{obs} is derived from the integral heat flux data obtained from the Highly Instrumented Plots (HIPs) fire behavior package (FBP) sensors [28]. I use the provided time-integrated values, averaging between all sensors with confirmed fire at the sensor location (as indicated by video footage [7]). I then obtain the mean value (in kinematic units) of 236 K ms^{-2} and multiply it by the average measured rate of spread (ROS) value of 0.38 m s^{-1} [7] for the same sensors to convert to spatially-integrated heat flux for a single fire line. I assume that this value is representative of the remaining three firelines, hence:

$$I_{obs} = 236 \cdot 0.38 \cdot 4 = 359 \tag{6.10}$$

in units of K m^{2}s^{-1}. Note, that raw data for both heat fluxes and ROS values have extremely large associated uncertainties. Observed ROS values vary by nearly a factor of two, depending on the measurement technique used. While I have included only locations with ignition confirmed by video footage in my calculations, heat fluxes still vary up to a factor of four between sensors.

For comparison, I also obtain an LES-based integrated fireline intensity value I_{LES}. Due to wind shear, as measured by the sounding launched prior to the burn, the CWI direction at the surface differs from the one used to estimate CWI smoke. I_{LES} was, hence, estimated by assuming 125 degree rotation of LES fields, based on the lowest available wind direction measurement. I use trapezoidal rule to numerically integrate the mean crosswind heat flux along the depth of the fireline (see Appendix B.3) and find $I_{LES} = 1002$ K m^{2}s^{-1}.

I apply the iterative solution (Equation 6.8) to find two z_{CL} estimates based on I_{obs} and I_{LES}, and compare them to the CWI smoke injection height obtained from the LES. The results are shown in Figure 6.6. The parameterized injection heights are underpredicted by 20 m and 70 m for LES- and observations- derived I values, respectively.

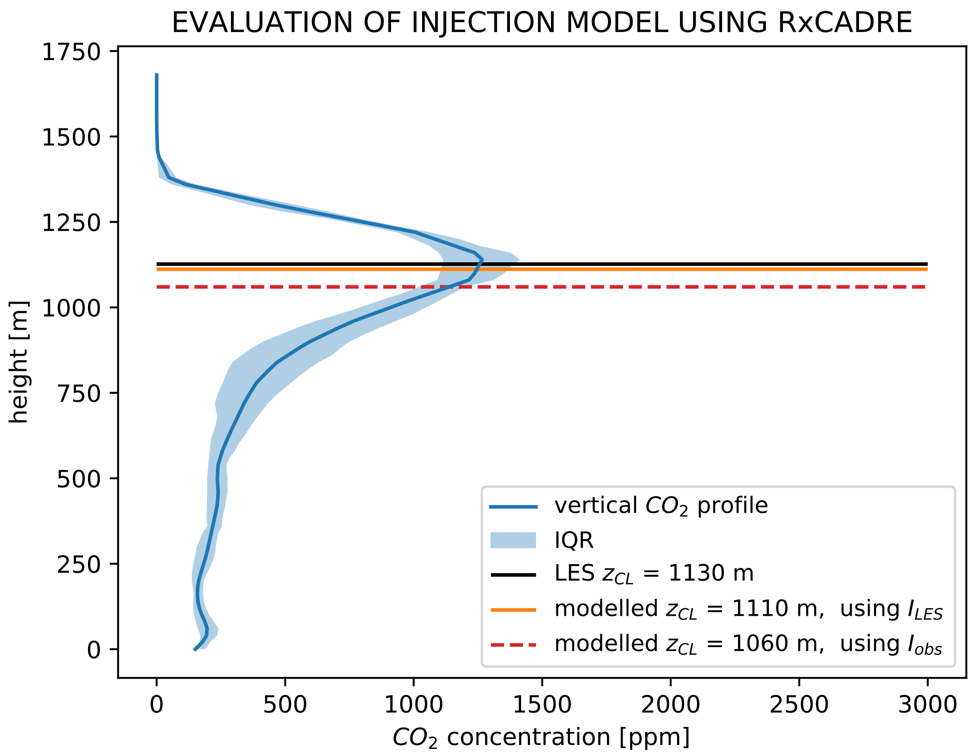

Figure 6.6: Model evaluation using a case-study of a real prescribed burn (RxCADRE 2012). CWI smoke concentration profile shown in blue. "True" z_{CL} obtained directly from LES shown in solid black. Solid orange and dashed red lines correspond to z_{CL} estimates obtained using the iterative solution of the proposed smoke injection height parameterization (Equation 6.8), based on LES- and observations- derived fireline intensities, respectively.

6.3 Discussion

6.3.1 Context and applications

The above model evaluation indicates encouraging performance for the proposed smoke injection parameterization (Equation 6.8) at little computational cost. An additional advantage of the method is that it does not require making simplifying assumptions regarding the shape and heat flux distribution of the fire. This allows me to easily apply this approach to complex heat sources, such as one produced with the strip head fire ignition pattern during the RxCADRE L2G prescribed burn (Figure 3.1).

Notably, this also makes direct comparison of the proposed method with existing schemes difficult. A vast majority of established plume-rise parameterizations consider a simplified fire geometry and a uniform (or total) heat flux as input parameters. [4, 6, 9, 20, 64]. Hence, applying these methods to my synthetic data would require making many simplifying assumptions regarding the heat source. Subsequent intercomparison would hardly be useful, as each scheme's performance would largely reflect how well the inputs are calibrated to the given plume-rise formulation.

Unlike most existing plume rise parameterizations, [6, 20, 64] I focus on a CWI centerline. The proposed scheme can be viewed as a "bulk method", having some common ground with the thermodynamic approach used in the FireWork modelling framework [4, 9] and the energy balance approach proposed by Sofiev et al. [69]. More specifically, I make no attempt to predict the full evolution of the rising plume centerline velocity or temperature before it reaches its equilibrium height. Rather, I focus on the energy balance of the plume within a "penetration layer".

Through analysis of the 140 LES experiments for plumes under variable fire and atmospheric conditions detailed in Chapter 5, I found that near-surface and boundary-layer plume dynamics are extraordinarily complex. While some aspects of plume mixing can be reasonably accounted for by making common entrainment assumptions, complicated features resulting from fire-atmosphere coupling, such as formation of lateral vortices and fireline wind convergence zone, are difficult to parameterize directly. Hence, I apply the energy balance approach to a layer well above the surface, starting from a reference height z_s close to the top of the ABL.

As noted in Section 6.1, the implicit functional form of my solution (Equation 6.8) can be interpreted as a characteristic timescale multiplied by the characteristic velocity scale w_f. By rearranging Equation 6.7 and substituting Equation 6.8 for z' it can be shown (see Appendix B.2) that the two expressions for w_f are equivalent, namely:

$$w_f = \left[\frac{I}{z_i \theta'}\right] = \left[\frac{gIz'}{\theta_s z_i}\right]^{\frac{1}{3}} \tag{6.11}$$

The scaling relationship between vertical plume velocity and cubic root of fire heat has been previously established with both Rio's and Freita's models [20, 64] (discussed in Section 2.2), although my formulation includes different variables inside the radical. While both of my forms for w_f and both model formulations (the simplified Equation 6.7 and the expanded Equation 6.8) are mathematically equivalent, conversion from one form to another requires repeated exponentiation. This results in large prediction errors; hence, for practical applications, the full Equation 6.8 should be used.

6.3.2 Dimensionless relationship

As discussed in Section 6.1, I can obtain an explicit solution for z_{CL} by making additional assumptions about the vertical profile of potential temperature above the ABL. This allows me to reduce Equation 6.9 to a similarity relationship with two dimensionless groups $\overline{z}$ and $\overline{H}$, denoting the left-hand side (LHS) and right-hand side (RHS) of Equation 6.12, respectively. Nondimensional $\overline{z}$ and $\overline{H}$ are linearly related, as shown in Figure 6.7. The simple relationship suggests that my modelling results could fairly easily be scaled to a wider range of fire and atmospheric conditions, beyond those captured by the synthetic dataset presented in Chapter 4.

$$\underbrace{\frac{z'}{z_i}}_{\overline{z}} = \underbrace{\left[\frac{\theta_s}{g\gamma^3}\right]^{\frac{1}{4}} \left[\frac{I}{z_i^3}\right]^{\frac{1}{2}}}_{\overline{H}} \tag{6.12}$$

6.3.3 Model bias

The raw, non-bias- corrected form of the proposed parameterization suffers from a positive bias for tall plumes, as suggested by Figure 6.3c and Figure 6.4c. In other words, z_{CL} is overpredicted for plumes injected high above the ABL. One could speculate that this is due to the simplifying assumption that most of the cooling, mixing, and dilution occurs below the reference level z_s in upper portion of the ABL.

As the distance between z_s and z_{CL} increases for tall plumes and as the smoke travels further into the free atmosphere, this assumption becomes increasingly less accurate. Additional radiative cooling and entrainment of ambient air is, therefore, unaccounted for, resulting in over-prediction for z_{CL}.

This issue may partially be corrected for my dataset with the applied bias-correction. However, cases with strong shear turbulence and active smoke mixing above the ABL are still likely to be overestimated.

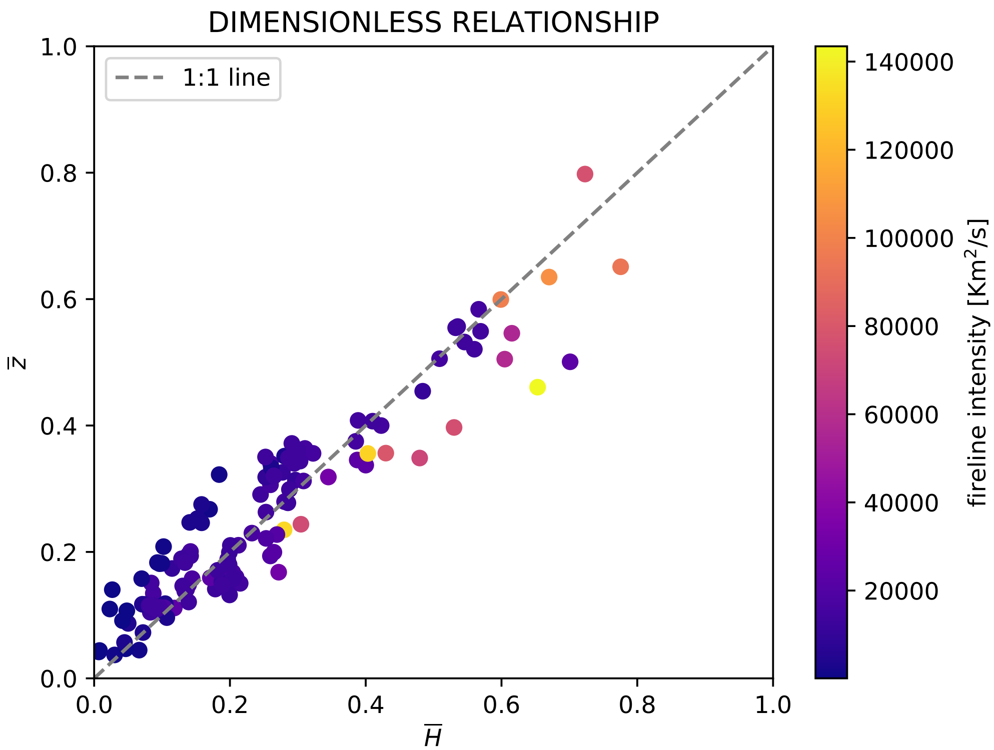

Figure 6.7: Similarity solution for dimensionless groups $\overline{H}$ and $\overline{z}$, corresponding to the RHS and LHS of Equation 6.12, respectively. Scatter points represent individual LES runs, colored by fireline intensity parameter I. 1:1 line is shown in dashed grey for reference.

6.4 Summary

In this chapter I present a simple parameterization (Equation 6.8) for predicting CWI smoke-plume centerline height from a wildfire of an arbitrary shape and intensity. I constrain and evaluate the proposed approach using the synthetic LES-derived plume dataset developed for a wide range of fire and atmospheric conditions detailed in Chapter 4. Based on the results of cross-evaluation with LES data as well as a real prescribed burn case study, the parameterization offers reasonable accuracy at little computational cost.

6.4.1 Limitations

The most significant limitation of the proposed smoke injection height parameterization is that it applies only to smoke plumes with no water vapor condensation. Latent heat effects are not considered. Hence, smoke injection level for extreme pyroconvective events (e.g. flammagenitus clouds [52]) will likely be grossly under-predicted with the given formulation.

Another limitation is the inherently implicit form of the full model Equation 6.8. While I have not encountered any issues using an iterative solver to find z_{CL}, atypical (or extremely noisy) ambient atmospheric soundings could potentially affect convergence. The explicit form (Equation 6.9) derived using the idealizing ambient sounding (Figure 6.2) offers a possible solution for such cases. However, it fails for weakly stable and adiabatic free atmosphere (eg. condition R8 in Figure 4.1), as θ_s is extrapolated into lower levels of ABL.

Lastly, the parameterization has been developed and tested only for typical daytime fair-weather atmospheric conditions. I have not assessed model performance for stable night-time atmospheric profiles or in the presence of strong vertical windshear.

6.4.2 Big picture

Given the above limitations, a reasonable question to ask is: **how useful is the proposed approach?** In its current form (without latent heat effects), it's unlikely to be suitable for large-scale applications (e.g. global chemical transport models). However, it has the potential to improve regional air quality tools, since wildfire emissions sources are largely dominated by in- or near- ABL non-condensing smoke plumes (Section 2.3). The method can also be applied as a classifier to distinguish penetrative vs. non-penetrative plumes, which is often vital for subsequent dispersion modelling [69], as discussed further in Chapter 7.

Given the energy-balance formulation of this plume rise parameterization, it may be possible to incorporate latent heat effects by including an extra PE term in Equation 6.1. Similarly to the iterative process for finding a level of neutral buoyancy with Equation 6.8 using potential temperature, it may be possible to predict plume condensation level using ambient humidity profile. A big obstacle to this development, however, is ensuring that WRF-SFIRE can capture aerosol microphysics, while accurately simulating input fire moisture fluxes. As noted in Section 3.2.1, my model evaluation of fire behavior within WRF-SFIRE is fairly primitive. Greater confidence in fire input parameters, following comprehensive evaluation of model microphysics, would most certainly pave the way for further plume rise parameterization improvement.

Chapter 7

Beyond injection height: Modelling the distribution of smoke in the atmosphere

The parameterization introduced in Chapter 6 enables one to predict the initial centerline height of a wildfire smoke plume. However, wildfire emissions are actually deposited over a greater depth between the surface and the equilibrium level, with significant portion remaining above the mean smoke injection height. Moreover, the physics that govern mixing and dispersion within the ABL differ from those in the entrainment layer and the free troposphere. Hence, in order to accurately predict downwind concentrations from a wildfire, we first need to know: **(i) Which plumes will penetrate the ABL?** Once penetrative plumes are identified, we then need to determine: **(ii) How far above the equilibrium level does the plume extend?** and **(iii) What fraction of wildfire emissions remains in the ABL?**. The following sections aim to answer these questions using ideas inspired by numerical experiments of Chapter 5, equations derived in Chapter 6 and synthetic data from Chapter 4.

7.1 Plume classification

Previous Chapter 6 applied an energy balance parameterization to predict the mean smoke injection height z_{CL} of a given penetrative plume. For this purpose, only plumes rising above ABL top z_i were included in the synthetic plume dataset used to constrain and evaluate the approach (see Table 4.3). In this section, I step back and consider all performed simulations, to determine whether the same equations can also be used to classify penetrative vs. non-penetrative plumes.

The synthetic dataset described in Chapter 4 consisted of 140 runs and excluded 7 simulations, where the plume remained trapped in the ABL (see Table 4.3 and Table 7.1). I determined this by visual analysis of CWI centerline and smoke fields. The excluded plumes typically exhibited oscillatory or irregular centerline behavior (within the ABL) with little or no smoke injected above z_i (see sample ABL plume in Appendix A.2). For several combinations of fire and atmospheric conditions, however, making the distinction was challenging. For this reason, I included these "marginally-penetrative" plumes in the dataset.

In real-world applications, classification is a fundamental first step in plume rise parameterization process [69]. A viable automated method for categorizing penetrative vs. non-penetrative plumes requires that the distinction be made based on available input parameters, rather then smoke observations (as such are typically not available at the time of making a forecast).

Conveniently, I can use Equation 6.8 to obtain a z_{CL} estimate for any combination of input parameters without prior knowledge of plume type. It can, hence, be applied as a classifier by requiring that for a penetrative plume

$$z_{CL} > z_{i+} \tag{7.1}$$

where z_{i+} denotes the height of the upper edge of the numerical grid box (or ambient atmospheric sounding) containing z_i. In other words, this definition ensures that z_i and z_{CL} are not in the same vertical model level. If this condition is not satisfied, the plume is assumed to be non-penetrative.

This approach correctly classifies all non-penetrative plumes that had been identified by visual analysis (Table 7.1). In addition, several plumes exhibiting marginal behavior are also classified by Equation 7.1) to be non-penetrative.

For the purpose of subsequent dispersion modelling within real-world applications, non-penetrative plumes (i.e. all plumes listed in Table 7.1) would be assumed to become uniformly mixed in the vertical within a few convective turnover distances downwind of the fire. Turbulent eddies within the ABL produce a well-mixed layer, resulting in relatively homogeneous vertical distribution of pollutants between the surface and z_i. In contrast, predicting the downwind smoke behavior for plumes that extend above z_i, spanning the ABL, the entrainment layer, and/or the free troposphere, is significantly more difficult. The goal of the following sections is, therefore, to parameterize the vertical smoke profiles of the remaining 133 synthetic plumes classified as "penetrative" by Equation 7.1.

Table 7.1: Identifying non-penetrative plumes using visual analysis vs. automated classification. Plume name denotes wind condition **W**, fuel type **F** and initial atmospheric profile **R**.

Plume	Visual analysis	Automated classification
W5F9R1	✓	✓
W5F1R3	✓	✓
W5F8R3	✓	✓
W5F9R3	✓	✓
W5F1R7	✓	✓
W5F8R7	✓	✓
W5F9R7	✓	✓
W5F1R0		✓
W5F1R1		✓
W5F8R1		✓
W5F10R3		✓
W5F11R3		✓
W5F1R4		✓
W5F11R4		✓

7.2 Predicting smoke distribution above z_{CL}

From hereon, for the identified penetrative plumes I will treat smoke injection height z_{CL} and plume penetration distance z' as "known". Hence, I will use the LES-derived, rather than estimated z_{CL} and z' values. This ensures that the errors associated with modelling the vertical smoke profile $C(z)$ are independent of mean plume rise parameterization.

7.2.1 Determining maximum rise

Recall from Section 5.5, that above ABL the **plume core** (represented by the centerline) experiences little mixing with the ambient environment. Yet due to momentum acquired during the initally-buoyant rise, the plume typically overshoots its equilibrium level. Naturally, one can expect some of the smoke to be detrained in the atmospheric levels between the peak centerline height z_{top} and z_{CL}. In other words, z_{top} is potentially a useful estimate for the upper edge of a given CWI smoke profile.

Amplitude of the initial centerline oscillation about its equilibrium level is likely to be roughly equal to the original "displacement" of the plume from z_{CL}. Therefore, I hypothesize that:

$$z_{top} = z_{CL} + z' \tag{7.2}$$

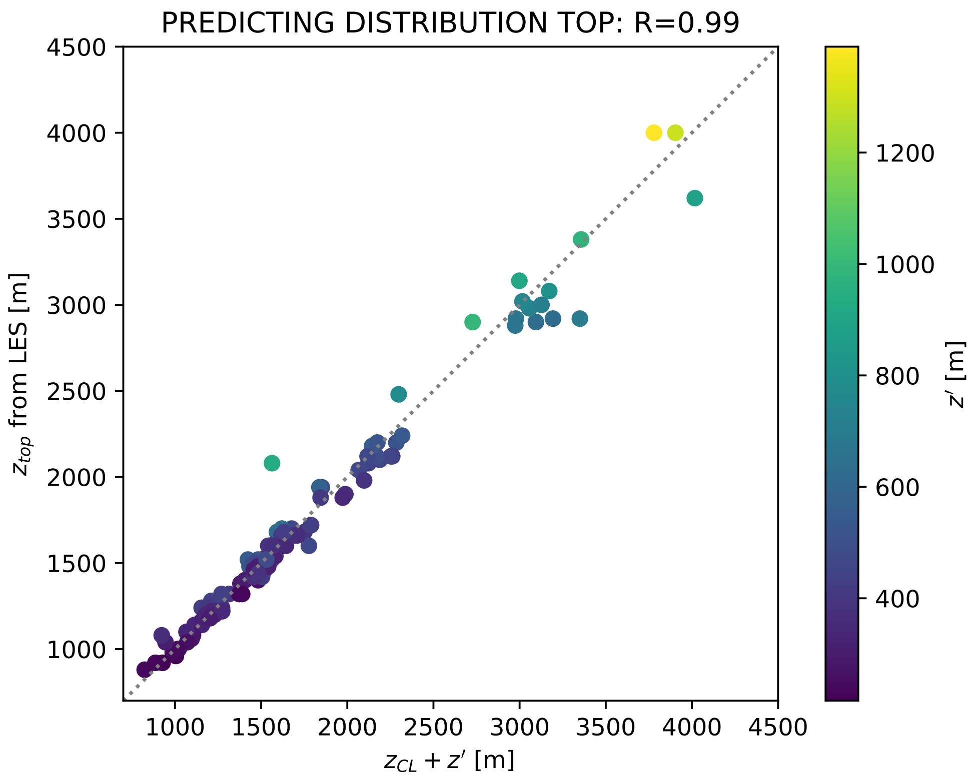

Figure 7.1: Estimation of plume top z_{top} using plume penetration distance z'. "Truth" value was obtained from the LES dataset of 133 penetrative plumes, assuming z_{top} is the height at which smoke concentration is equal to 0.15% of the maximum value at z_{CL} ($\approx$3 standard deviations from the peak for Gaussian distributions). Colors correspond to penetration distance z'. Unity slope (dashed grey) is shown for reference.

This relationship is plotted in Figure 7.1, suggesting a good fit to LES data (Pearson correlation coefficient R=0.99). To determine the "true" top of CWI smoke profiles from LES , I defined the upper plume edge such that $C(z_{top}) = 0.0015 \cdot C(z_{CL})$. This, assuming Gaussian spread, corresponds to a smoke concentration three standard deviations from the peak. Based on this definition, the scatter points generally fall on or close to the unity line (dashed grey), suggesting the above hypothesis (Equation 7.2) is not unreasonable. Greater overshoot distance (as indicated by scatter point color) tends to be associated with increased scatter about unity. However, overall this appears to be a viable approach for predicting z_{top}.

7.2.2 Determining spread above z_{CL}

In order to model CWI smoke distribution above the mean injection level, I assume that the concentration drop off between the maximum at z_{CL} and z_{top} is roughly Gaussian. In such case, the upper portion of the smoke profile $C(z)$ can be described with the following equation:

$$C(z)|_{z>z_{CL}} = Ae^{-(z-\mu)^2/\left(2\sigma_{top}^2\right)} \tag{7.3}$$

where $A = C(z_{CL})$ is the distribution amplitude, $\mu = z_{CL}$ is the location parameter, and σ_{top} is a scale factor representing mean smoke spread above z_{CL}.

Typically, actual absolute concentration values of wildfire emissions are calculated outside of plume rise parameterization scheme (by corresponding fuel consumption and emissions modules) within the host smoke modelling framework. Therefore, for the purpose of this chapter I assume $C(z_{CL})$ is known. For air quality applications, the **normalized** dimensionless smoke profiles $C_N(z)$ can be obtained by setting $A = 1$.

Based on the definition of z_{top} from Section 7.2.1 (i.e. upper edge of the plume corresponds to concentrations 3 standard deviations below the maximum), I can estimate σ_{top} as:

$$\sigma_{top} = \frac{(z_{top} - z_{CL})}{3} = \frac{z'}{3} \tag{7.4}$$

Given Equation 7.4 and assuming Gaussian functional form of Equation 7.3, I can parameterize the smoke distribution above z_{CL} using only z' value obtained from Equation 6.8. Sample fits produced with this approach are shown in Figure 7.2 and Figure 7.3 for typical low and high wind conditions, respectively.

For the low wind case (Figure 7.2), I have intentionally selected a run with appreciable error in z_{top}. Notably, as indicated by the relatively small discrepancy between the modelled (orange) and LES-derived (dotted grey) curves above z_{CL}, this error doesn't translate into large differences between the distributions.

The vertical smoke profile in Figure 7.2 appears to be well-captured by a single Gaussian curve. Namely, the profile below and above z_{CL} can be modelled using the same σ. In contrast, the distribution in Figure 7.3 is markedly wider below z_{CL} than above. The following section explores possible explanations for this behavior.

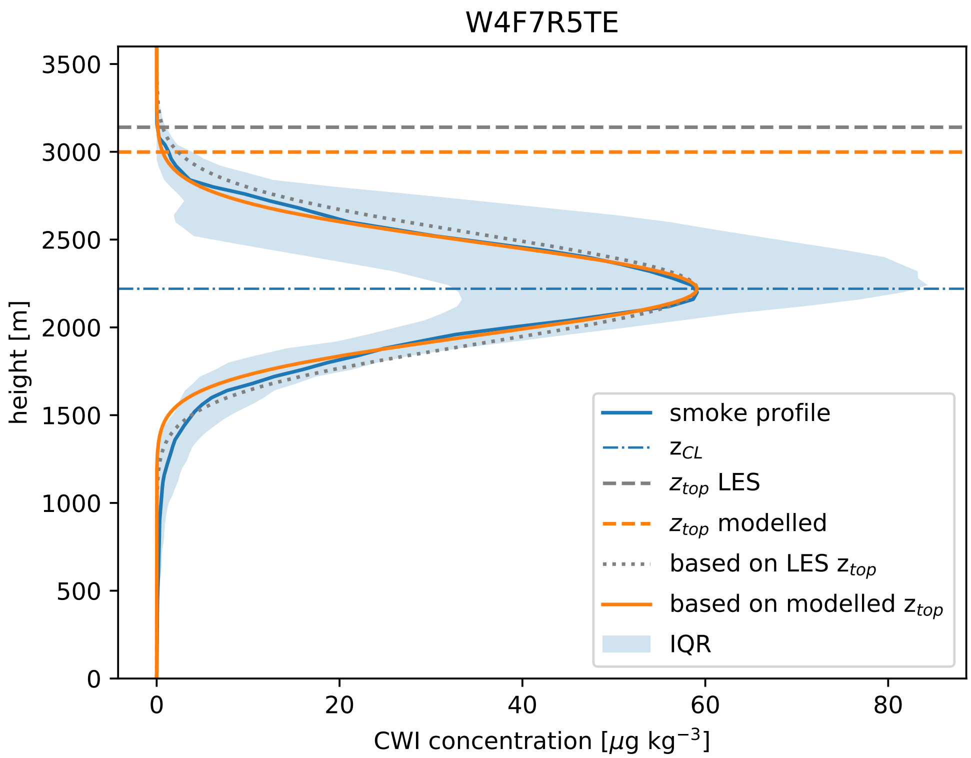

Figure 7.2: LES-derived (blue) and parameterized (orange) smoke distribution under low (4 ms$^{-}1$) ambient wind conditions. LES-derived and parameterized z_{top} values are plotted in dashed orange and dashed grey, respectively. Also shown, IQR range of LES smoke profile (blue shading), z_{CL} (dash-dotted blue) and parameterized distribution based on LES-derived z_{top}.

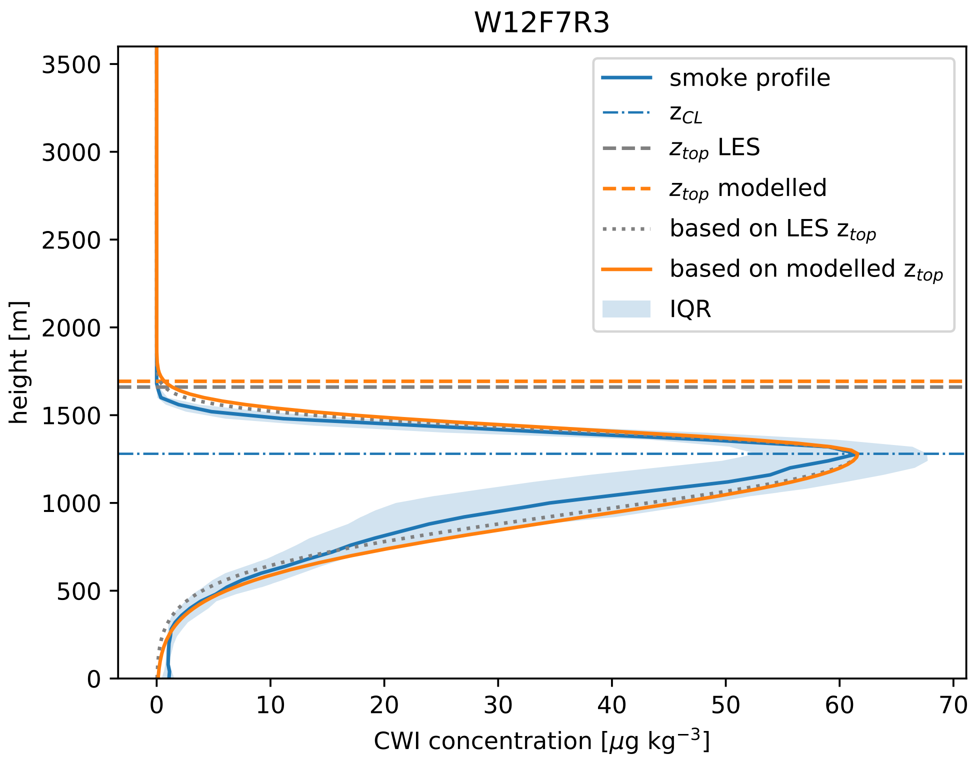

Figure 7.3: LES-derived (blue) and parameterized (orange) smoke distribution under high (12 ms^{-1}) ambient wind conditions. LES-derived and parameterized z_{top} values are plotted in dashed orange and dashed grey, respectively. Also shown, IQR range of LES smoke profile (blue shading), z_{CL} (dash-dotted blue) and parameterized distribution based on LES-derived z_{top}.

7.3 Predicting smoke distribution below z_{CL}

7.3.1 Accounting for ambient environmental mixing in the ABL

We know from boundary layer theory that mixing within the ABL is typically governed by surface buoyancy flux and wind stress [70]. Due to strong near-surface shear, high wind conditions are typically associated with mechanically-generated turbulence (forced convection). In contrast, under calm conditions mixing is largely the result of continual turnover of buoyant thermals rising from the surface (free/convective turbulence). Often the relative importance of each type of convection is expressed as the dimensionless Richardson number Ri, corresponding to the ratio of buoyant and shear production of TKE.

In a similar fashion, LES data suggests that the width of the smoke distribution below z_{CL} appears to be a function of the relative magnitudes of fire updraft and ambient convection. Previously, in Section 6.3, I introduced an expression for the characteristic fire velocity w_f (Equation 6.11). Using w_f I can estimate the relative (to background thermals) updraft speed w_r as

$$w_r = w_f - w^* \tag{7.5}$$

where w^* is the Deardorff velocity scale, representing the mean vertical velocity of background thermals, given by

$$w^* = \left[\frac{g z_i S}{T_v}\right]^{\frac{1}{3}} \tag{7.6}$$

T_v and S denote virtual absolute temperature of the ABL and kinematic surface sensible heat flux, respectively. To obtain a characteristic horizontal ABL wind U_a, I use the average value from the ambient sounding between $0.5z_i$ and z_i. I exclude the bottom half of the ABL, as various roughness lengths associated with different fuel types produce variable surface layer depths. I then define a dimensionless ratio R_w, such that

$$R_w = \begin{cases} \frac{U_a}{w_r}, & \frac{w_f}{w^*} \geq 1.5 \\ \frac{U_a}{w_f}, & \frac{w_f}{w^*} < 1.5 \end{cases} \tag{7.7}$$

This conditional formulation ensures that R_w remains reasonable for cases with $w_f \approx w_r$. I determined the absolute threshold based on informal sensitivity analysis of LES data. Finally, I define the spread of the smoke profile below z_{CL} as:

$$\sigma_{bot} = R_w \sigma_{top} \tag{7.8}$$

Substituting σ_{bot} in place of σ_{top} in Equation 7.3, I can obtain the bottom portion of the smoke profile, as shown in Figure 7.2 and Figure 7.3. For low wind case (Figure 7.2) $R_w \approx 1$, producing a roughly symmetrical (about z_{CL}) Gaussian curve. For high wind case with $R_w > 1$ (Figure 7.3) there is an obvious skew in the distribution, with larger portion of smoke remaining in the ABL.

In the following section I examine how accurately this approach partitions the smoke between the ABL and the free troposphere under the variety of fire and wind conditions captured by the synthetic plume dataset.

7.3.2 Estimating errors

Using the approach introduced in this chapter, I parameterize the normalized vertical smoke distributions of all penetrative plumes in the LES dataset (as identified by the classification condition in Section 7.1). To isolate potential sources of error, I calculate two separate solutions using (i) LES-derived z_{top} and (ii) modelled z_{top} values. Sample curves representing the two solutions are plotted in dotted grey and solid orange in Figure 7.2 and Figure 7.3.

For each solution, I then calculate mean absolute error (MAE) separately for values below and above z_i, as well as over the entire depth of the smoke column. The results are summarized in Figure 7.4.

As expected, LES-derived z_{top} generally produces slightly more accurate solutions than the modelled z_{top}, though the differences are not statistically significant. Overall, the proposed approach appears to properly partition smoke between the ABL and the free atmosphere above, accurately allocating 90-95% of normalized emissions.

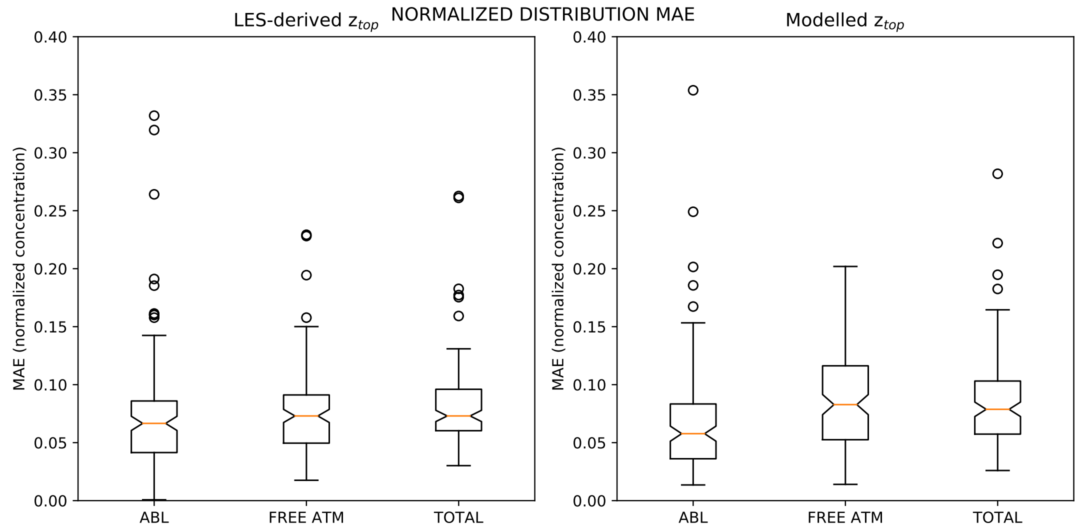

Figure 7.4: MAE of parameterized smoke distributions $C_N(z)$ based on LES-derived (left) and modelled (right) z_{top}. Orange line corresponds to median value. The box and whiskers span IQR and 1.5×IQR, respectively, with the notch denoting the 95% confidence interval of the median (median±1.57×IQR/n$^{\frac{1}{2}}$).

7.4 Distributing smoke laterally

The parameterizations presented in the previous and current chapters focused entirely on CWI smoke vertical distributions. This approach is largely motivated by its most likely application: a smoke modelling framework.

My numerical plume dataset contained fires with lengths ranging from 1 to 4 kilometers in the cross-wind direction. For comparison, typical grid-spacing of a regional smoke dispersion modelling system is $\approx$10 km [9, 66]. While common in the real world, the simulated fires captured by the dataset would, therefore, be treated as a subgrid-scale effect within these systems. This means that the smoke distribution in the cross-wind (y) direction would be considered to be uniform across the width of the cell y containing the fire. In other words:

$$C_N^*(y_j, z) = \frac{C_N(z)}{\Delta y} \tag{7.9}$$

where j denotes subgrid-scale index, $C_N(z)$ is normalized CWI concentration in units of mass/area, $C_N^*(y_j, z)$ is normalized concentration in units of mass/volume and Δy is the horizontal resolution of the host model in the cross-wind direction. The parameterized CWI smoke profile would be applied to the vertical column directly above the ignited cell (i.e. plume tilt and/or other local-scale effects would not be relevant within these coarse-grid applications). Dispersion and plume growth would be subsequently handled by the appropriate modules within the host smoke modelling framework.

A wide range of factors affect the lateral distribution of smoke within the plume. Among them are the shape and curvature of the fireline, ambient convection, vertical potential temperature profile, winds, vorticity, fire intensity and many others. While beyond the scope of both the synthetic dataset and of this dissertation, the remainder of this section offers some ideas for future investigation.

Shown in Figure 7.5a is the total normalized smoke of a sample simulated plume, as integrated over the depth of the domain in the along-wind direction. For most of my simulations along-wind integrated (AWI) plumes are not symmetrical, as the fires were not ignited instantaneously. A representative lateral smoke distribution can be obtained by taking a cross-section at z_{CL} (Figure 7.5b). By comparing cross-sections of different simulated plumes, I can examine the effects of some parameters in my synthetic dataset on the width and shape of the lateral (cross-wind) distribution (Figure 7.6).

Specifically, I compare runs with different (a) fire intensities, (b) fireline lengths and (c) ambient winds, while holding other simulation conditions constant (Figure 7.6). Of course, as many of the parameters interact in complex non-linear ways, these comparisons do not constitute true controlled experiments. Generally, LES data suggests that the extent to which the plume widens is largely governed by the shape and intensity of the fire.

Recall from Chapter 5 that wildfire plumes often exhibit anvil-like behavior, with smoke outflow levels marked by increased advection relative to ambient winds. One can speculate, that this radial outflow may contribute to plume widening. Hence, more intense fires, associated with stronger updrafts and fire-induced winds appear to have broader lateral smoke distributions than weaker fires (Figure 7.6a).

In a similar fashion to Section 7.2, I can characterize the strength of the updraft and the associated lateral spread using the fire velocity scale w_f (Equation 6.11). This does not in any way constitute a method for parameterizing the smoke distribution in the cross-wind direction. However, an **extremely crude** normalized approximation can be described as follows:

$$C_N^*(y,z) = e^{-(y-y_f)^2\left(2\sigma_y^2\right)} \tag{7.10}$$

where y_f is the cross-wind location of the center of the fire and $\sigma_y = 1870 + 215 * w_f$. I determined the fit parameters for σ_y (Equation 7.10) from linear regression on LES data

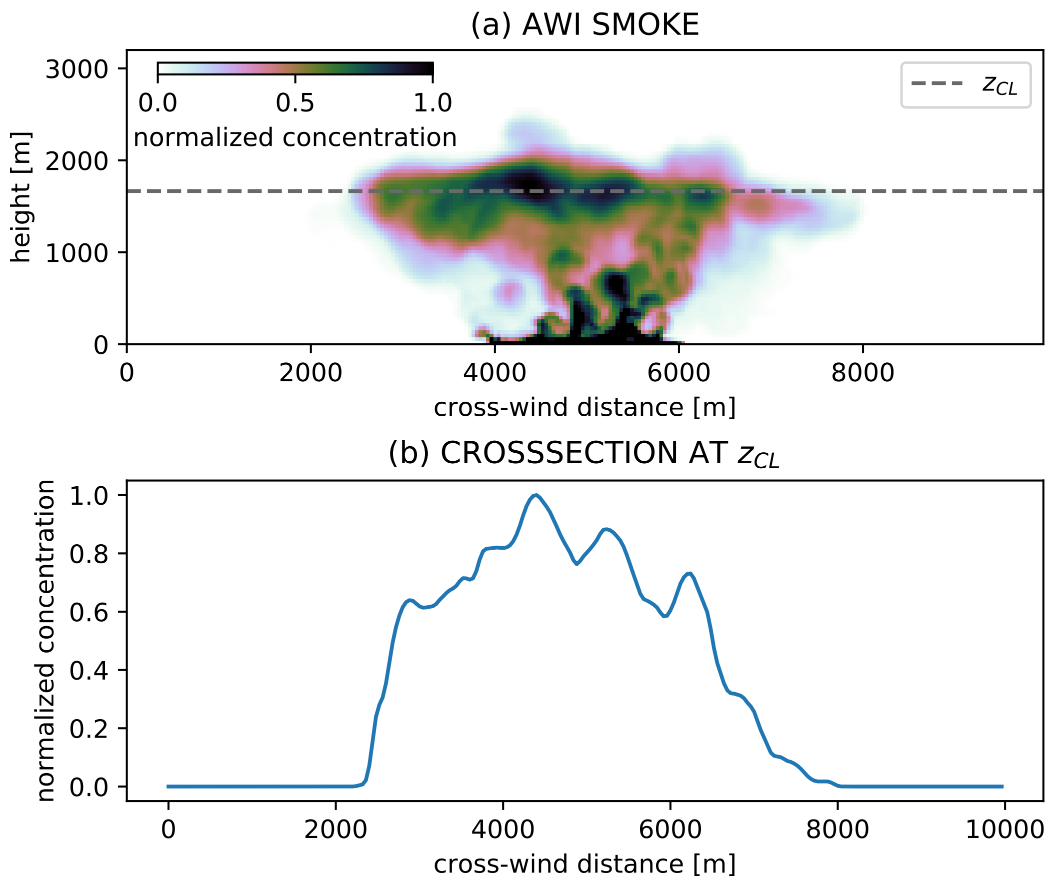

Figure 7.5: Lateral smoke spread from a sample simulated wildfire plume. (a) Total normalized along-wind (y,z) smoke. Dashed grey line denotes smoke injection level z_{CL} (b) Horizontal cross-section obtained from above at z_{CL}.

(R=0.80). The approximated lateral smoke distributions obtained using this approach are shown as dotted lines in Figure 7.6.

In conclusion, although parameterizations for the initial lateral spread of the smoke can be devised, most operational applications, with coarse-grid dispersion models, will inject the smoke plume into one grid column. Hence, initial lateral spread is not needed, because the injected smoke is assumed to to be distributed uniformly within each grid cell.

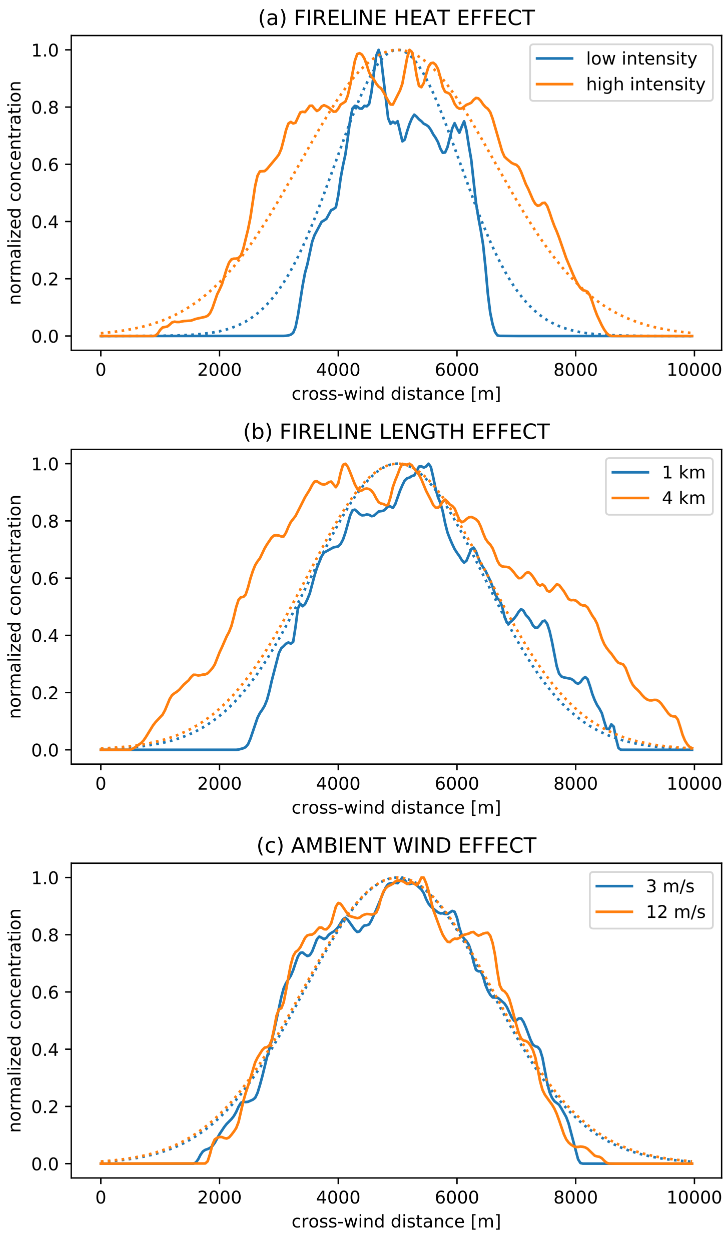

Figure 7.6: Parameters affecting lateral smoke spread from a wildfire. Solid and dotted lines denote true (LES) and approximated (Equation 7.10) cross-sections, respectively. (a) Low (blue) vs. high (orange) fireline intensity. (b) 1 km (blue) vs. 4 km (orange) firelines. (c) Low (blue) vs. high (orange) winds.

7.5 Summary of approach

In this chapter I introduce a simple method for predicting the **normalized** vertical distribution $C_N(z)$ of CWI smoke from a wildfire under known daytime ambient atmospheric conditions. The approach can be summarized with the following steps:

1. For a given wildfire, obtain z_{CL} and z' (Equation 6.8)
2. Perform automated plume classification (Equation 7.1)
   (a) For non-penetrative plumes assume uniform smoke distribution between the surface and z_i
   (b) For penetrative plumes proceed to the following steps
3. Calculate σ_{top} (Equation 7.4)
4. Calculate σ_{bot}
   (a) Calculate w_f (Equation 6.11)
   (b) Obtain $w*$ and U_a from ambient atmospheric and surface data
   (c) Calculate R_w (Equation 7.7) and σ_{bot} (Equation 7.8)
5. Model the full normalized vertical smoke profile of CWI concenration:

$$C_N(z) = e^{-(z-z_{CL})^2/\left(2\sigma^2\right)} \tag{7.11}$$

   where

$$\sigma = \begin{cases} \sigma_{top}, & z \geq z_{CL} \\ \sigma_{bot}, & z < z_{CL} \end{cases}$$

To obtain actual concentrations, it may be necessary to make additional assumptions about how the smoke is distributed in the cross-wind direction (Section 7.4), although most dispersion models will not need the initial lateral spread.

7.6 Limitations

The overall encouraging error statistics presented in Section 7.3.2 should be treated with caution, as all simulations in the synthetic plume dataset were initialized with the same ambient sensible heat flux at the lower domain boundary. Various ABL depths and temperatures corresponding to different **R** conditions produce a wide range of w^* values, however, S is constant for the entire dataset.

The dependence of the parameterization on w^* is in itself a limitation, as in real-world (rather then numerical modelling) applications observations of surface fluxes are typically not available. However, rough estimates can be made in the field using Pasquill-Gifford methods [21], such as considering insolation, cloud cover and wind speed. Also, while the approach doesn't appear to be very sensitive to errors in z_{top}, it, never-the-less, relies on the relative definition of the plume penetration distance z' from the previous Chapter 6.

Lastly, Section 7.4 merely skims the surface of the complex analysis required to understand what processes govern smoke distribution in the cross-wind direction.

7.6.1 Big picture

A truly robust assessment of uncertainties associated with the proposed parameterization would require expanding the parameter space of the LES plume dataset. In particular, it would be important to include directional shear in the imposed ambient winds, while also varying the surface sensible heat flux. Never-the-less, even in its current form it is likely going to offer an advantage over "single-level" smoke injection schemes or those relying on "uninformed" assumptions (e.g. linear interpolation of concentrations between the injection height and the surface; single Gaussian distribution with a fixed spread).

While encouraging, these results are still dependent on accurate input parameters from other components of smoke modelling systems. Namely, the methods presented here rely on fire behavior information to predict the mean smoke injection level and plume penetration distance, as well as emissions estimates to convert the normalized profiles to absolute concentration values. Moreover, much theoretical work is needed to understand how the smoke is distributed in the cross-wind direction. More broadly, the tools presented in this chapter are merely small elements of a complex modelling chain.

Chapter 8

Conclusions

Modelling plume rise from wildfires is a complex challenge that lies at the interface of fluid dynamics, atmospheric physics and fire behavior science. To date, it remains one of the weakest links in our ability to predict where and how smoke from wildfires travels in the atmosphere. This dissertation was guided by a set of research questions, aiming to fill the knowledge gaps in our current state of knowledge on the subject. As I revisit them below, I hope that my answers contribute to the interdisciplinary effort to improve our understanding of wildfire atmospheric dynamics.

- **Can a coupled fire-atmosphere numerical model accurately simulate smoke plume rise from a real fire?**

  In short, yes. The model evaluation case study presented in this thesis (Chapter 3) compared fire and smoke behavior from a WRF-SFIRE simulation to observations from a comprehensive field experiment (RxCADRE). While rudimentary in some aspects, the analysis suggested that the model reasonably captures plume kinematics and can serve as a useful tool for learning about the physical processes involved.

- **What can we learn about the behavior of the atmosphere around the fire from numerical experiments?**

  Detailed synthetic data produced by WRF-SFIRE (Chapter 4) allowed me to experiment with a range of fire and atmospheric conditions well beyond the capacity of any observational campaign. Complex dynamical features (including flow convergence, vorticity, interactions with boundary layer turbulence) revealed by these numerical experiments challenge several common assumptions about how smoke plumes mix with the atmosphere (Chapter 5). Most aspects of fire-atmosphere interactions detailed in this work remain to be quantified.

- **Can synthetic data be used to parameterize smoke plume rise for air quality applications?**

  Based on insights gained from the numerical experiments, I developed a simple energy-balance approach, which allows to determine:

  - **What is the mean smoke injection height of a given wildfire plume?**

    The proposed parameterization (Chapter 6) allows to predict the centerline height of a CWI penetrative plume from a fire of arbitrary shape and intensity under a wide range of ambient conditions. I demonstrated that for daytime fair-weather plumes there exist a linear dimensionless relationship and a characteristic fire velocity scale, which govern the vertical penetration distance of the plume in the atmosphere above the ABL.

  - **Which plumes will penetrate the ABL?**

    Using equations from Chapter 6, I showed that the proposed energy-balance approach can also be applied as an automated classifier to distinguish penetrative vs. non-penetrative plumes.

  - **How are wildfire emissions vertically distributed in the atmosphere?**

    In Chapter 7 I demonstrated that parameterized plume penetration distance and fire velocity scale can be used to predict the full vertical profile of smoke emissions above and below the mean injection height.

  In Section 7.5 I provide a complete set of algorithms needed to incorporate the new plume rise parameterization into an air quality model.

The natural next step beyond this thesis is the implementation of the new plume rise scheme within a regional smoke prediction system (e.g. BlueSky Canada). Much work remains to be done to ensure that the new methods are calibrated to work well with the existing fire behavior and emissions models. Moreover, the inherently numerical perspective of this thesis is bound to be challenged, when the ideas and methods presented here are put to trial in real-world applications.

As extreme wildfire events become more common under a changing climate, our ability to reduce the health risks and mortality associated with smoke exposure will become critically important. My hope is that the contributions presented here will help advance our current smoke modelling tools and mitigate some of the negative impacts of wildfires for human health and the environment.

8.1 Contributions

The specific contributions of this thesis are as follows:

- Analysis of WRF-SFIRE model performance using an integrated observational RxCADRE dataset (Chapter 3). The results and methods (as well as sample initialization files) of this evaluation study can be used for model development and improvement.

- A synthetic plume dataset consisting of 133 penetrative and 14 non-penetrative plumes over a wide range of atmospheric and fire conditions (Chapter 4, Table 4.3), to facilitate smoke dispersion research in the absence of detailed observational data.

- An analytical method for determining the mean injection height of a smoke plume from an arbitrarily shaped wildfire in a daytime atmosphere (Chapter 6). The approach can be applied as a classifier to distinguish penetrative and non-penetrative plumes (Section 7.1) as well as a plume rise parameterization within a host smoke modelling system.

- A Gaussian-based method for predicting the vertical distribution of CWI wildfire emissions in the atmosphere (Chapter 7), which can be applied within air quality and dispersion models.

8.2 What's ahead?

Methods and ideas presented in this thesis are aimed at improving a single link in a long and complex modelling chain of smoke prediction systems. Due to lack of scientific theory connecting the numerous physical processes involved, many components of these frameworks still rely on simplifying parameterizations. Hence, in the short term, I hope that the methods contributed by this work can be implemented within existing air quality systems and help improve their accuracy.

Yet I imagine that the next generation of smoke modelling frameworks could harness the power of increasingly more affordable cloud computing resources. This would eventually allow us to replace parameterized components (like combustion and smoke dynamics) of our numerical systems with directly computed full-physics models. This, in turn, could help capture many dynamical feedbacks that exist between the fire, the smoke and the atmosphere. The importance of understanding these feedbacks extends well beyond air quality, and carries fundamental consequences for climate prediction.

Hence, my long-term vision and hope is that accurate and intelligent smoke modelling systems of the future will have no need for parameterizations akin to ones contributed by this thesis.

Bibliography

[1] G. L. Achtemeier, S. A. Goodrick, Y. Liu, F. Garcia-Menendez, Y. Hu, and M. T. Odman. Modeling smoke plume-rise and dispersion from southern united states prescribed burns with daysmoke. *Atmosphere*, 2(3):358–388, 2011. → page 7

[2] R. Ahmadov, G. Grell, E. James, S. Freitas, G. Pereira, I. Csiszar, M. Tsidulko, B. Pierce, S. McKeen, S. Peckham, et al. A high-resolution coupled meteorology-smoke modeling system hrrr-smoke to simulate air quality over the conus domain in real time. *EGUGA*, page 10841, 2017. → page 5

[3] H. E. Anderson. Aids to determining fuel models for estimating fire behavior. *The Bark Beetles, Fuels, and Fire Bibliography*, page 143, 1982. → pages 20, 36

[4] K. Anderson, A. Pankratz, and C. Mooney. 9.2 a thermodynamic approach to estimating smoke plume heights. In *Proceedings of Ninth Symposium on Fire and Forest Meteorology, Palms Springs, CA*, pages 17–21, 2011. → pages 8, 51, 59, 69

[5] D. M. Bowman, J. K. Balch, P. Artaxo, W. J. Bond, J. M. Carlson, M. A. Cochrane, C. M. D'Antonio, R. S. DeFries, J. C. Doyle, S. P. Harrison, et al. Fire in the earth system. *science*, 324(5926):481–484, 2009. → page 4

[6] G. Briggs. *Plume Rise Equations*, pages 59–111. AMS: Boston, MA, USA, 1975. → pages 6, 51, 59, 69

[7] B. Butler, C. Teske, D. Jimenez, J. O'Brien, P. Sopko, C. Wold, M. Vosburgh, B. Hornsby, and E. Loudermilk. Observations of energy transport and rate of spreads from low-intensity fires in longleaf pine habitat –rxcadre 2012. *International Journal of Wildland Fire*, 25(1):76–89, 2016. URL http://dx.doi.org/10.1071/WF14154. → pages 16, 17, 21, 24, 67

[8] J. Canfield, R. Linn, J. Sauer, M. Finney, and J. Forthofer. A numerical investigation of the interplay between fireline length, geometry, and rate of spread. *Agricultural and Forest Meteorology*, 189:48–59, 2014. → page 54

[9] J. Chen, K. Anderson, R. Pavlovic, M. D. Moran, P. Englefield, D. K. Thompson, R. Munoz-Alpizar, and H. Landry. The firework v2.0 air quality forecast system with biomass burning emissions from the canadian forest fire emissions prediction system v2.03. *Geoscientific Model Development*, 12(7):3283–3310,

2019. doi:10.5194/gmd-12-3283-2019. URL https://www.geosci-model-dev.net/12/3283/2019/. → pages 5, 6, 8, 45, 69, 83

[10] C. B. Clements, S. Zhong, S. Goodrick, J. Li, B. E. Potter, X. Bian, W. E. Heilman, J. J. Charney, R. Perna, M. Jang, et al. Observing the dynamics of wildland grass fires: Fireflux—a field validation experiment. *Bulletin of the American Meteorological Society*, 88(9):1369–1382, 2007. → page 9

[11] C. B. Clements, N. P. Lareau, D. Seto, J. Contezac, B. Davis, C. Teske, T. J. Zajkowski, A. T. Hudak, B. C. Bright, M. B. Dickinson, B. W. Butler, D. Jimenez, and J. K. Hiers. Fire weather conditions and fire–atmosphere interactions observed during low-intensity prescribed fires –rxcadre 2012. *International Journal of Wildland Fire*, 25(1):90–101, 2016. URL http://dx.doi.org/10.1071/WF14173N2-. → pages 16, 17

[12] C. B. Clements, A. K. Kochanski, D. Seto, B. Davis, C. Camacho, N. P. Lareau, J. Contezac, J. Restaino, W. E. Heilman, S. K. Krueger, et al. The fireflux ii experiment: a model-guided field experiment to improve understanding of fire–atmosphere interactions and fire spread. *International journal of wildland fire*, 28(4):308–326, 2019. → page 9

[13] J. Clyne, P. Mininni, A. Norton, and M. Rast. Interactive desktop analysis of high resolution simulations: application to turbulent plume dynamics and current sheet formation. *New Journal of Physics*, 9(8):301, 2007. → pages vi, 21, 49, 50, 55

[14] J. L. Coen, M. Cameron, J. Michalakes, E. G. Patton, P. J. Riggan, and K. M. Yedinak. Wrf-fire: Coupled weather–wildland fire modeling with the weather research and forecasting model. *Journal of Applied Meteorology and Climatology*, 52(1):16–38, 2015/09/29 2012. doi:10.1175/JAMC-D-12-023.1. URL http://dx.doi.org/10.1175/JAMC-D-12-023.1. → page 12

[15] J. L. Coen, M. Cameron, J. Michalakes, E. G. Patton, P. J. Riggan, and K. M. Yedinak. Wrf-fire: Coupled weather–wildland fire modeling with the weather research and forecasting model. *Journal of Applied Meteorology and Climatology*, 52(1):16–38, 2015/09/29 2012. doi:10.1175/JAMC-D-12-023.1. URL http://dx.doi.org/10.1175/JAMC-D-12-023.1. → pages 8, 9, 17

[16] P. Cunningham, S. L. Goodrick, M. Y. Hussaini, and R. R. Linn. Coherent vortical structures in numerical simulations of buoyant plumes from wildland fires. *International Journal of Wildland Fire*, 14(1):61–75, 2005. → page 48

[17] B. Cushman-Roisin. Atmospheric boundary layer. *Environmental Fluid Mechanics*, pages 165–186, 2014. → page 59

[18] J.-B. Filippi, F. Bosseur, X. Pialat, P.-A. Santoni, S. Strada, and C. Mari. Simulation of coupled fire/atmosphere interaction with the mesonh-forefire models. *Journal of Combustion*, 2011. → page 11

[19] J. M. Forthofer and S. L. Goodrick. Review of vortices in wildland fire. *Journal of Combustion*, 2011, 2011. → page 48

[20] S. R. Freitas, J. Carvalho, K. Longo, R. Chatfield, D. Latham, M. Silva Dias, M. Andreae, E. Prins, J. Santos, and R. Gielow. Including the sub-grid scale plume rise of vegetation fires in low resolution atmospheric transport models. *Atmospheric Chemistry and Physics*, pages 3385–3398, 2007. → pages 6, 7, 51, 69

[21] F. A. Gifford. Use of routine observations for estimating atmospheric dispersion. *Nuclear Safety*, 2:47–57, 1961. → page 88

[22] W. E. Heilman, Y. Liu, S. Urbanski, V. Kovalev, and R. Mickler. Wildland fire emissions, carbon, and climate: Plume rise, atmospheric transport, and chemistry processes. *Forest Ecology and Management*, 317:70–79, 2014. → page 6

[23] S. B. Henderson, M. Brauer, Y. C. MacNab, and S. M. Kennedy. Three measures of forest fire smoke exposure and their associations with respiratory and cardiovascular health outcomes in a population-based cohort. *Environmental health perspectives*, 119(9):1266–1271, 2011. → page 5

[24] A. Hudak, B. Bright, R. Kremens, and M. Dickinson. Rxcadre 2011 and 2012: Wildfire airborne sensor program long wave infrared calibrated image mosaics. https://doi.org/10.2737/RDS-2016-0008, 2015. → pages 16, 17

[25] A. T. Hudak and B. C. Bright. Rxcadre 2008, 2011, and 2012: Burn blocks. https://doi.org/10.2737/RDS-2014-0031, 2014. → page 16

[26] A. T. Hudak, B. C. Bright, B. W. Williams, and J. K. Hiers. Rxcadre 2011 and 2012: Ignition data. https://doi.org/10.2737/RDS-2017-0065, 2017. → pages 16, 17, 19

[27] C. Ichoku, R. Kahn, and M. Chin. Satellite contributions to the quantitative characterization of biomass burning for climate modeling. *Atmospheric Research*, 111:1 – 28, 2012. ISSN 0169-8095. doi:https://doi.org/10.1016/j.atmosres.2012.03.007. URL http://www.sciencedirect.com/science/article/pii/S0169809512000750. → page 9

[28] D. Jimenez and B. Butler. Rxcadre 2012: Rxcadre 2012: In-situ fire behavior measurements, 2016. → page 67

[29] F. Johnston, I. Hanigan, S. Henderson, G. Morgan, and D. Bowman. Extreme air pollution events from bushfires and dust storms and their association with mortality in sydney, australia 1994–2007. *Environmental research*, 111(6): 811–816, 2011. → page 5

[30] F. H. Johnston, S. B. Henderson, Y. Chen, J. T. Randerson, M. Marlier, R. S. DeFries, P. Kinney, D. M. Bowman, and M. Brauer. Estimated global mortality attributable to smoke from landscape fires. *Environmental health perspectives*, 120(5):695–701, 2012. → page 5

[31] R. A. Kahn, Y. Chen, D. L. Nelson, F.-Y. Leung, Q. Li, D. J. Diner, and J. A. Logan. Wildfire smoke injection heights: Two perspectives from space. *Geophysical Research Letters*, 35(4), 2008. → page 9

[32] S. Kartsios, T. Karacostas, I. Pytharoulis, and A. Dimitrakopoulos. Coupled weather-wildland fire model for fire behavior interpretation. In *12th International Conference on Meteorology, Climatology and Atmospheric Physics COMECAP 2014*, 05 2014. → page 17

[33] S. Kartsios, T. S. Karacostas, I. Pytharoulis, and A. P. Dimitrakopoulos. The role of heat extinction depth concept to fire behavior: An application to wrf-sfire model. In T. Karacostas, A. Bais, and P. T. Nastos, editors, *Perspectives on Atmospheric Sciences*, pages 137–142. Springer International Publishing, 2017. ISBN 978-3-319-35095-0. → page 33

[34] A. Kochanski, M. Jenkins, J. Mandel, J. Beezley, and S. Krueger. Real time simulation of 2007 santa ana fires. *Forest Ecology and Management*, 294:136 – 149, 2013. ISSN 0378-1127. doi:http://dx.doi.org/10.1016/j.foreco.2012.12.014. URL http://www.sciencedirect.com/science/article/pii/S0378112712007372. The Mega-fire reality. → pages 12, 30

[35] A. K. Kochanski, M. A. Jenkins, J. Mandel, J. D. Beezley, C. B. Clements, and S. Krueger. Evaluation of wrf-sfire performance with field observations from the fireflux experiment. *Geosci. Model Dev.*, 6(4):1109–1126, 08 2013. doi:10.5194/gmd-6-1109-2013. URL http://www.geosci-model-dev.net/6/1109/2013/. → pages 12, 17, 32, 33

[36] A. K. Kochanski, M. A. Jenkins, K. Yedinak, J. Mandel, J. Beezley, and B. Lamb. Toward an integrated system for fire, smoke and air quality simulations. *International Journal of Wildland Fire*, 25(5):534–546, 2016. → page 12

[37] A. K. Kochanski, D. V. Mallia, M. G. Fearon, J. Mandel, A. H. Souri, and T. Brown. Modeling wildfire smoke feedback mechanisms using a coupled fire-atmosphere model with a radiatively active aerosol scheme. *Journal of Geophysical Research: Atmospheres*, 124(16):9099–9116, 2019. → page 12

[38] N. P. Lareau and C. B. Clements. The Mean and Turbulent Properties of a Wildfire Convective Plume. *Journal of Applied Meteorology and Climatology*, 56 (8):2289–2299, 08 2017. ISSN 1558-8424. doi:10.1175/JAMC-D-16-0384.1. URL https://doi.org/10.1175/JAMC-D-16-0384.1. → page 4

[39] N. K. Larkin, S. M. O'Neill, R. Solomon, S. Raffuse, T. Strand, D. C. Sullivan, C. Krull, M. Rorig, J. Peterson, and S. A. Ferguson. The bluesky smoke modeling framework. *International Journal of Wildland Fire*, 18(8):906–920, 2010. → pages 5, 6, 45

[40] P. Lee, J. McQueen, I. Stajner, J. Huang, L. Pan, D. Tong, H. Kim, Y. Tang, S. Kondragunta, M. Ruminski, et al. Naqfc developmental forecast guidance for fine particulate matter (pm2. 5). *Weather and Forecasting*, 32(1):343–360, 2017. → page 5

[41] R. Linn, J. Reisner, J. J. Colman, and J. Winterkamp. Studying wildfire behavior using firetec. *International journal of wildland fire*, 11(4):233–246, 2002. → page 11

[42] D. Mallia, A. Kochanski, S. Urbanski, and J. Lin. Optimizing smoke and plume rise modeling approaches at local scales. *Atmosphere*, 9(5):166, 2018. → pages 8, 12, 15, 29

[43] D. V. Mallia, A. K. Kochanski, K. E. Kelly, R. Whitaker, W. Xing, L. E. Mitchell, A. Jacques, A. Farguell, J. Mandel, P.-E. Gaillardon, et al. Evaluating wildfire smoke transport within a coupled fire-atmosphere model using a high-density observation network for an episodic smoke event along utah's wasatch front. *Journal of Geophysical Research: Atmospheres*, 125(20):e2020JD032712, 2020. → page 44

[44] D. V. Mallia, A. K. Kochanski, S. P. Urbanski, J. Mandel, A. Farguell, and S. K. Krueger. Incorporating a canopy parameterization within a coupled fire-atmosphere model to improve a smoke simulation for a prescribed burn. *Atmosphere*, 11(8):832, 2020. → page 12

[45] J. Mandel, J. D. Beezley, and A. K. Kochanski. Coupled atmosphere-wildland fire modeling with wrf 3.3 and sfire 2011. *Geoscientific Model Development*, 4(3): 591–610, 2011. → pages 11, 17, 35

[46] J. Mandel, S. Amram, J. Beezley, G. Kelman, A. Kochanski, V. Kondratenko, B. Lynn, B. Regev, and M. Vejmelka. Recent advances and applications of wrf–sfire. *Natural Hazards and Earth System Sciences*, 14(10):2829–2845, 2014. → pages 11, 17, 35

[47] C. J. Matz, M. Egyed, G. Xi, J. Racine, R. Pavlovic, R. Rittmaster, S. B. Henderson, and D. M. Stieb. Health impact analysis of pm2. 5 from wildfire smoke in canada (2013–2015, 2017–2018). *Science of The Total Environment*, 725:138506, 2020. → page 5

[48] J. Meadley. Dalyup fire column, February 2016. URL https://www.abc.net.au/news/2016-02-03/dalyup-fire-column/7134540?nw=0. → pages vi, 2

[49] W. Mell, M. A. Jenkins, J. Gould, and P. Cheney. A physics-based approach to modelling grassland fires. *International Journal of Wildland Fire*, 16(1):1–22, 2007. → page 11

[50] N. Moisseeva and R. Stull. Capturing plume rise and dispersion with a coupled large-eddy simulation: Case study of a prescribed burn. *Atmosphere*, 10(10):579, 2019. URL https://www.mdpi.com/2073-4433/10/10/579/s1. → pages 18, 19, 20, 29

[51] D. L. Nelson, M. J. Garay, R. A. Kahn, and B. A. Dunst. Stereoscopic height and wind retrievals for aerosol plumes with the misr interactive explorer (minx). *Remote Sensing*, 5(9):4593–4628, 2013. → page 9

[52] W. M. Organization. *International Cloud Atlas*. World Meteorological Organization, 2017. URL https://cloudatlas.wmo.int/en/flammagenitus.html. → pages 8, 72

[53] R. D. Ottmar and J. C. Restaino. Rxcadre 2008, 2011, and 2012: Ground fuel measurements from prescribed fires. https://doi.org/10.2737/RDS-2014-0028, 2014. → page 17

[54] R. D. Ottmar, J. K. Hiers, B. W. Butler, C. B. Clements, M. B. Dickinson, A. T. Hudak, J. J. O'Brien, B. E. Potter, E. M. Rowell, T. M. Strand, and T. J. Zajkowski. Measurements, datasets and preliminary results from the rxcadre project –2008, 2011 and 2012. *International Journal of Wildland Fire*, 25(1):1–9, 2016. URL http://dx.doi.org/10.1071/WF14161. → pages vi, 8, 10, 15

[55] K. Overholt, J. Cabrera, A. Kurzawski, M. Koopersmith, and O. Ezekoye. Characterization of fuel properties and fire spread rates for little bluestem grass. *Fire Technology*, 50(1):9–38, 2014. → page 20

[56] R. Paugam, M. Wooster, S. Freitas, and M. Val Martin. A review of approaches to estimate wildfire plume injection height within large-scale atmospheric chemical transport models. *Atmospheric Chemistry and Physics*, 16(2):907–925, 2016. doi:10.5194/acp-16-907-2016. URL https://www.atmos-chem-phys.net/16/907/2016/. → pages 4, 7, 8, 9

[57] R. Pavlovic, J. Chen, K. Anderson, M. D. Moran, P.-A. Beaulieu, D. Davignon, and S. Cousineau. The firework air quality forecast system with near-real-time biomass burning emissions: Recent developments and evaluation of performance for the 2015 north american wildfire season. *Journal of the Air & Waste Management Association*, 66(9):819–841, 2016. → page 6

[58] B. E. Potter. The role of released moisture in the atmospheric dynamics associated with wildland fires. *International Journal of Wildland Fire*, 14(1):77–84, 2005. URL http://dx.doi.org/10.1071/WF04045. → page 8

[59] B. E. Potter. Atmospheric interactions with wildland fire behaviour–ii. plume and vortex dynamics. *International Journal of Wildland Fire*, 21(7):802–817, 2012. → page 48

[60] S. Prichard, S. O'Neill, and S. Urbanski. Evaluation of revised emissions factors for emissions prediction and smoke management. https://www.epa.gov/sites/production/files/2017-10/documents/prichard.pdf, 2017. → pages 20, 36

[61] S. Prichard, N. S. Larkin, R. Ottmar, N. H. French, K. Baker, T. Brown, C. Clements, M. Dickinson, A. Hudak, A. Kochanski, et al. The fire and smoke model evaluation experiment—a plan for integrated, large fire–atmosphere field campaigns. *Atmosphere*, 10(2):66, 2019. → pages vi, 10, 11, 12, 15, 45

[62] S. M. Raffuse, K. J. Craig, N. K. Larkin, T. T. Strand, D. C. Sullivan, N. J. Wheeler, and R. Solomon. An evaluation of modeled plume injection height with satellite-derived observed plume height. *Atmosphere*, 3(1):103–123, 2012. → page 6

[63] C. E. Reid, M. Brauer, F. H. Johnston, M. Jerrett, J. R. Balmes, and C. T. Elliott. Critical review of health impacts of wildfire smoke exposure. *Environmental health perspectives*, 124(9):1334–1343, 2016. → page 5

[64] C. Rio, F. Hourdin, and A. Chédin. Numerical simulation of tropospheric injection of biomass burning products by pyro-thermal plumes. *Atmospheric Chemistry and Physics*, 10, 04 2010. doi:10.5194/acp-10-3463-2010. → pages 7, 51, 69

[65] J. Roberts, M. Trainer, D. Murphy, S. Brown, A. Brewer, R.-S. Gao, and D. Fahey. Fire influence on regional to global environments and air quality (firex-aq), 2020. → page 10

[66] R. Schigas and R. Stull. Bluesky canada part 3—bluesky canada wildfire smoke: Status at ubc. *Can. Smoke Newslett*, 2013:29–32, 2013. → pages 5, 45, 83

[67] D. Seto and C. B. Clements. Rxcadre 2012: Csu-maps wind lidar velocity and microwave temperature/relative humidity profiler data. https://doi.org/10.2737/RDS-2015-0026, 2015. → page 17

[68] D. Seto and C. B. Clements. Rxcadre 2012: In-situ wind, air temperature, barometric pressure, and heat flux time series data. https://doi.org/10.2737/RDS-2015-0048, 2015. → pages 17, 18

[69] M. Sofiev, T. Ermakova, and R. Vankevich. Evaluation of the smoke-injection height from wild-land fires using remote-sensing data. *Atmospheric Chemistry and Physics*, 12(4):1995–2006, 2012. doi:10.5194/acp-12-1995-2012. URL https://www.atmos-chem-phys.net/12/1995/2012/. → pages 7, 8, 13, 59, 69, 72, 75

[70] R. B. Stull. *An Introduction to Boundary Layer Meteorology*. Springer Netherlands, 1988. doi:10.1007/978-94-009-3027-8. → pages 4, 81

[71] J. Turner. Turbulent entrainment: the development of the entrainment assumption, and its application to geophysical flows. *Journal of Fluid Mechanics*, 173:431–471, 1986. → page 48

[72] S. P. Urbanski. Rxcadre 2012: Airborne measurements of smoke emission and dispersion from prescribed fires. https://doi.org/10.2737/RDS-2014-0015, 2014. → pages 17, 25

[73] M. Val Martin, J. A. Logan, R. A. Kahn, F.-Y. Leung, D. L. Nelson, and D. J. Diner. Smoke injection heights from fires in north america: analysis of 5 years of satellite observations. *Atmospheric Chemistry and Physics*, 10(4):1491–1510, 2010. doi:10.5194/acp-10-1491-2010. URL https://www.atmos-chem-phys.net/10/1491/2010/. → pages 9, 13, 44

[74] M. Val Martin, R. A. Kahn, J. A. Logan, R. Paugam, M. Wooster, and C. Ichoku. Space-based observational constraints for 1-d fire smoke plume-rise models. *Journal of Geophysical Research: Atmospheres*, 117(D22), 2012. → pages 6, 8

[75] M. Val Martin, R. Kahn, and M. Tosca. A global analysis of wildfire smoke injection heights derived from space-based multi-angle imaging. *Remote Sensing*, 10(10):1609, 2018. → pages 9, 13, 28

[76] J. Vaughan, B. Lamb, C. Frei, R. Wilson, C. Bowman, C. Figueroa-Kaminsky, S. Otterson, M. Boyer, C. Mass, M. Albright, et al. A numerical daily air quality forecast system for the pacific northwest. *Bulletin of the American Meteorological Society*, 85(4):549–562, 2004. → page 5

Appendix A

Working with synthetic data

A.1 Initialization files

Sample initialization files used to generate a smoke plume can be obtained from Supplementary Material available at:
https://acp.copernicus.org/preprints/acp-2020-827/acp-2020-827-supplement.zip

A.2 Sample non-penetrative plume

Shown in Figure A.1 is an example of a simulated plume classified as non-penetrative by visual analysis. Note that the centerline exhibits oscillatory behavior and very little smoke is injected above ABL top. Such plumes are likely to remain trapped in the ABL and eventually become uniformly mixed throughout the depth of the convective mixed layer.

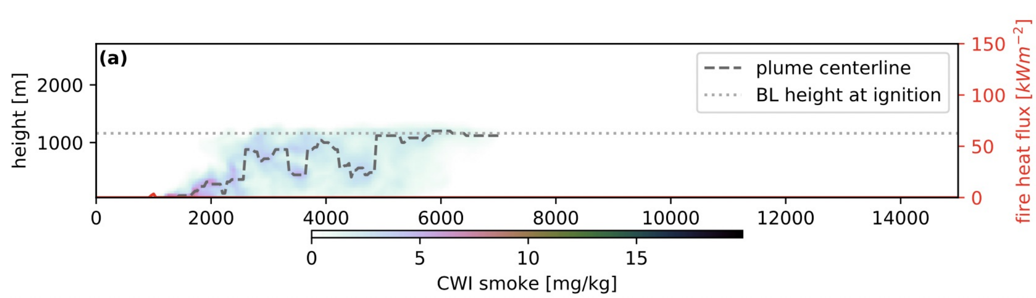

Figure A.1: True aspect ratio plot of CWI smoke from a sample non-penetrative plume. Plume centerline and z_i shown in dashed and dotted grey, respectively.

A.3 Identifying quasi-stationarity

I define the quasi-stationary downwind region for each plume based on two factors: the height of the centerline and tracer concentration gradient along the centerline. My filter attempts to extract only those portions of the downwind CWI smoke distribution, where both of these factors are changing slowly.

First, I remove the effect of random turbulent oscillations by applying a smoothing function (Savitzky-Golay filter provided by SciPy library with polynomial order set to 3) to both the concentration gradient along the centerline and the centerline height. I vary the size of the smoothing window as a function of mean ambient wind condition **W**, such that $window\_length = max(\mathbf{W} \cdot 10 + 1, 51)$ grid points.

The filter then applies the following criteria to extract quasi-stationary regions:

- smoothed tracer concentration along the plume centerline varies by less then 10% of the maximum concentration gradient
- smoothed centerline height varies by less then a 100 m
- the location is downwind of the maximum tracer concentration gradient
- the location is at least 10 grid points away from the maximum in smoothed and non-smoothed centerline height
- the location is at least 50 grid points away from the downwind endpoint of the centerline

The above thresholds were determined through an informal sensitivity analysis (not shown), based on the filter's ability to effectively identify regions of near-stationary plume centerline height for all simulations in our dataset.

A.4 Access to plume dataset

Data archive is available at:
https://doi.org/10.20383/102.0314

Appendix B

Plume rise scheme: mathematical formulations and implementation

B.1 Expanded form of plume penetration equation

Energy-balance formulation for plume penetration distance (Equation 6.1) can be converted into expanded form Equation 6.8) as follows:

$$\frac{z' g\theta'}{\theta_s} = c\left[\frac{I}{z_i\theta'}\right]^2 \tag{B.1}$$

Rearranging gives

$$\frac{z' g\theta'^3}{\theta_s} = c\left[\frac{I}{z_i}\right]^2$$

Multiplying both sides by z'

$$z'\left[\frac{gz'\theta'^3}{\theta_s}\right]^{\frac{1}{2}} = \tilde{c}\left[\frac{Iz'}{z_i}\right]$$

and rearranging gives

$$z' = \tilde{c}\left[\frac{gz'\theta'^3}{\theta_s}\right]^{-\frac{1}{2}}\left[\frac{Iz'}{z_i}\right]$$

Expanding the RHS

$$z' = \tilde{c}\left[\frac{gz'\theta'^3}{\theta_s}\right]^{-\frac{1}{2}}\left[\frac{gIz'}{z_i\theta_s}\right]\left[\frac{\theta_s}{g}\right]$$

and rearranging gives

$$z' = \tilde{c}\left[\frac{1}{z'\theta'^3}\right]^{\frac{1}{2}}\left[\frac{gIz'}{z_i\theta_s}\right]\left[\frac{\theta_s}{g}\right]^{\frac{3}{2}}$$

Multiplying both sides by z'^2

$$z'^3 = \tilde{c}\left[\frac{z'}{\theta'}\right]^{\frac{3}{2}}\left[\frac{gIz'}{z_i\theta_s}\right]\left[\frac{\theta_s}{g}\right]^{\frac{3}{2}}$$

and taking a cube root of the above expression

$$z' = C\underbrace{\left[\frac{\theta_s z'}{g\theta'}\right]^{\frac{1}{2}}}_{\frac{1}{N}}\underbrace{\left[\frac{gIz'}{z_i\theta_s}\right]^{\frac{1}{3}}}_{w_f}$$

where N is Brunt-Vaïsälä frequency (units of s^{-1}) over the penetration region with mean atmospheric lapse rate $\frac{\theta'}{z'}$ and w_f is the fire velocity scale (in ms^{-1}). Expanding z' and θ' gives

$$z_{CL} - z_s = C\left[\frac{g(\theta_{CL}-\theta_s)}{\theta_s(z_{CL}-z_s)}\right]^{-\frac{1}{2}}\left\{\frac{gI(z_{CL}-z_s)}{\theta_s z_i}\right\}^{\frac{1}{3}} \tag{B.2}$$

B.2 Expressions for w_f

I have two expressions for convective fire velocity w_f:

$$w_{f1} = \frac{I}{z_i\theta'} \tag{B.3}$$

and

$$w_{f2} = \left[\frac{gIz'}{\theta_s z_i}\right]^{\frac{1}{3}} \tag{B.4}$$

Using Equation 6.7 and setting $C \approx 1$ (based on LES data), I can rewrite Equation B.3 as

$$\begin{aligned} w_{f1} &= \left[z' g\frac{\theta'}{\theta_s}\right]^{\frac{1}{2}} \\ &= z'\left[\frac{g\theta'}{z'\theta_s}\right]^{\frac{1}{2}} \end{aligned}$$

Now substituting Equation 6.8 for z' into the above and cancelling terms in square brackets I obtain:

$$\begin{aligned} w_{f1} &= \left[\frac{g\theta'}{\theta_s z'}\right]^{-\frac{1}{2}} \left\{\frac{gIz'}{\theta_s z_i}\right\}^{\frac{1}{3}} \left[\frac{g\theta'}{z'\theta_s}\right]^{\frac{1}{2}} \\ &= \left\{\frac{gIz'}{\theta_s z_i}\right\}^{\frac{1}{3}} \\ &= w_{f2} \end{aligned}$$

Hence, the two expressions are equivalent.

B.3 Estimating model input parameters

Summarized in Table B.1 are parameters associated with an iterative solution for z_{CL} using Equation 6.8. Below is my approach to estimating these parameters from LES data.

As noted above, I consider the problem in crosswind direction. Given a three-dimensional fire of an arbitrary shape (eg. Figure 4.2b) and an ambient atmospheric sounding, I first average the fire kinematic heat flux for all ignited cells (where heat flux > 1 kW m^{-2}) over the crosswind (y) direction at the surface (red line on Figure 4.2a). Due to surface wind shear this direction may differ from the one used for calculating CWI smoke concentrations (as shown in Section 6.2.3). To obtain fireline intensity parameter I I numerically integrate the crosswind averaged heat fluxes over the depth of the fireline in the along-wind (x) direction.

I use pre-ignition potential temperature profile (i.e. the ambient environment upwind of the fire) averaged over the entire LES domain as an environmental sounding.

Table B.1: Variable descriptions and units used in smoke injection parameterization.

Variable	Unit	Description
I	K m^{2}s^{-1}	fireline integrated heat flux
g	ms^{-2}	gravity constant = 9.81
θ_{CL}	K	ambient potential temperature at z_{CL}
θ_s	K	ambient potential temperature at z_s
z_{CL}	m	smoke injection height
z_i	m	boundary layer height
z_s	m	reference height

All model fields are interpolated to have a 20 m vertical increment. z_i is defined as the height of the strongest environmental lapse rate gradient, and $z_s = \frac{3}{4}z_i$, based on informal model sensitivity analysis (not shown). The exact choice of z_s has little effect on model performance as long as it remains within the upper portion of the uniform potential temperature well-mixed layer.

The values of θ_s and θ_{CL} are then determined from the pre-ignition sounding for each simulation using the definitions of z_s and z_{CL} (as described in Section 4.2).

B.4 Iterative solution for z_{CL}

The numerical implementation of my iterative solution using SciPy's fsolve function (scipy.optimize.fsolve) is as follows. I rewrite bias corrected Equation 6.8 into an input function $toSolve$ as:

$$toSolve = lambda\ z : z - B_1(z_s + \left[\frac{g(T0[int(\frac{z}{dz})] - \theta_s)}{\theta_s(z - z_s)}\right]^{-\frac{1}{2}} \left[\frac{gI(z - z_s)}{\theta_s z_i}\right]^{\frac{1}{3}}) - B_2 \tag{B.5}$$

where $B_1 = 0.919$ and $B_2 = 137.919$ are bias correction parameters, $T0$ is the potential temperature sounding vector, dz is the vertical step and $int()$ is a standard Python function converting the bracketed value into an integer.

A possible issue for some solvers is that we are, effectively, iterating over the vertical index of the column vector $T0$ corresponding to z_{CL}. As the numerical solver attempts to converge on a solution it may query a non-existent index and fail. I am able to obtain a fast and consistent performance by ensuring I set z_i as the initial guess for z_{CL} and by minimizing the initial step bound option of the solver

$$z_{CL} = fsolve(toSolve, z_i, factor = 0.1) \tag{B.6}$$